UNIVERSITY OF CALIFORNIA

San Diego

Some Astrophysical Problems Involving Plasmas and Plasma-Solid Systems:

I. On the Mechanism of Formation of Loop Prominences

II. Electric Potential on Solid Spheres in a Plasma

III. Physical Conditions in the Meteorite Condensation Environment

IV. Origin of the Ocean

A dissertation submitted in partial satisfaction of the

requirements for the degree Doctor of Philosophy

in Applied Physics

by

Bibhas Ranjan De

Committee in charge:

Professor Hannes Alfvén, Chairman
Professor Gustaf Arrhenius, Co-Chairman
Professor James R. Arnold
Professor W. Ian Axford
Doctor D. Asoka Mendis, Lecturer

1973

The dissertation of Bibhas Ranjan De is approved, and it is acceptable in quality and form for publication on microfilm:

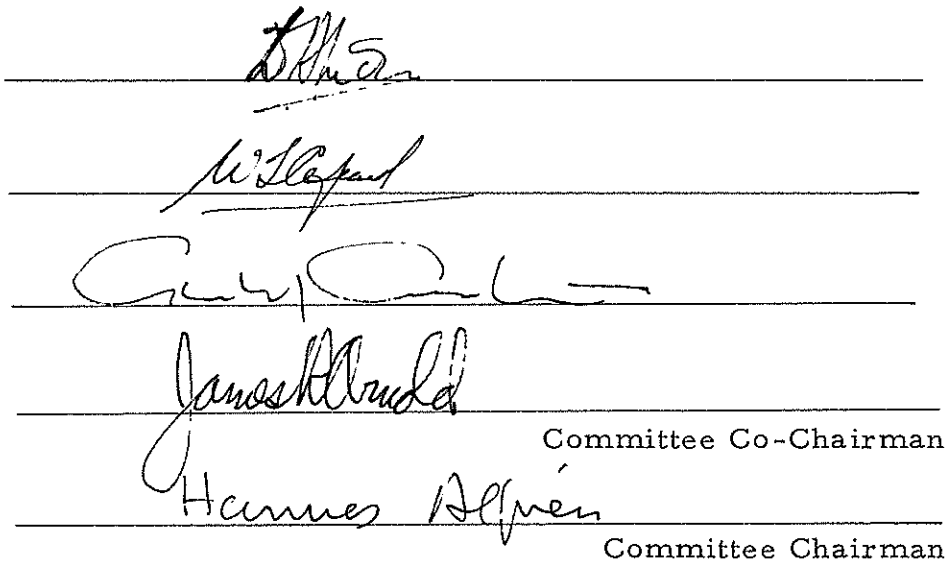

Committee Co-Chairman

Committee Chairman

University of California, San Diego

1973

TABLE OF CONTENTS

		Page
LIST OF FIGURES AND TABLES		v
PREFACE		vii
ACKNOWLEDGMENT		viii
VITA, LIST OF PUBLICATIONS AND FIELDS OF STUDY		x
ABSTRACT		xii
I.	ON THE MECHANISM OF FORMATION OF LOOP PROMINENCES	1
	1. INTRODUCTION	2
	2. OBSERVATIONAL BASIS	2
	3. THE FORMATION MECHANISM	5
	4. COOLING OF PLASMA IN CONTRACTING FILAMENT	9
	5. EQUILIBRIUM AT THE END OF COMPRESSION	15
	6. MASS DOWNFLOW	18
	7. LIFETIME OF A PROMINENCE LOOP	20
	8. REMARKS	22
	REFERENCES FOR I	23
II.	ELECTRIC POTENTIAL ON SOLID SPHERES IN A PLASMA	25
	1. INTRODUCTION	26
	2. THE ELECTRIC POTENTIAL ON A SPHERE	28
	3. THE EFFECT OF PLASMA DRIFT	34
	4. SUBMICRON SIZE METAL SPHERES: THE EFFECT OF IMAGE FORCE	37
	5. THE SEMI-CLASSICAL CASE	44
	6. LOWERING OF BARRIER BY IMAGE FORCE	47
	7. LIMITATION OF THE POTENTIAL	48
	8. EMISSION OF ELECTRONS	55
	9. REMARKS	56
	REFERENCES FOR II	58

Page

III. PHYSICAL CONDITIONS IN THE METEORITE CONDENSATION ENVIRONMENT 59

1. INTRODUCTION 60
2. THE CONDENSATION ENVIRONMENT ACCORDING TO SOME CURRENT INTERPRETATIONS 62
3. THE CONDENSATION ENVIRONMENT 103
4. THE CONDENSATION PROCESS IN THE STATE OF TEMPERATURE DISEQUILIBRIUM 130
5. SUMMARY AND IMPLICATIONS 135

REFERENCES FOR III 136

IV. ORIGIN OF THE OCEAN 138

1. SOURCES OF NEW INFORMATION 139
2. FORMATION OF THE SOLAR SYSTEM 141
3. OCCLUSION OF VOLATILES IN SOLID CONDENSATES 143
4. PRIMORDIAL GRAINS AS CARRIERS OF ATMOSPHERIC AND OCEANIC COMPONENTS 147
5. THE IMMEDIATE PRECURSOR STAGES 152
6. ACCRETION OF PLANETARY EMBRYOS 155
7. HEAT RELEASE AND VOLATIZATION OF WATER AT ACCRETION 163
8. TEMPERATURE DISTRIBUTION IN THE GROWING PROTOPLANET 165
9. A SIMPLE MODEL FOR ACCUMULATION OF WATER 167
10. ACCRETIONAL HEAT FRONT AND STATE OF WATER 171
11. DETAILS OF MODEL 172
12. VOLATILES IN THE LITHOSPHERE 178
13. THE OCEAN AND THE EARTH-MOON SYSTEM 183
14. FUTURE DEVELOPMENTS 186

REFERENCES FOR IV 188

LIST OF FIGURES AND TABLES

Figure		Page
I-1	Change in temperature with time of the contracting filamentary plasma	14
II-1	The potential of solid spheres in a hydrogen plasma as a function of the plasma temperature	33
II-2	The potential barrier	39
II-3	The position r_m of the maxima of the potential hill as a function of the number of electrons Z on the surface of the sphere	42
II-4	The transmission coefficient $P(\epsilon_r)$ of an electron as a function of ϵ_r for two different radii of the sphere: 0.01 μ and 0.1μ	46
II-5	The potential of solid spheres in a hydrogen plasma as a function of the sphere radius in units of $\underline{s}$, the radius of the Debye sheath which has been taken to be 1 m	50
II-6	Limitation of potential due to field emission of electrons	54
III-1	A conceptual sketch of a primitive solar nebula	66
III-2	Temperatures of grains in thermal equilibrium with gas and radiation field	74
III-3	Cooling to equilibrium temperature of an iron grain which has been raised to a high temperature (here 2000°K) by some transient process	87
III-4	Cooling of gas due to refrigeration by the grains	91
III-5	Temperature of gas, grains and radiation field as a function of optical depth in a disc-shaped cloud around the Sun as sketched in Figure III-1	98
III-6	Asymptotic approach to the "equal temperature" state	101

Figure Page

III-7 The equilibrium grain temperatures including the effects of dissociation and ionization of the gas 117

III-8 The ranges of gas pressure in the meteorite condensation environment as a function of the grain temperature 125

III-9 Condensation and evaporation rates of solids in the plasma limit 133

IV-1 Delicate leafy crystals of the magnesium-iron silidates of olivine and pyroxene, frequently twinned, and loosely adhering to each other 145

IV-2 Formation of jet streams 154

IV-3 Heat structure and the accumulation of water 162

IV-4 Noncatastrophic capture 185

Table

III-1 Total Emissivity of Various Non-Black Substances . . . 82

IV-1 Oxygen Reservoir of the Earth 174

PREFACE

Part IV of this thesis is a contribution to the Sillén Memorial Volume of The Sea invited from Professors Gustaf Arrhenius and Hannes Alfvén, who were very kind to introduce me to certain problems in this work. It appeared under the joint authorship of Gustaf Arrhenius, Hannes Alfvén and myself.

ACKNOWLEDGMENT

My association with Professors Hannes Alfvén and Gustaf Arrhenius, my thesis advisors, has been rewarding to me in many ways. In the academic sphere, I have enjoyed the privilege of being introduced to the great intuition and thought processes of these two men. Outside the academia, I have enjoyed discussions with them on many and varied topics and these have enriched my vision greatly. On the material side, they have always sought to alleviate the economic difficulties of a foreign student trying to make both ends meet. For all these kindnesses and many more, I shall remain ever grateful. Their role to me has truly been one of a "friend, philosopher and guide."

The members of my thesis advisory committee, Professors James Arnold and Ian Axford and Dr. Asoka Mendis, have patiently given me of their time and attention, for which I remain thankful.

I have benefitted from many discussions with my wife Gopa during the years of fruition of this thesis, for which I wish to express my greatest appreciation.

I also wish to thank many other people who have helped me along the way. Among them are Mss. Joanne Guy, Lola Lindsay, Dawn Rawls, Marge Sinkankas and Annetta Whiteman, who typed this thesis with great care.

And to conclude, I wish to express my deepest gratitude to the late Professor M. G. J. Minnaert, who as the President of Commission 38 of I. A. U. had taken an interest in me through correspondences when I was a fresh graduate student in India, and had greatly expedited the matter of my coming to study in the United States. He passed away before I had a chance to meet him.

VITA

January 22, 1946 - Born - Silchar, Assam, India

1967	B.Sc., University of Calcutta, India
1970	M.S., University of Michigan, Ann Arbor, Mich.
1972	C. Phil., University of California, San Diego, La Jolla, Ca.
1970-1971	Graduate Research Assistant, Apprentice Observer and Electronic Technician, University of Michigan Radioastronomy Observatory
1971-1973	Graduate Research and Teaching Assistant in Applied Physics, University of California, San Diego

Honors, Awards

Government of India National Scholarship, 1964-1968; Joint Fellowship from International Astronomical Union and UNESCO to undertake graduate studies in the U.S.A., 1968; Wheeler-Lawton Graduate Fellowship in Astronomy, University of Michigan, 1969; Elected to National Honor Society of Phi Kappa Phi, 1970. Citation in Transactions of the I.A.U. (1970) for scholastic achievement.

PUBLICATIONS

"A Survey of Man-made Radio Signals between 4 GHz and 11.5 GHz," University of Michigan Radioastronomy Observatory Report 70-7, 1970

"Origin of the Ocean," with G. Arrhenius and H. Alfvén, The Sea, vol. 5, Wiley-Interscience, New York, 1973

"On the Mechanism of Formation of Loop Prominences," Solar Physics, 1973 (in press)

"Equilibrium Condensation in a Solar Nebula," with G. Arrhenius, Meteoritics, vol. 8, No. 4, 1973

FIELDS OF STUDY

Major Fields: Physics and Astronomy

Studies in Theoretical and Observational Radioastronomy
Professor Fred T. Haddock
University of Michigan

Studies in Radioastronomy Instrumentation
Professor Fred T. Haddock
University of Michigan

Studies in Plasma Physics
Professor Herschel Weil
University of Michigan

Studies in Microwave Engineering
Professor Brice Carnahan
University of Michigan

Studies in Theoretical Astrophysics
Professors Richard L. Sears and Gunther H. Elste
University of Michigan

Studies in Solar System Astrophysics
Professors Hannes Alfvén and Gustaf Arrhenius
University of California, San Diego

ABSTRACT OF THE DISSERTATION

Some Astrophysical Problems Involving Plasmas and Plasma-Solid Systems:

I. On the Mechanism of Formation of Loop Prominences

II. Electric Potential on Solid Spheres in a Plasma

III. Physical Conditions in the Meteorite Condensation Environment

IV. Origin of the Ocean

by

Bibhas Ranjan De

Doctor of Philosophy in Applied Physics

University of California, San Diego, 1973

Professor Hannes Alfvén, Chairman

Professor Gustaf Arrhenius, Co-Chairman

In Part I, a mechanism is suggested for the formation of loop-type prominences in solar-active regions following flare events. The mechanism is based on the already existing idea of compression of a coronal plasma element resulting in enhanced radiation and consequent cooling of the element. A model is suggested for such a compression based on the concept of a contracting, force-free filamentary structure.

If the current in a filament increases with time, then there is a radial contraction of the filament. Since the coronal plasma is frozen into the magnetic field lines of the filament, a contraction of the filament causes a compression of the filamentary plasma. This model of compression is shown to be in approximate qualitative and quantitative agreement with observations.

In Part II, it is shown that the steady electric potential that develops on a solid body immersed in a plasma is dependent on the dimension of the body relative to the Debye shielding distance in the plasma. In this paper we derive the general expression for this potential on a solid sphere showing the dependence of the potential on the radius $\underline{a}$ of the sphere and $\underline{s}$ of the plasma sheath that develops around the sphere. In the limit where the radius $\underline{a}$ is much larger than the sheath thickness $\underline{s} - \underline{a}$ we recover from this expression the well-known result for the potential on an infinite wall in contact with a plasma. On the other extreme where $\underline{s}$ is much larger than $\underline{a}$, we get the result derived by Spitzer (1941) for the potential on spherical grains in the interstellar plasma. Since the surface of the sphere forms a sink for the charged particles, there is a net drift of the plasma towards the surface. The effect of this drift on the potential is examined. Finally, for very small metallic spheres, two possible effects leading to a revision of the potential are discussed. These are the lowering of the potential barrier for the electrons due to the

image force and the possibility of electrons tunnelling through the resulting potential hill. Both these effects are shown to be important for submicron size grains. The various effects limiting the potential on spheres are discussed.

In Part III we examine the assumption in many currently popular theories of the meteorite condensation environment that the condensing solids and the ambient gas had the same temperature. This assumption is found to be irreconcilable with our knowledge of space and the fundamental laws of physics. A fresh attempt is made to deduce the physical conditions in the primordial gas at condensation basing on the assumption that the temperature of the solids at condensation was in the range 2000-200°K. The conclusion is that the gas temperature was in the range 3000-10,000°K, perhaps closer to the upper limit. Elemental iron, a major constituent of many meteorites, is chosen as an example for the discussion of the condensation process. The upper limit of total gas pressure for growth of solid iron grains is shown to be of the order of 10^{-5} - 10^{-4} atm, the corresponding total gas densities being of the order of 10^{13} - 10^{14} cm^{-3}. The condensation is essentially a slow process - the upper limit of growth rate for iron grains being about 100 Å per day.

Part IV is a preliminary attempt to understand the problem of the origin of the ocean starting from the assumption of a plasma condensation origin of the material that now form the earth. It is

suggested that the primordial grains that formed the earth already carried in them the seeds of the present ocean in the form of water bound in crystal lattices. This water was released during the accretion process by impact heating of the grains and was initially retained as an atmosphere around the growing hot embryonic earth. When at a later stage of accretion the conditions became favorable, the water vapor condensed to form liquid water. Quantitative aspects of the problem are examined and found consistent with the above suggestion.

I. ON THE MECHANISM OF FORMATION OF LOOP PROMINENCES

1. INTRODUCTION

The loop type prominences are observed in solar active regions following flare events. They become visible roughly 30 min after a flare has been observed. Motion pictures of loop prominence formation suggest that they form out of the surrounding coronal material and not for instance from material thrown up from the underlying photosphere or the chromosphere. The prominence material first becomes visible in Hα at the top of the loop and then falls downward on one or both sides of the loop. In this paper we suggest a mechanism for the formation of loop type prominences consistent with observations. Our discussion is based on the already existing idea of compression of a coronal plasma element resulting in enhanced cooling (see e.g. Lüst and Zirin, 1960), but we attempt to provide a model for this compression on the basis of observations and well known physical processes.

2. OBSERVATIONAL BASIS

The loop prominences form in active regions typically 30 min after proton flare events (Bruzek, 1964a, b; Jefferies and Orrall, 1965a, b). We can therefore make the reasonable assumption that the loop prominences start forming at the time of flare and hence the formation time is of the order of 30 min. The lifetime of a loop prominence system is of the order of 10^4 sec or more (Jefferies and Orrall, 1965b).

The electron density in the prominence loop is $\geq 10^{11}$ cm^{-3}, while the electron density in the surrounding corona is of the order of 10^{8} - 10^{9} cm^{-3}. The magnetic field in the prominence is of the order of 50 - 300 G, being predominantly axial. Such fields are impossible to represent by a current-free approximation. The magnetic field in the prominence region prior to the formation of the prominence may be taken to be of the order of a few gauss. The temperature at the edge and the top of the loop is about 12000 K, and the temperature near the central region is about 6000 - 7000 K. The temperature in the surrounding corona is of the order of 10^{6} K. The active region prominence data quoted above are taken from a recent report on prominence research by Bruzek and Kuperus (1972). The typical length of a prominence loop is about 10^{10} cm and the cross-sectional diameter of the loop is about 5×10^{8} cm. Note that under these conditions the gas pressure in the loop is negligible compared to the pressure of the magnetic field. Let us define at this point two time scales: the time scale of formation $\tau_f \approx 30$ min $\approx 10^{3}$ sec, and the lifetime $\tau_\ell \geq 10^{4}$ sec.

There do not seem to be any direct evidence of the existence of an electric current in the loop type prominences. However, in active region sunspot type prominence threads ('microspots') measurement of transverse magnetic field component indicates the existence of vertical electric current of the order of 10^{11} amp (Beckers and

Schröter, 1968; Stenflo, 1969). In the bright knots that precede the solar flare events and the subsequent formation of loop prominences in the same region, similar measurement also indicates vertical current of the order of 10^{11} amp (Moreton and Severny, 1968). Carlqvist (1969) and Stenflo (1969) have suggested that these bright knots and the microspots are force-free filamentary current paths. The current flows along a magnetic flux tube and forms an arch between two points between which a voltage difference exists. The circuit thus formed is essentially inductive, the resistivity being very low, and hence the current increases with time. The current, however, cannot increase indefinitely with time. It may either be interrupted by an instability such as discussed by Carlqvist (1969), or it may reach a steady value when for instance the resistive voltage drop across the loop equals the voltage between its foot points.

Observations of loop type prominences also indicate a continual downflow of matter from the prominence tube back into the photosphere and the chromosphere. This downflow takes place during a period of time which is shorter than the lifetime of the loop prominence system (Kleczek, 1963; Jefferies and Orall, 1965a, b). The downflowing material is visible in Hα and hence must consist largely of neutral hydrogen. Most of the material reaches the photosphere with a velocity of about 100 km sec^{-1}, somewhat less than the free-fall velocity. Orrall (see Bruzek and Kuperus, 1972) has estimated that

a single prominence thread loses about 10^{34} proton masses per sec back into the photosphere.

We shall not here go into the question as to what sources drive the electric current (see Stenflo, 1969, for a possible explanation of this), but assume that loop prominences are inductive filamentary current paths that begin to form following a flare. The current in the filament increases with time during the formation time τ_f, reaching a steady value of the order of 10^{11} amp at the end of this time.

3. THE FORMATION MECHANISM

The filamentary structure of a magnetic flux tube carrying current has been discussed among others by Chandrasekhar (1956), Schlüter (1957), Alfvén (1961, 1968) and Murty (1962). It has often been suggested that the solar prominences are such structures. The current in a prominence flows along the magnetic field lines so that the resulting $\underset{\sim}{J} \times \underset{\sim}{B}$ force vanishes. The result is that the magnetic field lines form helices around the axis of symmetry (z axis of a cylindrical coordinate system). The necessity of this force-free state arises from the fact that the gas pressure in the prominence is insufficient to balance the pressure of the magnetic field.

In the following discussion we shall neglect the curvature of the prominence loop and treat the loop as a straight cylindrical filament. The magnetic field in this filament derives partly from an

external axial field $\underset{\sim}{B}_{zo}$ in the undisturbed medium, and partly from the field generated by the current. If a filament of effective radius R forms by compressing the initial axial flux in a cylindrical region of radius r, then the total axial flux in the filament is

$$\Phi = \pi r^2 B_{zo} \tag{1}$$

which will be treated as a constant for our discussion. The distribution of current and magnetic field within the filament may be found by solving the Maxwell's equation

$$\text{curl } \underset{\sim}{B} = \frac{4\pi}{c} \underset{\sim}{J} \tag{2}$$

subject to the conditions

$$\text{div } \underset{\sim}{B} = 0 \tag{3}$$

$$\underset{\sim}{J} \times \underset{\sim}{B} = 0 \tag{4}$$

The last condition ensures that the configuration is force-free. Alfvén (1961) obtained a solution to these equations with cylindrical symmetry in the presence of an initial axial field under the assumption that the conductivity of the medium has a constant and non-zero value only along the field lines. It was later shown by Murty (1962) that a solution similar to Alfvén's could be obtained without making any special assumption about the conductivity except that it is very high. Both Alfvén and Murty find that the current and the magnetic field in a

filament are almost entirely confined within a radius R given by

$$R = A \Phi I^{-1} \tag{5}$$

where A is a constant whose value is 4×10^9 in gaussian units, and I is the total current in the filament. Hence equation (5) may be taken as a definition of the effective radius R of a filamentary tube. The total magnetic flux in such a filament is given by

$$\Phi \approx \pi R^2 B_z \tag{6}$$

where B_z is the magnetic field at the axis. Comparing equation (6) with equation (1) we find

$$\left(\frac{r}{R}\right)^2 = \frac{B_z}{B_{zo}} \tag{7}$$

In the highly conducting coronal plasma, the assumption of frozen-in field lines is valid. Hence a compression of the magnetic flux tube results in a compression of the plasma, so that if n and N are the initial density in the region in which the filament forms and the density in the filament respectively, we must have

$$\frac{N}{n} = \left(\frac{r}{R}\right)^2 = \frac{B_z}{B_{zo}} \tag{8}$$

If we substitute order-of-magnitude values $B_{zo} \approx 1$ G and $B_z \approx 10^2$ G for a filament in its final steady state, we find $R \approx 0.1\ r$ and

$N \approx 10^2 n$. With the coronal density of $n \approx 10^8 - 10^9$ cm^{-3}, the density in the filament becomes $N \approx 10^{10} - 10^{11}$ cm^{-3}, consistent with observations. If the temperature in the filament is such that some of the plasma can recombine, then the neutral gas will fall down to the photosphere under gravitation. This will be discussed in Section 6.

From equation (5) we note that if the current in the filament increases with time, its effective radius decreases. This results in a contraction of the filament, causing a compression of the plasma. If the current changes slowly, the evolution of the filament may be considered as consisting of a series of quasi-stationary states. Thus the velocity of contraction of the filamentary tube will be given by the rate of change of R as given by equation (5) with increasing I, that is

$$v_c = \frac{dR}{dt} = - A \Phi I^{-2} \left(\frac{dI}{dt} \right) \tag{9}$$

The assumption of quasi-static contraction made above will be valid if v_c is much smaller than the Alfvén velocity in the region. The Alfvén velocity in the filamentary region is of the order of $10^8 - 10^9$ cm sec^{-1} whereas the maximum value of v_c in our case would be of the order of 10^7 cm sec^{-1}. This justifies the assumption in equation (9).

The current I at any time t from the beginning of contraction may be written as

$$I = I_o + at \tag{10}$$

where I_o is the current at $t = 0$ and $a = dI/dt$ is a constant for our discussion. A finite current at $t = 0$ is necessary in order to avoid singularity in equation (9). This current corresponds to an arrangement of the initial undisturbed magnetic flux into a filamentary configuration prior to the beginning of contraction, and is given from equation (5) by

$$I_o = \frac{A\Phi}{r} \tag{11}$$

The time taken by the filamentary tube to contract from the initial radius r to the final radius R can be found from equations (9) and (10). We define this time as the formation time τ_f

$$\tau_f = \frac{1}{b}\left(\frac{r - R}{R}\right) \tag{12}$$

where $b = a/I_o$. With $B_{zo} \approx 1$ G, $\tau_f \approx 10^3$ sec and $R = 0.1\, r = 2.5 \times 10^8$ cm, we find $I_o \approx 10^{10}$ amp and $a \approx 10^8$ amp sec^{-1} and hence $b \approx 10^{-2}$ sec^{-1}. The total current at the end of τ_f would then be 1.1×10^{11} amp, which is roughly what we expect.

4. COOLING OF PLASMA IN CONTRACTING FILAMENT

The density of the plasma in the filament at any time t can be found by combining equations (5), (8) and (10) to be

$$N = n\,(1 + bt)^2 \tag{13}$$

The compression of the plasma in our case may be assumed to be adiabatic except for the heat conduction through the end faces of the filamentary tube, which we shall take into account separately. Assuming an ideal gas, the rate of adiabatic heating during compression is

$$\left(\frac{dT}{dt}\right)_{compr} = 2\gamma\, b\, T_o (1 + bt)^{2\gamma - 1} \tag{14}$$

where T_o is the initial temperature of the plasma ($\approx 10^6$ K) and γ is the ratio of specific heats and will be taken to be equal to 5/3 in our case.

The plasma in the filament also loses heat by thermal conduction along the magnetic flux tube. Heat flows from the compressed hot plasma through the end faces of the flux tube to the cooler regions where the prominence loop is anchored. The rate of this cooling is given by (Shklovsky, 1965)

$$\left(\frac{dT}{dt}\right)_{cond} = \frac{10^{-6}}{k\ell^2}\ \frac{T^{5/2}(T - T_B)}{N} \tag{15}$$

where ℓ is the length of the prominence loop, k is the Boltzmann constant and T_B is the temperature at the base of the prominence loop and may be taken to be roughly equal to the photospheric temperature of about 6000 K.

The other sources of heat loss from the compressed plasma are the enhanced free-free, free-bound and bound-bound radiations. Assuming a hydrogen-helium plasma, the rates of cooling due to these processes may be written as (see Lüst and Zirin, 1960 for expressions of heat loss)

$$\left(\frac{dT}{dt}\right)_{ff} = \frac{1}{\frac{3}{2}Nk}\left[E_{ff}(\text{loss}) - E_{ff}(\text{gain})\right]$$

$$= \frac{1}{\frac{3}{2}Nk}\left[1.92\times10^{-27}\, N^2 T^{1/2} - 1.92\times10^{-27}\, n^2 T_o^{1/2}\right] \quad (16)$$

$$\left(\frac{dT}{dt}\right)_{fb+bb} = \frac{1}{\frac{3}{2}Nk}\left[E_{fb+bb}(\text{loss}) - E_{fb+bb}(\text{gain})\right]$$

$$= \frac{1}{\frac{3}{2}Nk}\left[1.26\times10^{-8}\,\frac{n^2}{T}\left(\frac{1}{2}kT + 1.08\times10^{-11}\right)\right. \quad (17)$$

$$\left. - 1.26\times10^{-8}\,\frac{n^2}{T_o}\left(\frac{1}{2}kT_o + 1.08\times10^{-11}\right)\right]$$

where E_{ff} and E_{fb+bb} are the rates in ergs per cm^3 per sec. In the above equations the second terms on the right hand sides represent the normal heat loss of the coronal plasma which must also be equal to the normal heat gain. The overall rate of change of temperature of the prominence plasma is now given by

$$\left(\frac{dT}{dt}\right) = \left(\frac{dT}{dt}\right)_{compr} - \left(\frac{dT}{dt}\right)_{cond} - \left(\frac{dT}{dt}\right)_{ff} - \left(\frac{dT}{dt}\right)_{fb+bb} \qquad (18)$$

In Figure I-1 we have plotted the change in temperature with time in the contracting filament for two different values of the initial gas density n. Our purpose here is to examine if the plasma in the filament will have cooled to sufficiently low temperatures by the time the compression has stopped, i.e. in a time of the order of τ_f or less. If $I_o = 10^{10}$ amp and $a = 10^8$ amp sec^{-1}, then $b = 10^{-2}$ sec^{-1}, corresponding to $\tau_f \approx 10^3$ sec. We find that whether we start with an initial density of 10^8 cm^{-3} or 10^9 cm^{-3}, the plasma cools within a time of the order of 10^3 sec. The temperature rises at first due to compressional heating, but falls off very steeply when the conductive cooling exceeds the compressional heating. In the case $n = 10^9$ cm^{-3}, the gas pressure at the peak temperatures becomes comparable with the magnetic pressure, but still does not exceed the latter substantially. This indicates that the gas pressure never builds up to high enough values during the compression to effectively counteract the compression.

It should be noted that although initially the cooling of the filamentary plasma is predominantly due to conduction, the cooling becomes predominantly radiative when the plasma has reached a temperature somewhat higher than 10^4 K. Hence the cooling phase preceding the appearance of $H\alpha$ is radiative. If the magnetic field

FIGURE I-1

Change in temperature with time of the contracting filamentary plasma. The temperature increases at first due to compressional heating, but decreases rapidly when heat loss due to thermal conduction along the filament exceeds the compressional heat gain.

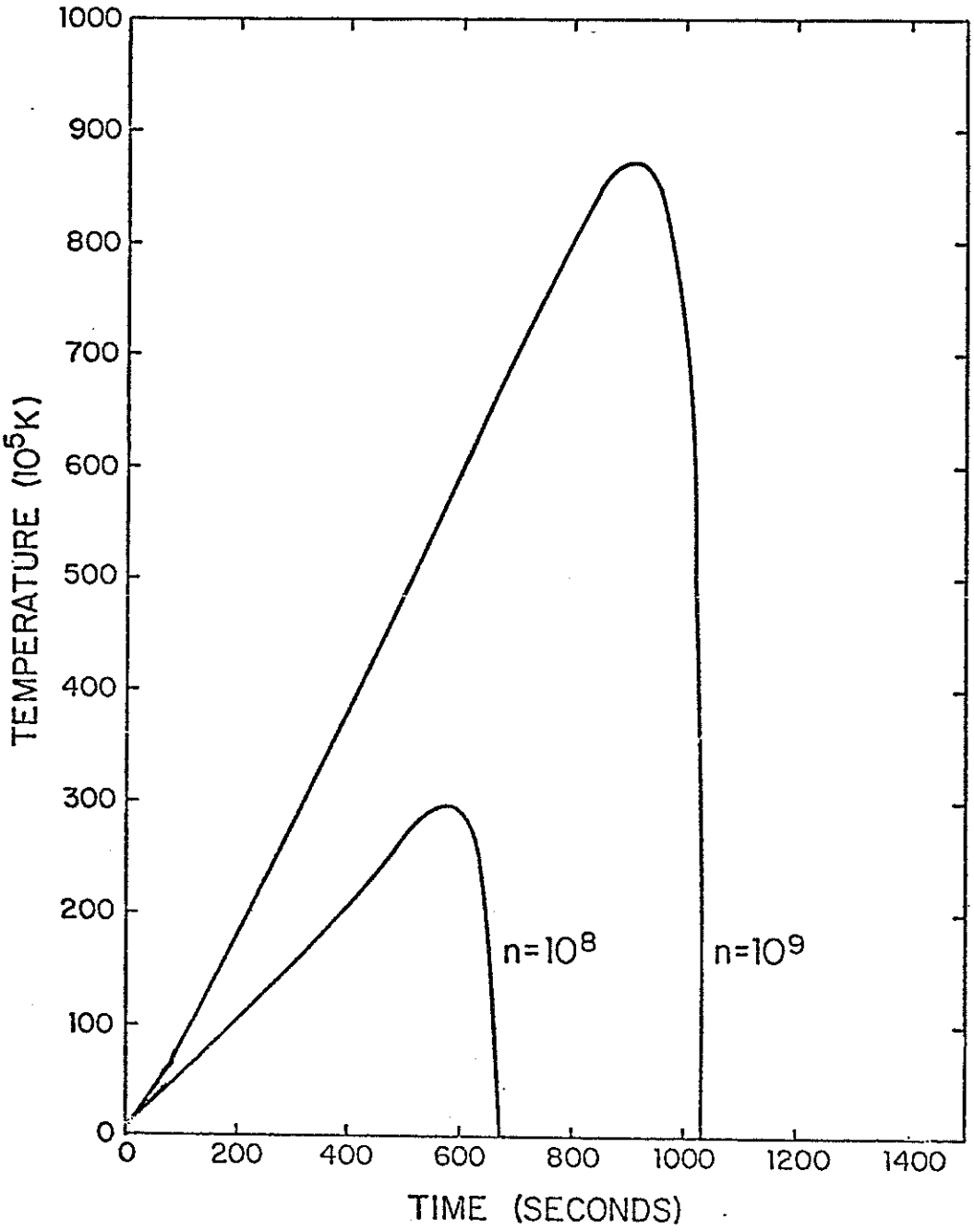
1000
900
800
700
600
500
400
300
200
100
0
TEMPERATURE (10^5K)
0
200
400
600
800
1000
1200
1400
TIME (SECONDS)
n=10^8
n=10^9

lines forming the filament are to some extent anchored in the photosphere, one would expect that the compression of the plasma would be slightly higher at the top of the loop than in the lower parts. If this is true, then the top of the loop, being the region of densest plasma, will cool faster than the rest of the loop and thus become visible in Hα first. This is one possible explanation of the observational fact that the loop becomes visible in Hα first at the top.

5. EQUILIBRIUM AT THE END OF COMPRESSION

The compression of the filamentary tube stops at the end of τ_f when the current I has reached a steady value. We shall not discuss in this thesis what determines this steady final value of the current. We have instead chosen a value of the order of 10^{11} amp on an empirical basis.

The thermal energy balance at the end of compression is determined by the fact that the heat loss from the compressed plasma is balanced by the heat gain from normal coronal energy sources. The temperature at the end of compression will become low enough so that a recombination of some of the plasma will take place. The recombination time is given by $\tau_{rec} \approx (N_e \alpha)^{-1}$ sec, where α is the recombination coefficient given by Allen (1963)

$$\alpha = 3 \times 10^{-10} T^{-3/4} \qquad (19)$$

At the end of compression $N_e \approx 10^{11}$ cm^{-3} and, if we take $T \approx 10^4 - 10^5$ K, we find that $\tau_{rec} \approx 30 - 180$ sec. Thus the plasma will recombine within a short time at the end of compression.

The equilibrium temperature at the end of compression should be given by the solution of the equation

$$E_{cond} + E_{ff}(\text{loss}) + E_{fb+bb}(\text{loss}) = E_{ff}(\text{gain}) + E_{ff+fb}(\text{gain}) \qquad (20)$$

where the density N in the expressions for the cooling rates as given by equations (16) and (17) must now be replaced by the electron density N_e, allowing for a recombination of the plasma. The total density N (ions plus neutrals) is related to N_e by the ionization equation. E_{cond} in equation (20) is equal to $3/2\ Nk\ (dT/dt)_{cond}$. Although not quite accurate, but perhaps an adequate description of the ionization in this case is given by Elwert's model (Elwert, 1952) of coronal ionization, which may be written for hydrogen as

$$\frac{N_e}{N - N_e} = 8.3 \times 10^5 \ \frac{kT}{\chi_H} \ \exp\left(-\frac{\chi_H}{kT}\right) \qquad (21)$$

where χ_H is the ionization potential of hydrogen. Since we know the value of N at the end of compression from equation (13), equation (21) gives us the value of N_e as a function of temperature. We shall not discuss here the ionization of a multicomponent plasma.

In the previous section we have not taken into account the energy loss through bound-bound radiation from heavy elements because the main source of heat loss at the temperatures involved was by far the thermal conduction. In determining the equilibrium temperature, however, we should include the line radiation from heavy elements, since the equilibrium temperature is presumably around 10^4 K and line radiation from heavy elements contribute substantially to the loss at these temperatures. Mendis (1968) has shown that at temperatures around 10^4 K, all such losses from a plasma with cosmic composition may be represented on an order-of-magnitude basis by the loss arising from excitation and deexcitation of the λ 3727 doublet line of O^+. The loss rate due to this source in ergs per cm^3 per sec may be written as

$$E_{O^+,bb} = 10^{-31} N_e^2 (T - 4000)^2, \quad T > 4000 \text{ K} \tag{22}$$

Finally, the equation determining the thermal equilibrium is given by

$$E_{cond} + E_{ff}(\text{loss}) + E_{fb+bb}(\text{loss}) + E_{O^+,bb}(\text{loss})$$

$$= E_{ff}(\text{gain}) + E_{fb+bb}(\text{gain}) \tag{23}$$

Equations (21) and (23) are two simultaneous equations in N_e and T. Solving them we find that if $n = 10^9$ cm^{-3} and hence $N = 1.2 \times 10^{11}$ cm^{-3}, then $T \approx 9000 - 9500$ K and $N_e \approx 10^{-3} - 3 \times 10^{-3}$ N. If on the other hand $n = 10^8$ cm^{-3} and hence

$N = 1.2 \times 10^{10}$ cm^{-3}, we find again $T \approx 9000 - 9500$ K and $N_e \approx 10^{-3} - 3 \times 10^{-3} N$. These values are not very different from the observed values. Note that if there is a radial density gradient established in the filament, which is what we should expect, the density at the axis being the greatest, then the temperature and the degree of ionization may both be lower near the axis than those indicated above. Similarly, the temperature and the degree of ionization may both be higher near the edge of the loop than the values found above. Thus, it is possible that the edge of the loop $N_e \approx N$. This would explain this observed value of the electron density of about 10^{11} cm^{-3}.

6. MASS DOWNFLOW

When some of the plasma in the filament recombines at the end of compression, the neutral particles will start to fall freely toward the photosphere under the action of solar gravitation. The ionized component of the gas in the filament cannot confine the neutrals in the axial direction. Let H be the height of a prominence loop ($H \approx \frac{1}{2} \ell$), v_g the free-fall velocity and g the gravity at the solar surface ($\approx 2 \times 10^4$ cm sec^{-2}). Let us take $\frac{1}{2} H$ as a representative height in the loop. The neutral atoms initially at this height will flow through the end faces of the loop down into the photosphere at a rate $2N_o v_g \pi R^2 \approx 2N (gH)^{1/2} \pi R^2 \approx 10^{34} - 10^{35}$ proton masses per sec, where N_o is the density of neutrals and is approximately equal to the total density N when the degree of ionization is low. The above

values may be taken as an order-of-magnitude estimate of the expected downflow rate, and are found to be consistent with Orrall's value (see Section 2) of 10^{34} proton masses per sec.

The total amount of matter in the prominence loop at the end of compression is $\pi R^2 \ell N \approx 10^{38}$ proton masses. Thus, a downflow at the observed rate would cause all the prominence material to fall down to the photosphere in a time of the order of 10^4 sec. However, this cannot happen due to the following reason: As a density depletion in the filament takes place due to the downflow, the plasma becomes hotter and hence the degree of ionization increases. The consequent decrease in the number of neutrals causes a decrease in the downflow rate. Thus we expect to observe the downflow during a part of the total lifetime beginning from the time of formation of the loop. This is consistent with the observational fact that the downflow takes place during a period of time short compared to the total lifetime.

Finally, we note that earlier observations by Kleczek (1963) and Jefferies and Orrall (1965b) indicate a total mass downflow from loop prominence systems of the order of 10^{15} - 10^{16} gm. We have found above that a single loop contains about 10^{38} proton masses or about 10^{14} gm. Thus a loop system containing several loops may contain a total mass of the order of 10^{15} gm. However, an amount of mass much higher than this seems unlikely on the basis of our model. Hence, although our model is not in conflict with the observations of

Kleczek and Jefferies and Orrall, the agreement remains somewhat unsatisfactory. A model which satisfactorily explains these mass requirements in loop prominences has been proposed by Jefferies and Orrall (1965b).

7. LIFETIME OF A PROMINENCE LOOP

One can think of a number of processes which may cause the filament to slowly "dissolve" once it has formed. We suggest two such processes here. When the plasma recombines, the conductivity in the filament decreases. This will cause the compressed axial magnetic flux to diffuse out of the filament. This diffusion of magnetic flux is similar to that in a magnetic pinch where a time-scale for the e-folding decay of the magnetic field is given by (see Glasstone and Lovberg, 1960)

$$\tau_{decay} \approx 2 \times 10^{-9} \frac{R^2}{\eta} \text{ sec} \tag{24}$$

where η is the resistivity of the medium in ohm-cm. The resistivity of a partially ionized gas may be written as

$$\eta = \frac{m_e v_e}{e^2} \sigma \left(\frac{N_o}{N_e} \right) \tag{25}$$

where m_e, v_e and e are the electronic mass, velocity and charge respectively and σ is effective cross-section for collision of electrons with the neutrals and is about 6×10^{-15} cm^2 (Kolesnikov and

Obukhov-Denisov, 1962). With the conditions in the filament we find $\tau_{decay} \approx 10^6 - 10^7$ sec, which is rather large compared to the observed lifetime of the loop prominences. However, this process may still be one of the factors contributing to the loss of a loop prominence.

Another process that may contribute to the loss of a loop prominence is the depletion of matter in the prominence either by the downflow or a radial outward diffusion of the neutrals. Such a depletion causes the prominence to heat up and merge with the corona. Since the prominence contains about 10^{38} proton masses, a downflow at the rate of 10^{34} proton masses per sec taking place during part of the lifetime would make the lifetime $\geq 10^4$ sec. The neutrals also diffuse radially out of the prominence due to the radial density gradient. They diffuse against a stationary background of a gas of ions and electrons. The time-scale for this diffusion is

$$\tau_D \approx \frac{R^2}{D} \tag{26}$$

where D is the diffusion coefficient which may be written as $D \approx \frac{1}{3} c \lambda_{ne}$, c being the average velocity of the neutrals and λ_{ne} the mean free path for collision between the neutrals and the ions or electrons. With $N_e \approx 10^{-3} N \approx 10^8$ cm^{-3} and $T \approx 10^4$ K, this time turns out to be of the order of 3×10^3 sec. However, since (a) the rate of diffusion would decrease with time due to decrease in density

gradient and (b) the electron density may be much higher near the edge of the loop, the lifetime due to this process may be much longer.

8. REMARKS

The model that we have suggested has been shown to be in approximate qualitative and quantitative agreement with observations. We should point out again that the idea of compression of a coronal plasma element to form a prominence is not new, although a specific mechanism for such a compression does not seem to have been suggested. We have attempted to suggest such a mechanism in this chapter. It is possible that the processes discussed here apply also to other types of filamentary structures in the solar atmosphere besides the loop prominences.

REFERENCES FOR I

Alfvén, H.: 1961, Arkiv. Fysik 19, 375.

Alfvén, H.: 1968, Ann. Geophys. 24, 341.

Allen, C. W.: 1963, Astrophysical Quantities, 2nd ed., Athlone Press, University of London, 90.

Beckers, J. M. and Schroter, E. H.: 1968, Solar Phys. 4, 142.

Bruzek, A.: 1964a, Ap. J. 140, 746.

Bruzek, A.: 1964b, J. Geophys. Res. 69, 2386.

Bruzek, A. and Kuperus, M.: 1972, Solar Phys. 24, 3.

Carlqvist, P.: 1969, Solar Phys. 7, 377.

Chandrasekhar, S.: 1956, Proc. Nat. Acad. Sci. (Washington) 42, 1.

Elwert, G.: 1952, Z. Naturforsch. 72, 432.

Glasstone, S. and Lovberg, R. H.: 1960, Controlled Thermonuclear Reactions, Van Nostrand, Princeton, New Jersey, 453.

Jefferies, J. T. and Orrall, F. Q.: 1965a, Ap. J. 141, 505.

Jefferies, J. T. and Or ll, F. Q.: 1965b, Ap. J. 141, 519.

Kleczek, J.: 1963, Joint AAS-NASA Symposium on Physics of Solar Flares, Washington, D.C., October, 1963.

Kolesnikov, V. N. and Obukhov-Denisov, V. V. : 1962, Zh. eksper. teor. Fiz. 42, 1001.

Lüst, R. and Zirin, H.: 1960, Zeitschr. f. Astrophys. 49, 8.

Mendis, D. A.: 1968, M. N. R. A. S. 140, 435.

Moreton, G. and Severny, A.: 1968, Solar Phys. 3, 282.

Murty, G. S.: 1962, Arkiv. Fysik 21, 203.

Schlüter, A.: 1957, Z. Naturforsch. 12a, 855.

Schklovsky, I. S.: 1965, Physics of the Solar Corona, 2nd ed., Addison-Wesley, Reading, Mass., 412.

Stenflo, J. O.: 1969, Solar Phys. 8, 115.

II. ELECTRIC POTENTIAL ON SOLID SPHERES IN A PLASMA

1. INTRODUCTION

A solid body immersed in a plasma is continually impacted on by ions and electrons. One normally assumes that the ions and electrons hitting the body stick to its surface. They may return to the plasma as neutral atoms, or in some cases the solid body may grow in size with time as a result of condensation of plasma on the surface. We shall assume here that the impinging electrons and the ions have the same probability of sticking to the surface. The analysis is easily modified to take into account the case where these probabilities are different but they have a fixed known ratio. Since the thermal velocity of the electrons is much higher than that of the ions, the electron flux to the surface initially far exceeds the ion flux. As a result there is an accumulation of electrons on the surface. The negative potential associated with these electrons provides an attractive force for the ions and a repulsive force for the electrons so that the ion flux increases and the electron flux decreases until an equilibrium is reached where these two fluxes are equal and the potential on the surface has a fixed negative value. This value has been calculated in the astrophysical context by Spitzer (1941, 1968), Wickramasinghe (1967) and others. In laboratory experiments dealing with electrical probes for measuring the physical conditions in a plasma, this potential has long been known as the floating potential. In many problems related to plasma-grain systems encountered in astrophysics as well as colloidal plasmas in

the laboratory it is useful to know the value of this potential.

In this chapter we shall evaluate the equilibrium potential on solid spheres immersed in a plasma following essentially the lines of early work of Langmuir on electrical probes (see e.g. Suits, 1961). We shall show that for a plasma of given density and temperature (i.e. given Debye shielding distance) there are three different domains of the radius of the sphere in which different approximations for the potential must be used. These domains may be characterized as (a) the thin sheath domain, where the radius $\underline{a}$ of the sphere is much larger compared to the thickness $\underline{s} - \underline{a}$ of the Debye sheath that forms around it ($\underline{s}$ = the radius of the Debye sheath), (b) the thick sheath domain, where $\underline{a}$ is much smaller than $\underline{s}$ and (c) the transition domain, where $\underline{a}$ is comparable to $\underline{s} - \underline{a}$. Finally, in each of these cases, for metallic spheres with radii in the submicron range, we shall discuss two effects which do not seem to have been included so far. These are: (1) the lowering of the potential barrier that an electron has to overcome in order to reach the surface of the sphere; this lowering results from the image force on the electron when it is close to the metal sphere. (2) From a semi-classical point of view, electrons having energies less than the maximum height of the barrier have a finite probability of arriving at the surface by tunnelling through the barrier. This last effect will be discussed and evaluated, but not included in our final calculation of the potential of the sphere. Finally,

we shall discuss the effects that set an upper limit to the potential for both metallic and dielectric spheres.

We shall assume throughout this chapter that within the Debye sheath of a given sphere, there are not enough spheres so as to effectively screen the sphere in question from the influx of plasma.

2. THE ELECTRIC POTENTIAL ON A SPHERE

We shall consider a sphere of radius a immersed in a fully ionized plasma where the atoms are singly ionized. The analysis given here is easily generalized for a partially ionized plasma or a plasma containing multiply ionized atoms, if the degree of ionization is known. We shall not consider any processes of emission of electrons from the sphere (other than field emission from metal spheres), but such processes will be discussed briefly in Section 8.

Let ϕ_a be the steady electric potential developed on the sphere. The radius s of the plasma sheath around the sphere is approximately given by

$$s \approx a + \lambda_D = a + 6.9 \left(\frac{T}{N}\right)^{1/2} \tag{1}$$

where λ_D is the Debye shielding distance, N is the electron density and T is the plasma temperature (assumed same for electrons and ions) in C.G.S. units. Leg q_α be the charge of a plasma particle (= -e for electrons and e for ions) and m_α be its mass (= m_e for

electrons and m_i for ions). If u and v are the radial and tangential components of the particle velocity, and the subscripts a and s refer to their values at the surface of the sphere and at the sheath boundary respectively, then for a particle that crosses the sheath and arrives at the surface, the laws of conservation of energy and angular momentum requires

$$\frac{1}{2} m_\alpha u_s^2 + \frac{1}{2} m_\alpha v_s^2 = \frac{1}{2} m_\alpha u_a^2 + \frac{1}{2} m_\alpha v_a^2 + q_\alpha \phi_a \qquad (2)$$

and

$$s v_s = a v_a \qquad (3)$$

For a particle which is barely able to arrive at the surface, we put $u_a = 0$ and find from the above two equations a value $V_{s\alpha}$ of v_s given by

$$V_{s\alpha}^2 = \frac{a^2}{s^2 - a^2} \left(u_s^2 - \frac{2 q_\alpha \phi_a}{m_\alpha} \right) \qquad (4)$$

Clearly, the particles for which v_s exceeds $V_{s\alpha}$ cannot arrive at the surface. Let us assume that at the sheath boundary the electrons and ions have Maxwellian velocity distribution. In our spherical coordinate system this distribution is given by

$$n_\alpha(u, v)\, du\, dv = 2\pi N \left(\frac{m_\alpha}{2\pi kT} \right)^{3/2} \exp\left[- \frac{m_\alpha}{2kT} (u^2 + v^2) \right] v\, du\, dv \qquad (5)$$

and hence the total flux of ions and electrons to the surface is given by

$$\Gamma_i = 4\pi s^2 \int_0^{\infty} \int_0^{V_{si}} n_i(u_s, v_s)\, u_s\, dv_s\, du_s \tag{6}$$

and

$$\Gamma_e = 4\pi s^2 \int_{U_{se}}^{\infty} \int_0^{V_{se}} n_e(u_s, v_s) u_s\, dv_s\, du_s \tag{7}$$

where U_{se} is the lowest radial electron velocity for which it can overcome the repulsive force due to the negative potential on the surface and is given by

$$\frac{1}{2} m_e U_{se}^2 = -e\phi_a \tag{8}$$

Evaluation of the above integrals give

$$\Gamma_i = 4\pi s^2 N \left(\frac{kT}{2\pi m_i}\right)^{1/2} \left\{1 - \frac{s^2 - a^2}{s^2} \exp\left[\frac{a^2}{s^2 - a^2} \frac{e\phi_a}{kT}\right]\right\} \tag{9}$$

$$\Gamma_e = 4\pi a^2 N \left(\frac{kT}{2\pi m_e}\right)^{1/2} \exp\left[\frac{e\phi_a}{kT}\right] \tag{10}$$

The potential ϕ_a is now given by the condition

$$\Gamma_i = \Gamma_e \tag{11}$$

or

$$\exp\left[\frac{e\phi_a}{kT}\right] = \left(\frac{m_e}{m_i}\right)^{1/2} \left(\frac{s}{a}\right)^2 \left\{1 - \frac{s^2 - a^2}{s^2} \exp\left[\frac{a^2}{s^2 - a^2} \frac{e\phi_a}{kT}\right]\right\} \tag{12}$$

If the electrons and the ions in the plasma have different temperatures T_e and T_i, then it is easily shown that the above result becomes

$$\exp\left[\frac{e\phi_a}{kT_e}\right] = \left(\frac{m_e T_i}{m_i T_e}\right)^{1/2} \left(\frac{s}{a}\right)^2 \left\{1 - \frac{s^2 - a^2}{s^2} \exp\left[\frac{a^2}{s^2 - a^2} \frac{e\phi_a}{kT_i}\right]\right\} \quad (13)$$

However we shall not discuss this case any further. We now observe the following two limiting cases of equation (12):

The thin sheath domain: If the conditions in the plasma are such that the sheath thickness $s - a$ is much smaller than the radius a of the sphere, then, since ϕ_a is negative, equation (12) reduces to

$$\exp \frac{e\phi_a}{kT} = \left(\frac{m_e}{m_i}\right)^{1/2} \quad (14)$$

For a fully ionized hydrogen plasma, this result becomes

$$\frac{e\phi_a}{kT} = -\frac{1}{2} \ln\left(\frac{m_i}{m_e}\right) \approx -3.76 \quad (15)$$

Note that for the plasma in the sheath, the surface of the sphere in this case behaves like a plane wall. Hence the result in equation (14) is the same as that for the potential on an infinite wall in contact with a plasma. In Figure II-1 we have plotted the potential as a function of the plasma temperature for the case of the hydrogen plasma.

FIGURE II-1

The potential of solid spheres in a hydrogen plasma as a function of the plasma temperature. The thick curve at the bottom corresponds to the thick sheath case with no image force [equation (16)], and the thin curves immediately above it correspond to the thick sheath case including the effect of image force [equation (38)] for various values of the radius of the sphere. The thick curve at the top is for the thin sheath case with no image force [equation (14)] and the thin curves above it are for the same case including the image force [equation (37)]. The thick curve in the middle is for an intermediate case [equation (12)] where the sheath thickness $\underline{s} - \underline{a}$ equals the radius $\underline{a}$ of the sphere. Note that the thick curves apply to both metallic and dielectric spheres while the thin curves apply only to metallic spheres. The results presented in this figure are subject to the constraint discussed in Section 7.

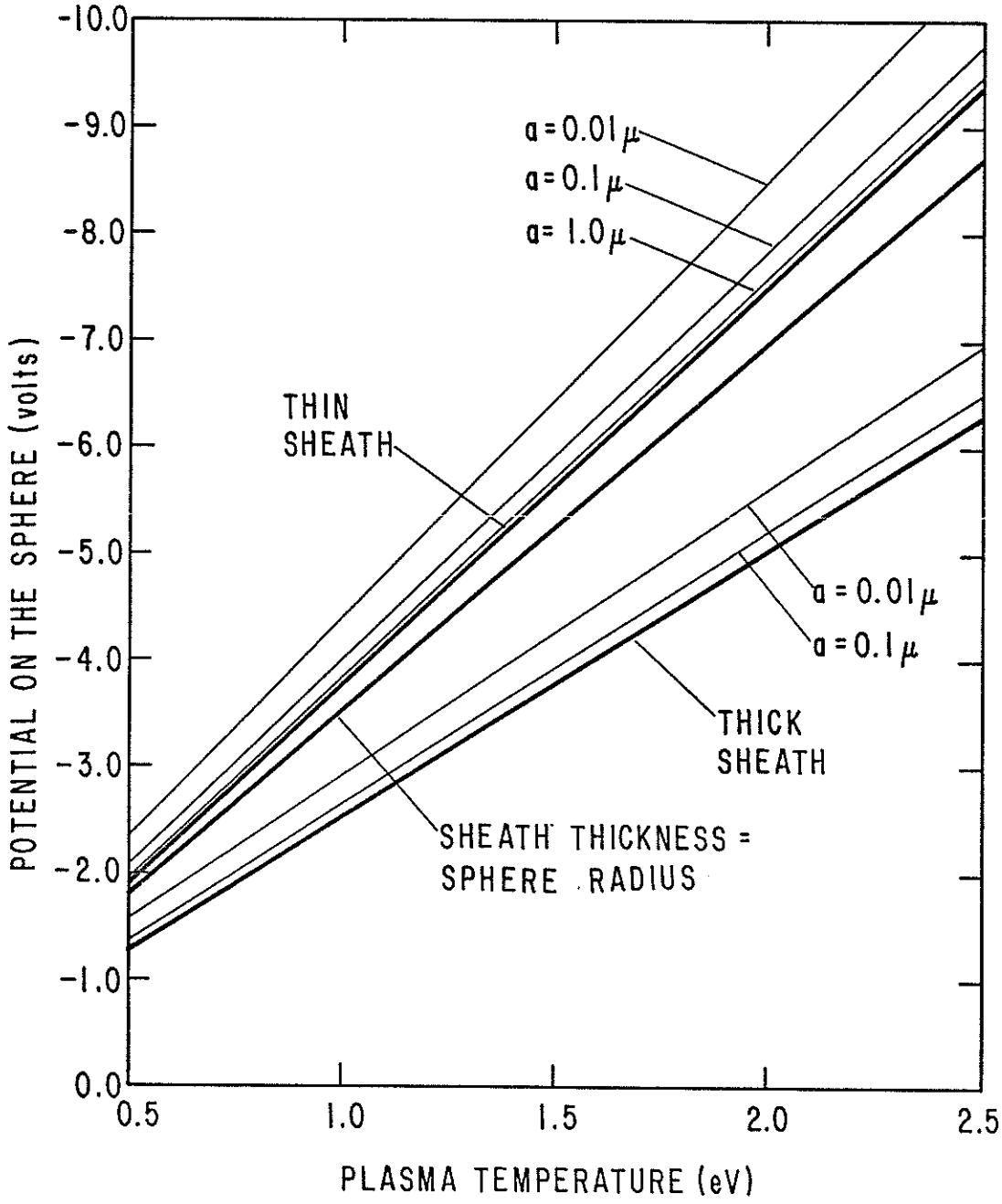
-10.0
-9.0
-8.0
-7.0
-6.0
-5.0
-4.0
-3.0
-2.0
-1.0
0.0
0.5
1.0
1.5
2.0
2.5
POTENTIAL ON THE SPHERE (volts)
PLASMA TEMPERATURE (eV)
a = 0.01 μ
a = 0.1 μ
a = 1.0 μ
THIN SHEATH
a = 0.01 μ
a = 0.1 μ
THICK SHEATH
SHEATH THICKNESS = SPHERE RADIUS

The thick sheath domain: On the other extreme if the conditions in the plasma are such that the sheath radius s is very large compared to the sphere radius a, then equation (12) reduces to

$$\exp\left[\frac{e\phi_a}{kT}\right] = \left(\frac{m_e}{m_i}\right)^{1/2}\left[1 - \frac{e\phi_a}{kT}\right] \tag{16}$$

which for a fully ionized hydrogen plasma becomes

$$\frac{e\phi_a}{kT} \approx -2.51 \tag{17}$$

This result is the same as that derived by Spitzer (1941, 1968) in the astrophysical context and probably applies to most situations of astrophysical interest, e.g. micron size grains in the tenuous interstellar plasma. In Figure II-1 we have also plotted equation (17).

The transition domain: In the cases where s is comparable to a however, we must use equation (12) without making any approximations. In Figure II-1 we have plotted a particular case where $s = 2a$.

3. THE EFFECT OF PLASMA DRIFT

One important effect often not included in the discussion of the potential on solid surfaces in contact with a plasma is the following: Since the plasma particles neutralize on the solid surface, this surface is in effect a sink for the plasma. This means that there is a net drift of the plasma towards the surface. We shall discuss this

effect only for the case of the plane wall, i.e. the thin sheath case.

From equation (9) we find that in the thin sheath case with $\underline{s} \approx \underline{a}$ the flux of the ions to the surface per unit area is given by

$$\gamma_i = N_a \left(\frac{kT}{2\pi m_i}\right)^{1/2} \tag{18}$$

where N_a is the value of N at the surface, for which a Boltzmann distribution must now be used, i.e.

$$N_a = N \exp\left[-\frac{e\phi_a}{kT}\right] \tag{19}$$

If the plasma has a net drift velocity u_D to the surface, then at a large distance from the surface the flux of ions towards the surface is $N u_D$. This must equal γ_i to a first approximation. Hence we can get an estimate of u_D:

$$u_D \approx \left(\frac{kT}{2\pi m_i}\right)^{1/2} \exp\left[-\frac{e\phi_a}{kT}\right] \tag{20}$$

The flux γ_{iD} of the ions including the effect of the drift may now be found by integrating from 0 to ∞ a one-dimensional Maxwellian distribution in u drifting with a velocity u_D. This gives

$$\gamma_{iD} = N\left(\frac{kT}{2\pi m_i}\right)^{1/2} \left[\exp(-X^2) + \pi^{1/2} X \{1 + \mathrm{erf}(X)\}\right] \tag{21}$$

where

$$X^2 = \frac{m_i u_D^2}{2kT} \quad .$$

On the other hand, electrons with insufficient velocity are repelled by the surface and hence the electron flux in this case is still given by equation (10), so that

$$\gamma_{eD} = N \left(\frac{kT}{2\pi m_e} \right)^{1/2} \exp \left[\frac{e\phi_a}{kT} \right] \tag{22}$$

Equating γ_{iD} and γ_{eD} and inserting the value of X, we find that the surface potential is now given by

$$\frac{e\phi_a}{kT} \approx -\frac{1}{4} \ln \left(\frac{m_i}{m_e} \right) \tag{23}$$

which is half the value found in equation (14). In the case of a hydrogen plasma, this relation becomes

$$\frac{e\phi_a}{kT} \approx -1.88 \tag{24}$$

A similar change in the potential will also result in the thick sheath case. Hence when the effect of the drift is included, the potential on the surface is substantially lowered. The results of the preceding section therefore represent an upper limit.

4. SUBMICRON SIZE METAL SPHERES: THE EFFECT OF IMAGE FORCE

If the sphere has charge -Ze on it, then in a spherical coordinate system with origin at the center of the sphere, the potential energy of an electron at points exterior to the sphere is given by

$$-e\Phi_r = \frac{Ze^2}{r} \tag{25}$$

This potential is shown by the dotted curve in Figure II-2(a).

An electron near the sphere is also attracted towards it due to its own image in the sphere. The corresponding potential energy is

$$e\Phi_i = -\frac{e^2a}{2(r^2 - a^2)} + \frac{e^2a}{2r^2} \tag{26}$$

This is shown by the broken line in Figure II-2(a). The full line in this figure shows the sum of these two energies:

$$-e\Phi = \frac{Ze^2}{r} - \frac{e^2a}{2(r^2 - a^2)} + \frac{e^2a}{2r^2} \tag{27}$$

This curve therefore gives us the potential barrier that an electron would have either to surmount or to tunnel through in order to reach the surface of the sphere. It is not necessary for our discussion to match the curve to a specific value at the surface of the sphere.

The position r_m of the barrier maxima (Figure II-2(b)) is given

FIGURE II-2

The potential barrier. (a) Dotted curve: Potential energy of an electron near a sphere of radius $\underline{a}$ due to a charge - Ze on the sphere. Broken curve: Potential energy of an electron near a metal sphere due to its own image force. Solid curve: The net potential energy of an electron near a metal sphere - the "potential hill."

(b) An electron tunnelling through the potential hill crosses the potential energy curve at two points r_1 and r_2 which are the two positive real roots of equation (30).

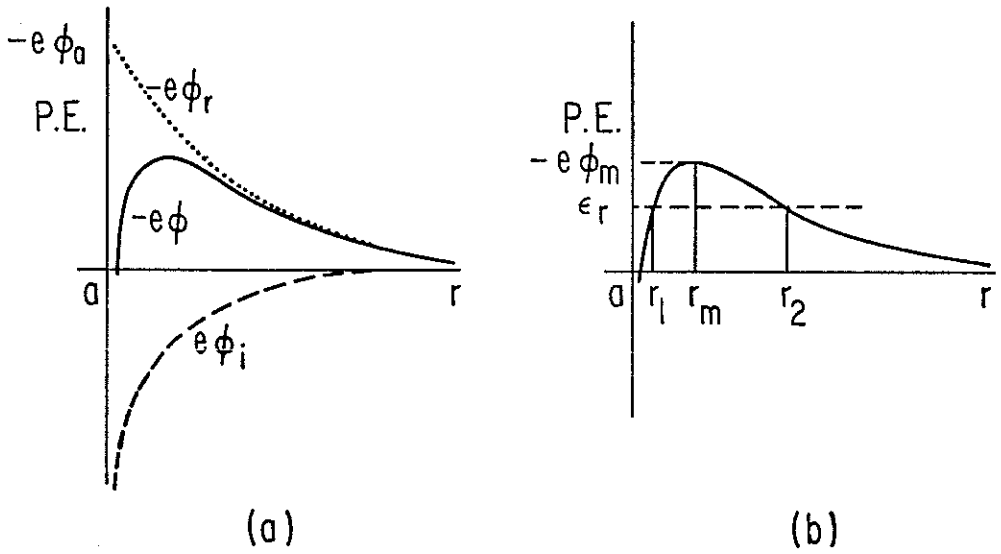
−e φa
P.E.
−eφr
−eφ
a
r
eφi
(a)
P.E.
− e φm
εr
a
r1
rm
r2
r
(b)

by the solution of the equation $d\Phi/dr = 0$. This equation can be solved numerically to get values of r_m for different values of Z. However, for our purpose it is very convenient to have an analytical expression for r_m as a function of Z. Such an expression was found by guessing and trial as

$$r_m = a\left[1 - \frac{0.17}{Z^{1/2}}\right]\left(\frac{1}{2Z}\right)^{1/2}\left[1 + (1 + 2Z)^{1/2}\right] \tag{28}$$

In Figure II-3 this analytical solution is found to be indistinguishable from the numerical solution. The agreement continues to be good for large values of Z. Note that equation (28) has the correct behavior in that r_m approaches $\underline{a}$ for very large values of Z. The energy $-e\Phi_m$ of the barrier maxima is now given by

$$-e\Phi_m = \frac{Ze^2}{r_m} - \frac{e^2a}{2(r_m^2 - a^2)} + \frac{e^2a}{2r_m^2} \tag{29}$$

If u is the radial component of the electron velocity, an electron with radial kinetic energy $\epsilon_r = \frac{1}{2} m_e u^2$ less than $-e\Phi_m$ may reach the surface by tunneling through the barrier, crossing the barrier at the two turning points r_1 and r_2 (Figure II-2(b)) which are the two real roots of the fourth degree equation

$$\frac{Ze^2}{r} - \frac{e^2a}{2(r^2 - a^2)} + \frac{e^2a}{2r^2} - \epsilon_r = 0 \tag{30}$$

FIGURE II-3

The position r_m of the maxima of the potential hill as a function of the number of electrons Z on the surface of the sphere. The solid curve represents the approximate solution [equation (28)]. The circles represent numerical solutions.

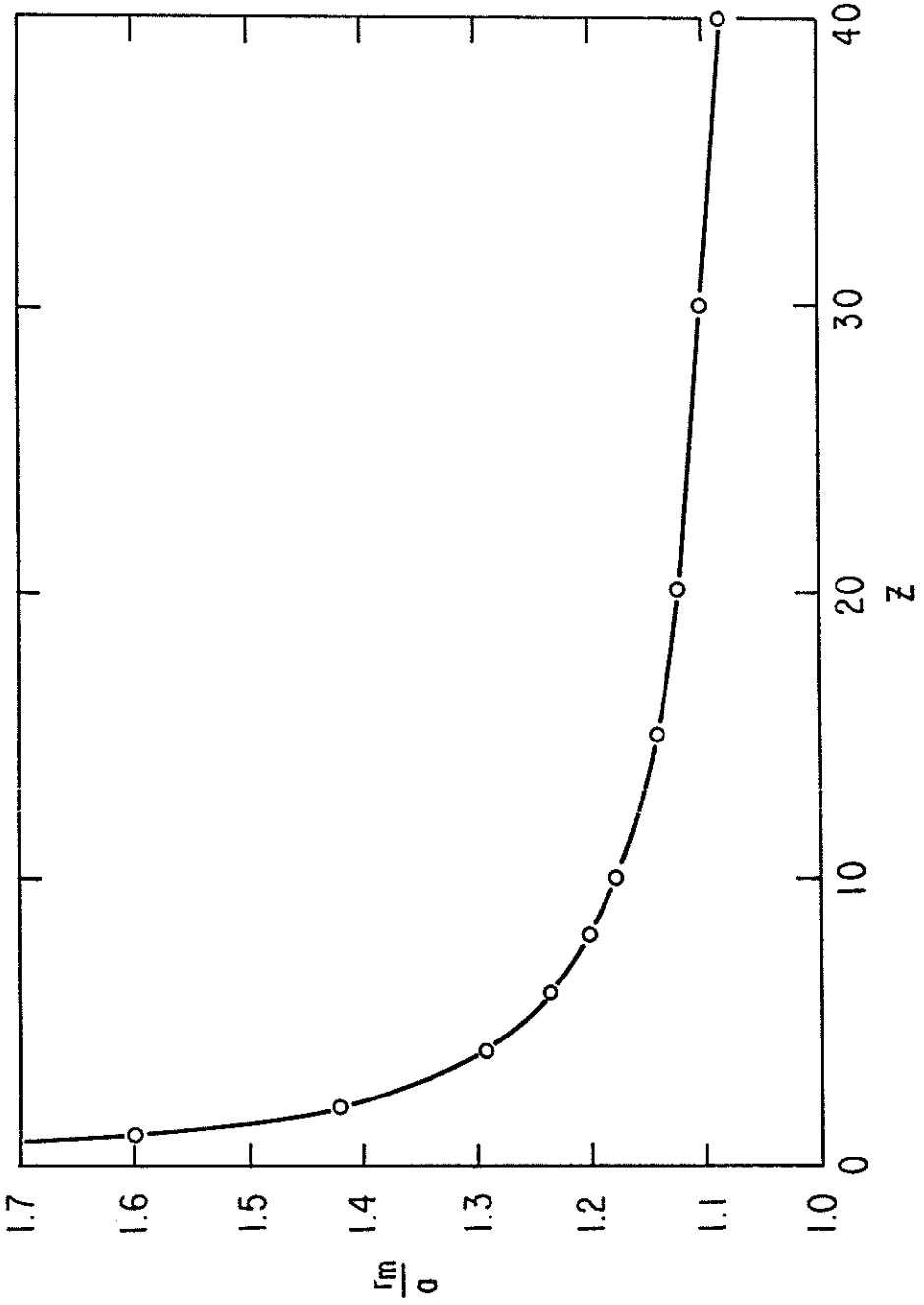
1.7
1.6
1.5
1.4
1.3
1.2
1.1
1.0
$\frac{r_m}{a}$
0
10
20
30
40
z

For an electron with $\epsilon_r > -e\phi_m$, these two real roots r_1 and r_2 go unambiguously to two complex roots. Since equation (30) is a real function, these two roots are complex conjugates. The root with positive imaginary part will be called r_1 in this case, and the root with negative imaginary part will be called r_2.

Referring to Figure II-2, we can divide the entire electron radial energy spectrum into three regions: Region I for $\epsilon_r > -e\phi_a$, Region II for $-e\phi_m \leq \epsilon_r \leq -e\phi_a$ and Region III for $0 \leq \epsilon_r < -e\phi_m$. We shall treat below Region I as classical and Regions II and III as semi-classical. Then the probability of arrival at the surface (the transmission coefficient) of an electron in Region II is (see Kemble, 1958)

$$P_{II}(u) = P_{II}(\epsilon_r) = \frac{1}{1 + \exp(-M)} \tag{31}$$

and that of an electron in Region III is

$$P_{III}(u) = P_{III}(\epsilon_r) = \frac{1}{1 + \exp M} \tag{32}$$

where

$$M = \int_{r_1}^{r_2} \left[\frac{8m_e}{\hbar^2}\left(\frac{Ze^2}{r} - \frac{e^2a}{2(r^2 - a^2)} + \frac{e^2a}{2r^2} - \epsilon_r\right)\right]^{1/2} dr \tag{33}$$

where m_e is the electron mass and $\hbar = h/2\pi$, h being the Planck's constant.

The probabilities given by equations (31) and (32) connect continuously at $\varepsilon_r = -e\phi_m$ with a value of 0.5. Figure II-4 shows this probability as a function of electron energy ε_r for two different sphere radii, 0.01 and 0.1 micron, and in each case for three different values of the surface potential Φ_a. Note that the tunnelling effect of electrons is very pronounced in the case of the smaller sphere.

5. THE SEMI-CLASSICAL CASE

If we want to include in our calculation of the surface potential ϕ_a the rounding effect of the image force from a semi-classical point of view, then we can again use equation (11) except that the electron flux Γ_e is now modified as follows

$$\Gamma_e = 4\pi s^2 \int_0^{\infty} \int_0^{V_{se}} n_e(u_s, v_s)\, u_s\, P(u_s)\, du_s\, dv_s \qquad (34)$$

where $P(u_s)$ is such that

$$P(u_s) = 1 \quad , \quad -\frac{2e\phi_a}{m_e} < u_s^2 \leq \infty$$

$$= P_{II}(u_s) \quad , \quad -\frac{2e\phi_m}{m_e} \leq u_s^2 \leq -\frac{2e\phi_a}{m_e}$$

$$= P_{III}(u_s) \quad , \quad 0 \leq u_s^2 < -\frac{2e\phi_m}{m_e}$$

FIGURE II-4

The transmission coefficient $P(\epsilon_r)$ of an electron as a function of ϵ_r for two different radii of the sphere: 0.01 μ and 0.1 μ. The horizontal axis, when multiplied by the factor f, gives the value of ϵ_r corresponding to any particular curve. The full horizontal scale then gives the value ϕ_a of the potential on the sphere. The value $-e\phi_m$ of the maxima of the potential hill corresponds to $P(\epsilon_r) = 0.5$.

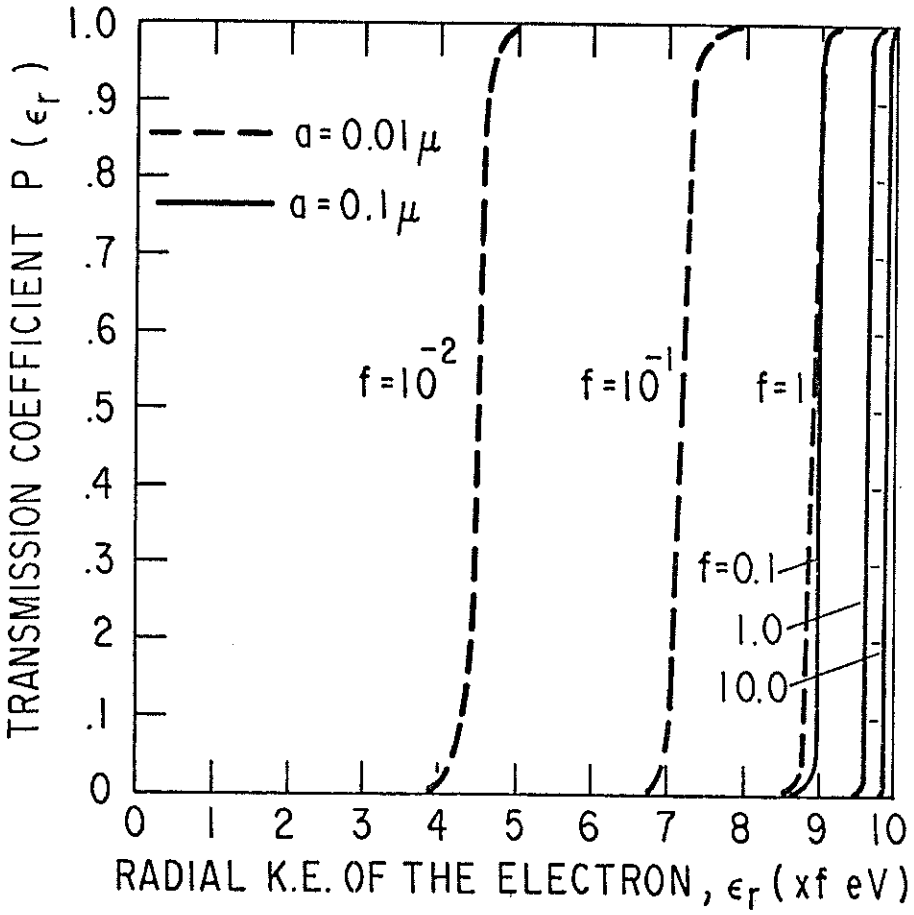
TRANSMISSION COEFFICIENT P (ε_r)
1.0
.9
.8
.7
.6
.5
.4
.3
.2
.1
0
a = 0.01 μ
a = 0.1 μ
f = 10^-2
f = 10^-1
f = 1
f = 0.1
1.0
10.0
0 1 2 3 4 5 6 7 8 9 10
RADIAL K.E. OF THE ELECTRON, ε_r (xf eV)

With this modification, equation (11) can be solved by using numerical techniques. However, the flux of electrons tunnelling through the barrier is very small, as is evident from Figure II-4 and hence the tunnelling effect is probably only of theoretical interest. In any case, it is unimportant for micron or larger size spheres.

6. LOWERING OF BARRIER BY IMAGE FORCE

The classical effect of the image force of lowering the energy barrier for incoming electrons from $-e\phi_a$ to $-e\phi_m$ is easily included in our analysis by replacing equation (8) by

$$\frac{1}{2} m_e U_{se}^2 = -e\phi_m \tag{35}$$

so that equation (12) for the surface potential ϕ_a now becomes

$$\exp\left[\frac{e\phi_m}{kT}\right] = \left(\frac{m_e}{m_i}\right)^{1/2} \left(\frac{s}{a}\right)^2 \left\{1 - \frac{s^2 - a^2}{s^2} \exp\left[\frac{a^2}{s^2 - a^2} \frac{e\phi_a}{kT}\right]\right\} \tag{36}$$

where the relationship between ϕ_m and ϕ_a is given by equations (28), (29) and the relation $\phi_a = -Ze/a$. Equation (14) for the thin sheath case now becomes

$$\exp\left[\frac{e\phi_m}{kT}\right] = \left(\frac{m_e}{m_i}\right)^{1/2} \tag{37}$$

and equation (16) for the thick sheath case becomes

$$\exp\left[\frac{e\phi_m}{kT}\right] = \left(\frac{m_e}{m_i}\right)^{1/2}\left[1 - \frac{e\phi_a}{kT}\right] \tag{38}$$

In Figure II-1 we have presented some results for the potential of the sphere as a function of plasma temperature including the image effect, for both the thin and thick sheath limits. When the image effect is included, the potential becomes a function of the radius of the sphere and the effect is unimportant for radii larger than $a = 1\mu$. In the thin sheath case, an additional condition for the image effect to be operative is that $\underline{s}$ must be larger than r_m. Note that since the image force permits a larger electron flux to the surface, the potential becomes larger when this effect is included.

In Figure II-5 we have plotted the potential on a sphere as a function of the ration s/a with $s = 1$ m. This figure shows the various domains of the quantity s/a in which different approximations for the potential should be used.

7. LIMITATION OF THE POTENTIAL

Our discussion so far indicates that the potential on a solid sphere in a plasma increases monotonically with increasing plasma temperature. However, this increase cannot take place indefinitely. In the case of dielectric spheres, a limit to the potential is set by either the dielectric breakdown phenomenon or a rupture of the sphere due to electrical forces, whichever occurs at a lower potential. If

FIGURE II-5

The potential of solid spheres in a hydrogen plasma as a function of the sphere radius in units of $\underline{s}$, the radius of the Debye sheath which has been taken to be 1 m.

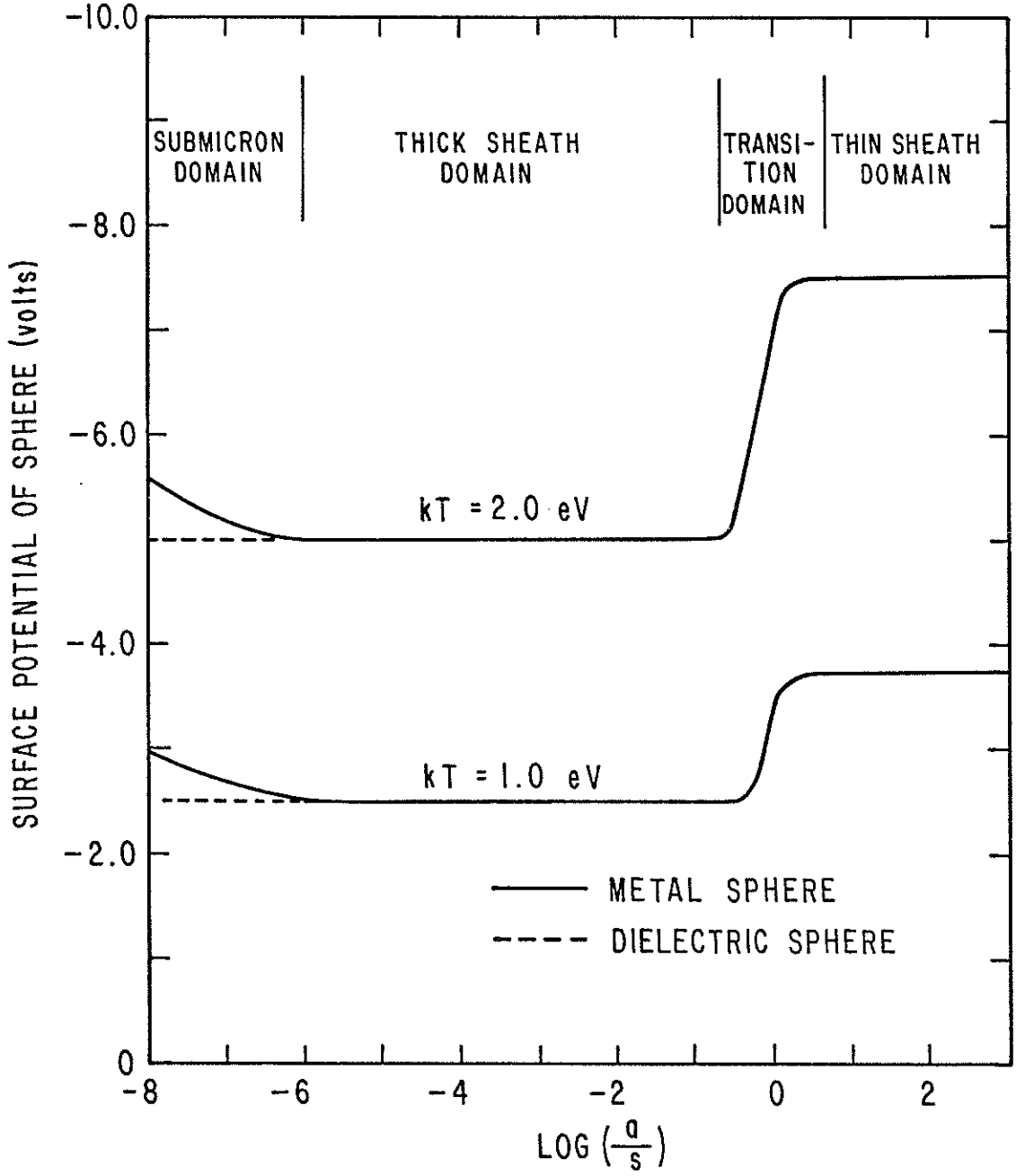
-10.0
-8.0
-6.0
-4.0
-2.0
0
SUBMICRON DOMAIN
THICK SHEATH DOMAIN
TRANSI-TION DOMAIN
THIN SHEATH DOMAIN
kT = 2.0 eV
kT = 1.0 eV
METAL SPHERE
DIELECTRIC SPHERE
SURFACE POTENTIAL OF SPHERE (volts)
-8
-6
-4
-2
0
2
LOG (a/s)

E_B is the breakdown electric field for the material of the sphere, then the maximum potential that the sphere can sustain is

$$\phi_a(\max) \approx a E_B \tag{39}$$

The criterion for rupture is hard to establish, but we can obtain a crude estimate in the following way. There is a uniform pressure $p = \phi_a^2/4\pi a^2$ over the surface of the sphere due to electrical forces. This pressure induces a tensile stress p throughout the body of the sphere. The criterion for a rupture of the sphere to occur is that p must exceed the tensile strength p_t of the material of the sphere. From this consideration, the maximum potential that the sphere can sustain without breaking up is given by

$$\phi_a(\max) \approx 600\, a(\pi p_t)^{1/2} \tag{40}$$

where ϕ_a is in volts and a and p_t are in C.G.S. units. As an example, for glass $\phi_a(\max)$ is about $1.3 \times 10^3\, a_\mu$ volts according to equation (39) and about $3 \times 10^3\, a_\mu$ volts according to equation (40), where a_μ is the radius of the sphere in microns.

For metal spheres, however, the limit is set by the field emission of electrons under the influence of the electric field

$$E = \frac{\phi_a}{a} \tag{41}$$

The flux of field-emitted electrons from a metal surface is given by

the Fowler-Nordheim equation (see e.g. Gomer, 1961)

$$\Gamma_{fem} = 4\pi a^2 \frac{(\beta/w)^{1/2}}{\xi^2(\beta + w)} E^2 \exp\left[58.9 - 6.8 \times 10^7 \, w^{3/2} \frac{\xi}{E}\right] \tag{42}$$

$$\xi = (1 - y)^{1/2}$$

$$y = 3.8 \times 10^{-4} E^{1/2}/w$$

and β and w are the Fermi energy and the work function for the metal in eV and E is in volts per cm. The Fowler-Nordheim equation includes the effect of the image force on the emitted electron. The steady potential on the sphere including the effect of field emission is given by the equation

$$\Gamma_i = \Gamma_e - \Gamma_{fem}/\chi \tag{43}$$

where χ is the sticking probability of electrons and ions and Γ_i and Γ_e are given by equations (9) and (10). Note that unlike the solution of equation (11), the solution of equation (43) depends on the value of N, the density of the ions or the electrons.

In Figure II-6 we have plotted the solution of equation (43) for a sphere of radius 0.01 μ and β = 11.6 eV and w = 3.0 (values for aluminum) for the thin sheath case, assuming χ = 1. Obviously, the effect of field emission is to put an upper limit to the potential on the sphere. This figure also shows the dependence of the solution on the plasma density N. To find the upper limit of the potential for a sphere of a different size, we have simply to multiply the upper limit shown in Figure II-6

FIGURE II-6

Limitation of potential due to field emission of electrons. The broken line represents the potential for the thin sheath case without including the effect of field emission [equation (14)] in the case of hydrogen plasma. The solid lines represent this potential in the same case including the effect of field emission [equation (43)] for a sphere of radius 0.01 μ and for various plasma densities N, assuming the sticking probability χ of the ions and the electrons to be equal to 1. However, note that the result for $N = 10^{10}$ and $\chi = 1$ for instance is the same as the result for $N = 10^{15}$ and $\chi = 10^{-5}$. This gives us an idea of the dependence of the result on χ. Note also that since the potential on dielectric spheres under similar conditions is given by the broken line, the potentials of metal and dielectric spheres in the same plasma may be very different.

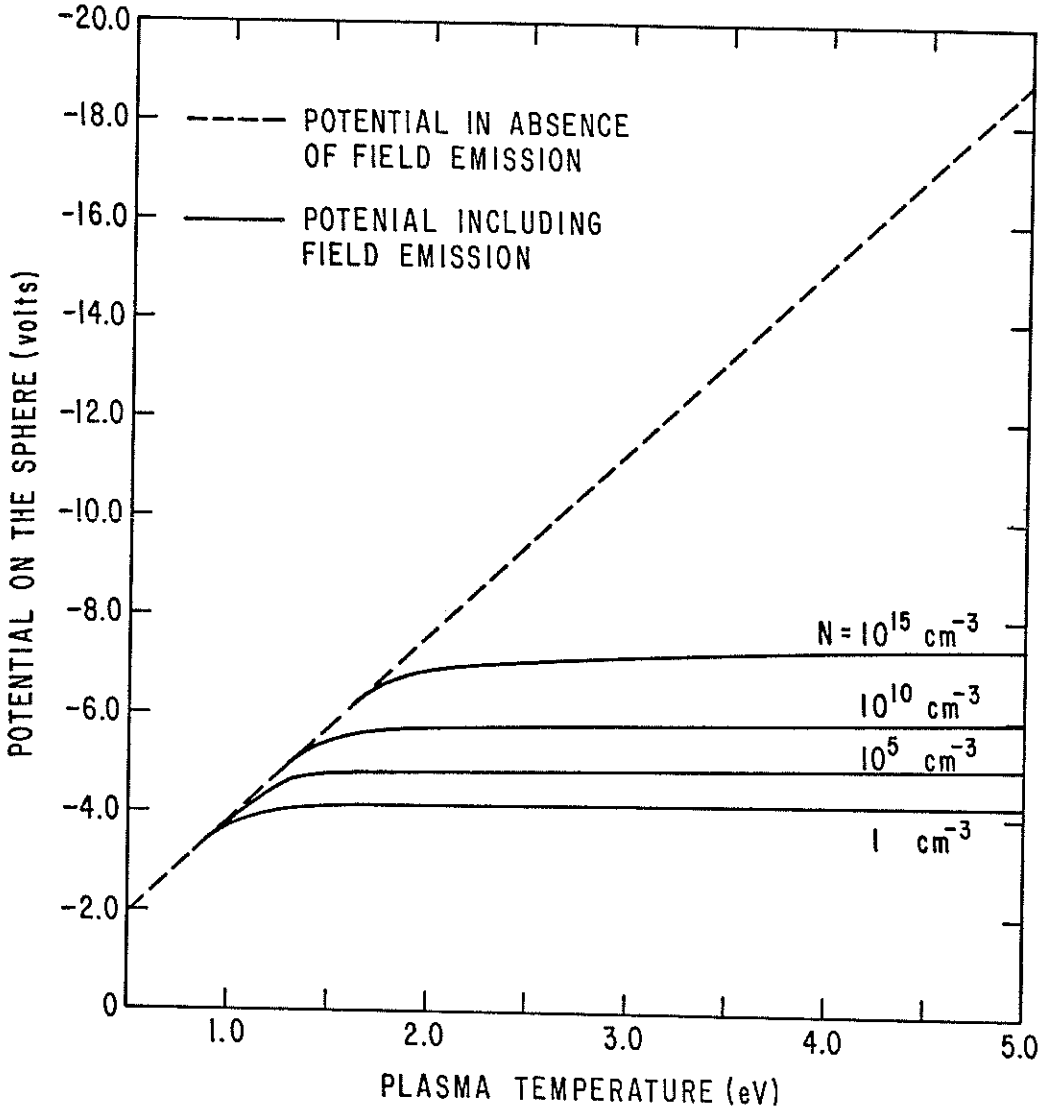
-20.0
-18.0
-16.0
-14.0
-12.0
-10.0
-8.0
-6.0
-4.0
-2.0
0
POTENTIAL ON THE SPHERE (volts)
POTENTIAL IN ABSENCE OF FIELD EMISSION
POTENIAL INCLUDING FIELD EMISSION
N = 10^15 cm^-3
10^10 cm^-3
10^5 cm^-3
1 cm^-3
1.0
2.0
3.0
4.0
5.0
PLASMA TEMPERATURE (eV)

by $10^2 a_\mu$. The upper limits found here do not change appreciably if we include in the electron flux Γ_e in equation (43) the effect of the image force as we have done in Section 6.

In the thick sheath case or in a general case, the upper limit of the voltage, in addition to being a function of $\underline{a}$ and N, becomes dependent on the radius $\underline{s}$ of the Debye sphere. This potential is easily calculated from equation (43).

The Fowler-Nordheim equation estimates the flux of field-emitted electrons from a plane surface. According to Dubey (1970), the flux from a spherical surface may be somewhat higher because whereas the classical criterion for an electron to escape from a plane surface is that its normal component of energy must exceed the surface barrier, the classical condition for escape from a spherical surface is that its total energy must exceed the surface barrier. If this effect is taken into account, the upper limit to the potential will be somewhat lower than the values we have found here.

8. EMISSION OF ELECTRONS

We have refrained in this thesis from including in our analysis the various processes of emission of electrons from the surface of the sphere. Such processes have been discussed in detail in literature and can be easily included in our analysis once the nature of the specific problem in question is known. For instance, in discussing photo-emission of electrons, we need a knowledge of the photon field in the

vicinity of the sphere as well as the electrical properties of the material of the sphere (see e.g., Spitzer, 1941). Once the efflux of electrons due to one or more of the various emission processes is known, this can be subtracted from the electron influx in equation (11). The solution of the resulting equation would give us the grain potential in this case.

The reader is referred to an excellent review of electron emission processes from solid surfaces by Sodha and Guha (1971). Because of the existence of this review, a discussion of the emission processes in this thesis does not seem worthwhile.

9. REMARKS

We have shown in this work that the potential on a solid sphere in a plasma is not given by any one formula such as equations (14) or (16), but it depends on the relative dimensions of the radius of the sphere and the Debye shielding distance in the plasma. Thus, in the same plasma the potentials of two spheres of different sizes may be different. Also, the potential on the same sphere may change if it moves in a plasma in which the density and/or the temperature is varying with space or time. We have further shown that for the submicron size metallic grains there is an increase in the potential due to the effect of the image force. Finally we have discussed the various factors that limit the potential on the spheres so that the

potential cannot increase indefinitely with increasing plasma temperature. We have not included in our discussion the processes of emission of electrons other than field emission, but they are easily included in a specific problem once the exact nature of the problem is known.

REFERENCES FOR II

Dubey, P. K.: 1970, J. Phys. D. 3, 145.

Gomer, R.: 1961, Field Emission and Field Ionization, (Harvard University Press, Cambridge, Mass.), 19.

Kemble, E. C.: 1958, The Fundamental Principles of Quantum Mechanics (Dover, New York), 109.

Sodha, M. S. and Guha, S.: 1971, Advances in Plasma Physics, A. Simon and W. B. Thompson, eds. (Interscience, New York), 4, 219.

Spitzer, L.: 1941, Ap. J. 93, 369.

Spitzer, L.: 1968, Diffuse Matter in Space (Interscience, New York).

Suits, G.: 1961, Collected Works of Irving Langmuir, Vol. 4 (Pergamon, New York), 118.

Wickramasinghe, N. C.: 1967, Interstellar Grains (Chapman and Hill, London).

III. PHYSICAL CONDITIONS IN THE METEORITE CONDENSATION ENVIRONMENT

1. INTRODUCTION

The various astrophysical theories of formation of the solar system assign a wide variety of physical conditions to the primitive solar nebula prior to or overlapping the period of formation of the planets and the satellites. Because of the very nature of the problem, a definitive choice between these theories with regard to the physical conditions at the time of condensation of solids has not been possible so far. In the recent years, a wealth of information bearing on the time period when the solar system was formed has been gathered from cosmochemical studies - particularly from the analysis of meteoritic materials, some of which are believed to be well-preserved primordial condensates. This information, when interpreted in a way consistent with our knowledge of the behavior of matter in space, provide us within rather certain limits the physical conditions in the environment in which these materials condensed.

A major limitation in the use of meteorites for the discussion of the condensation environment comes from the fact that we do not know in which region of space the meteorites condensed. The condensation of phases that we observe in them could, for all we know have taken place in the planetary region of the solar system, in the transplanetary region or for some components even in some source region outside of our solar system. However, even in the absence of this information, some general conclusions can be drawn from the meteoritic material, and these can be compared with the boundary

conditions on condensation phenomenon in the vicinity of our sun.

The purpose of this part is twofold: First, we examine the physical consistency of the conclusions regarding the meteorite condensation environment derived in some widely discussed theories in this field (see e.g. comprehensive reviews by Anders (1971a, 1972a, 1972b)). We find that some of the current conclusions regarding the conditions in a gas from which meteoritic material could have condensed are irreconcilable with fundamental laws of physics. Of special interest is the crucial assumption made in some theories that the solid condensate and the ambient gas had the same temperature at condensation. A number of conclusions have been made basing on this state of thermodynamic equilibrium. We show that there is no conceivable way in which such a state could exist in a region of condensation. Furthermore, the assumption of a gas pressure in the range obtainable by smearing out the matter now contained in the planets and the satellites together with a complement of hydrogen and helium over a nebula of some specific geometry is also unrealistic.

The second object of this part is to derive the realistic physical conditions in the condensing gas basing primarily on the known properties of solid phases occurring in meteorites on one hand, and the radiation laws for solids, gases and plasmas on the other. The conclusions arrived at in this way indicate that: (1) the condensation of materials such as found in meteorites took place from a gas

phase at a temperature substantially higher than the temperature of the solid "grains" growing from this gas; (2) this conclusion is independent of the opacity in the cloud where condensation took place and (3) for temperatures of condensing refractory grains the corresponding gas temperatures are sufficiently high so that many abundant chemical species in the gas would be extensively ionized while others would remain neutral.

2. THE CONDENSATION ENVIRONMENT ACCORDING TO SOME CURRENT INTERPRETATIONS

2.1 Summary of cosmochemical inferences

The present status of our information from meteorite research possibly bearing on the early states of the solar system together with some aspects of interpretation has been summarized in recent reviews for example by Anders (op. cit.). The main import of these discussions is that the condensation of solids took place from a neutral gas of "cosmic" composition during its cooling from temperatures of the order of 2000°K down to about 200°K. The solid condensate is suggested to have the same temperature as the ambient gas at all times. This assumption is of fundamental importance in discussing the condensation process - it implies that this process can be described in terms of chemical and thermodynamic equilibria between phases which are at the same temperature.

The inferred gas pressures at condensation are in the range of 10^{-6} - 10^{-3} atmospheres. Neither the time span of condensation nor

the cooling mechanism for the gas are specified. However, some exemplary results are presented where the cooling time in one case is taken to be of the order of minutes to hours (where the solids would condense practically without interdiffusion) and in another case of the order of years to centuries (with complete diffusional equilibration, permitting the formation of solid solutions to the limit of solubility).

2.2 Premises of inference

In trying to examine the conclusion drawn with regard to the temperatures of gas and solids, we find that the inference that these have the same temperature is an aesthetically determined choice without any physical or chemical basis. It is thus really not an inference, but a postulate. It depicts a situation which can be easily materialized in a wide range of temperature in the terrestrial laboratories, but which can be achieved only under very special circumstances in space.

Furthermore, the inference that the gas is cooling at the same rate as the solids during the process of condensation appears not to be independently considered. A scrutiny of the literature reviewed by Anders indicates that this is also an ad hoc assumption introduced to satisfy the "equal temperature" assumption. The fact that the cooling processes of a gas in space and of solids, and hence their cooling rates, are not identical, does not appear to have been taken into account.

There is also no clear explanation for the specific range of gas pressures used in these discussions. Grossman (1973) has deduced an

upper limit of gas pressure of about 2.2×10^{-3} atmospheres during the condensation of calcium and aluminum rich inclusions in carbonaceous chondrites. However, this estimate was made under the assumption of thermodynamic equilibrium. In general, the pressures used in these discussions are such as would be obtained by smearing out the material now existing in the planets and satellites together with its appropriate complement of hydrogen and helium over a "solar nebula" of reasonable dimensions. The pressures referred to are generally those that would exist in the interior of such a nebula.

2.3 Thermal equilibrium

For the sake of discussion we shall accept here the conceptual nebular models (Figure III-1) invoked in most current cosmochemical discussions, although these models suffer from a number of drawbacks in terms of physical consistency (for a discussion of these questions see Alfvén and Arrhenius 1973a; Arrhenius 1972a and references contained therein).

2.3.1 Basis of discussion

We shall use the state of thermal equilibrium between the gas and the solid condensates ("grains") as a basis for discussing the conditions for condensation and evaporation. We use the term thermal equilibrium in a special sense here - it is an equilibrium in the sense that the heat loss and heat gain rates of the grains are equal. However, the entire system consisting of gas and grains continue to lose energy

FIGURE III-1

A conceptual sketch of a primitive solar nebula. This nebula has been adopted (solely for the sake of discussion) in this paper, and it shows the region in which the meteoritic source material is supposed to have condensed. The commonly postulated physical conditions in this region during condensation are also indicated.

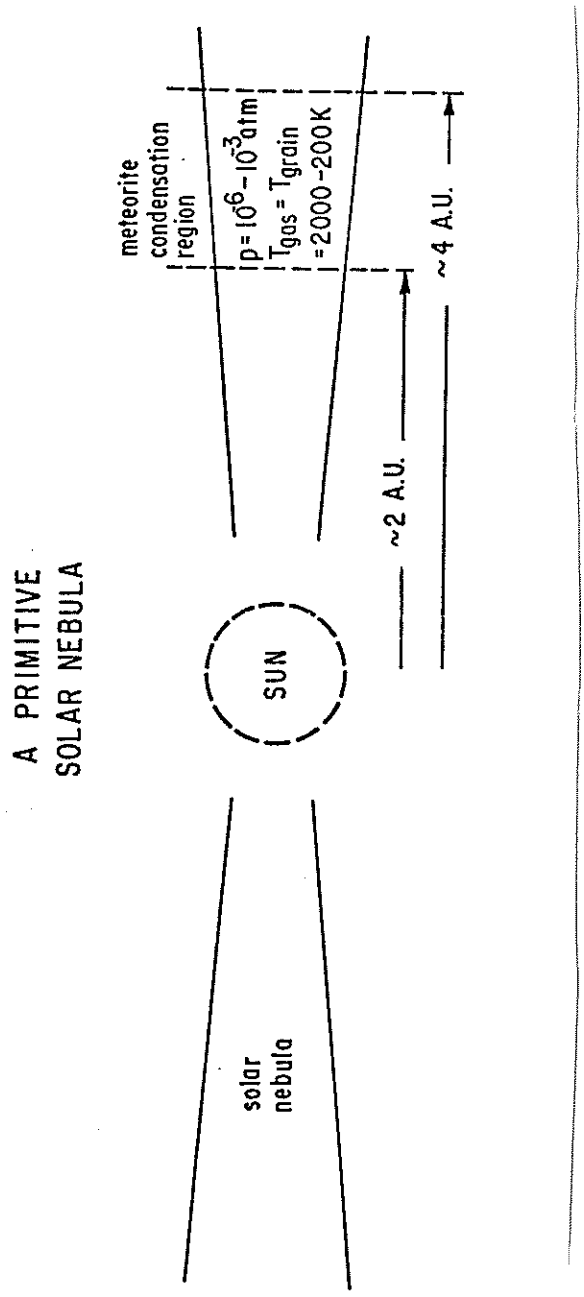
A PRIMITIVE
SOLAR NEBULA
meteorite
condensation
region
p = 10^-6 - 10^-3 atm
T_gas = T_grain
= 2000 - 200K
~2 A.U.
~4 A.U.
SUN
solar
nebula

with time as will be shown in Section 2.7, and hence the system is not in thermodynamic equilibrium. This state of heat balance of the grains does not necessarily imply a temperature equilibrium. Let us recognize that when we speak of temperatures of gas and solids in space, we have in fact to deal with three different temperatures which may be defined as follows:

1) A kinetic temperature T may be assigned to a body of gas in space if the particles in the gas have achieved a Maxwellian velocity distribution. There is no blackbody (cavity) radiation associated with a body of neutral gas in space.

2) A solid (or liquid) body in space has a temperature T_g, which to a fair approximation may be called a blackbody temperature. When this solid body is immersed in the above gas, T and T_g are usually not identical.

3) A star radiates like a blackbody (with superimposed emission and absorption lines) because the photons emitted by the excited and ionized gases assume an equilibrium distribution (the Bose-Einstein distribution for photons, i.e. the Planck distribution). The space in the vicinity of a star has a blackbody radiation field due to the stellar radiation. This field may be locally characterized by a blackbody temperature T_o. This is the equilibrium temperature that would be attained by a rapidly rotating blackbody placed in empty space near the star.

The equilibrium temperature T_g of a solid body in the vicinity of

a star and immersed in a gas of temperature T is, among other parameters, a function of T and T_o. This temperature is given by the condition that the rate of heat loss by the solid body equals its rate of heat gain.

2.3.2 Energy exchange between gas and grains

Suppose that a gas particle with mean energy ϵ is incident on a solid surface with mean molecular (or atomic) energy ϵ_g. If there is no condensation of the gas particles, it returns to the gas phase with a diminished energy ϵ_r. Then the ratio of energy that the incident gas particle transfers to the solid surface to the energy it would have transferred if condensation took place is

$$C = \frac{\epsilon - \epsilon_r}{\epsilon - \epsilon_g} = \frac{T - T_r}{T - T_g} \tag{1}$$

where T is the gas temperature, T_g is the temperature of the solid and T_r is a "temperature" of the reflected particle related to its mean energy. The quantity C is known as the accommodation coefficient, but it is conventionally defined in the literature as

$$C = \lim_{T \to T_g} \frac{T - T_r}{T - T_g} \tag{2}$$

and the experiments to determine C are usually performed with T close to T_g. In our case, however, T and T_g will be found to differ substantially. With this reservation, we shall continue to call C the accommodation coefficient throughout our discussion.

Let N and m be the density of the gas and the mass of a gas particle. In a spherical coordinate system centered on the grain (assumed spherical for the sake of simplicity), the Maxwellian velocity distribution function may be written as

$$n(u, v)\, du\, dv = 2\pi N \left(\frac{m}{2\pi kT}\right)^{3/2} \exp\left[-\frac{m}{2kT}\,(u^2 + v^2)\right] v\, du\, dv \tag{3}$$

where u is the radial velocity component and v is the resultant of the two tangential velocity components, k being the Boltzmann constant. The flux of the gas particles to the grain surface is then given by

$$\Gamma = \int_0^\infty \int_0^\infty n(u, v)\, u\, du\, dv$$

$$= N\left(\frac{kT}{2\pi m}\right)^{1/2} \tag{4}$$

and the corresponding energy flux to the grain surface is given by

$$E_{in} = \int_0^\infty \int_0^\infty n(u, v)\, \frac{1}{2}\, m(u^2 + v^2)\, u\, du\, dv$$

$$= N\left(\frac{kT}{2\pi m}\right)^{1/2} 2\,kT \tag{5}$$

If we assume that the reflected particles have a Maxwellian distribution corresponding to a temperature T_r, then the particle and the energy fluxes of the reflected particles is similarly given by

$$\Gamma_{out} = f\left(\frac{kT_r}{2\pi m}\right)^{1/2} \tag{6}$$

$$E_{out} = f\left(\frac{kT_r}{2\pi m}\right)^{1/2} 2kT_r \tag{7}$$

where f is a quantity which we determine by requiring Γ_{out} to be equal to Γ. Hence

$$E_{out} = N\left(\frac{kT}{2\pi m}\right)^{1/2} 2kT_r \tag{8}$$

However, the assumption that the reflected particles have a Maxwellian distribution is reasonable only if $T \approx T_g$. But notice that if the reflected particles have a known energy distribution, then they have definable mean energy ϵ_r and a cooresponding "temperature" T_r so that $\epsilon_r \approx 2kT_r$. Since the energy carried away by the reflected particles must equal the particle flux times the mean energy, we again have

$$E_{out} = N\left(\frac{kT}{2\pi m}\right)^{1/2} 2kT_r \tag{9}$$

The flux of energy imparted to the grain surface is now given by

$$G = E_{in} - E_{out} = N\left(\frac{kT}{2\pi m}\right)^{1/2} 2k(T - T_r) \tag{10}$$

which, on using equation (1), becomes

$$G = N\left(\frac{kT}{2\pi m}\right)^{1/2} C\, 2k(T - T_g) \tag{11}$$

2.3.3 The state of equilibrium

If the gas is in the composition range referred to as "cosmic," then we may fairly assume that it is predominantly hydrogen. Suppose that a grain immersed in hydrogen gas at temperature T and subjected to solar radiation at the present rate has an equilibrium blackbody temperature T_g (departures from the blackbody character are discussed in Section 2.5). At the site of the grain the solar radiation field has a temperature T_o. Then the amount of heat that the grain receives from the radiation field is

$$G_r = \sigma T_o^4 \text{ ergs cm}^{-2} \text{ sec}^{-1} \tag{12}$$

where σ is the Stefan-Boltzmann constant.

The heat input from the impinging gas molecules to the grain is given by equation (11):

$$G_m = N\left(\frac{kT}{2\pi m_m}\right)^{1/2} C_m\, 2k(T - T_g) \tag{13}$$

where m_m and C_m are the mass and the accommodation coefficient for hydrogen molecule. The rate of radiative heat loss from the grain, assumed to be a blackbody, is

$$L = \sigma T_g^4 \text{ ergs cm}^{-2} \text{ sec}^{-1} \tag{14}$$

The condition for thermal equilibrium is now given by

$$G_r + G_m = L \tag{15}$$

The value of the constant C_m is likely to be less than 1 in an actual situation (see Section 2.4). However, we shall put $C_m = 1$ in the present calculations and understand that the grain temperatures that we thus obtain are an upper limit.

Notice in equation (15) that one possible solution is $T_g = T_o = T$. All other solutions must have all three temperatures unequal. The former situation would be brought about if we put a quantity of gas at some initial temperature inside a solid "black" enclosure and put the enclosure in empty space. After some time both the gas and the enclosure will be found to have the same temperature as the local radiation field. The role of the walls of the enclosure is vital in bringing about this equilibrium. In the case of the solar nebula under discussion the solid grains, if present in substantial amount, play this role and tend to bring the gas temperature down to the temperature T_o of the radiation field, their own temperature approaching T_o at the same time. However, until and unless the final state of equality of all the three temperatures has been reached, all three temperatures remain unequal. This is the situation that we are interested in.

Figure III-2(a) shows the grain temperature as a function of gas temperature calculated from equation (15) for two different regions: the terrestrial region where we have assumed $T_o = 300°K$ and the

FIGURE III-2

Temperatures of grains in thermal equilibrium with gas and radiation field. Such equilibrium would in the models discussed here pertain in the entire nebula in the incipient stages of condensation. It would persist in regions where condensation could by definition continue, regardless of developing grain opacity.

Two values of the radiation field temperature T_o are chosen: $T_o = 300°K$ roughly corresponding to terrestrial region and $T_o = 150°K$ roughly corresponding to the asteroidal region. Each pair of curves corresponds to a fixed gas density and hence the gas pressure varies along these curves. Figure (a) shows the solutions for a "black" grain while Figure (b) shows the solutions including the effects of grain size and non-black emissivity.

The pressure range shown is within the one commonly assumed in "instant nebula" type models. In these the total amount of planetary matter with a complement of hydrogen and helium are assumed at one given time all to be distributed in the disc formed by the rotating solar nebula. The difficulties encountered in such models are discussed in the references in Section 2.3.

Note also the insensitivity of the grain temperature to the assumed value of T_o for relatively high pressures.

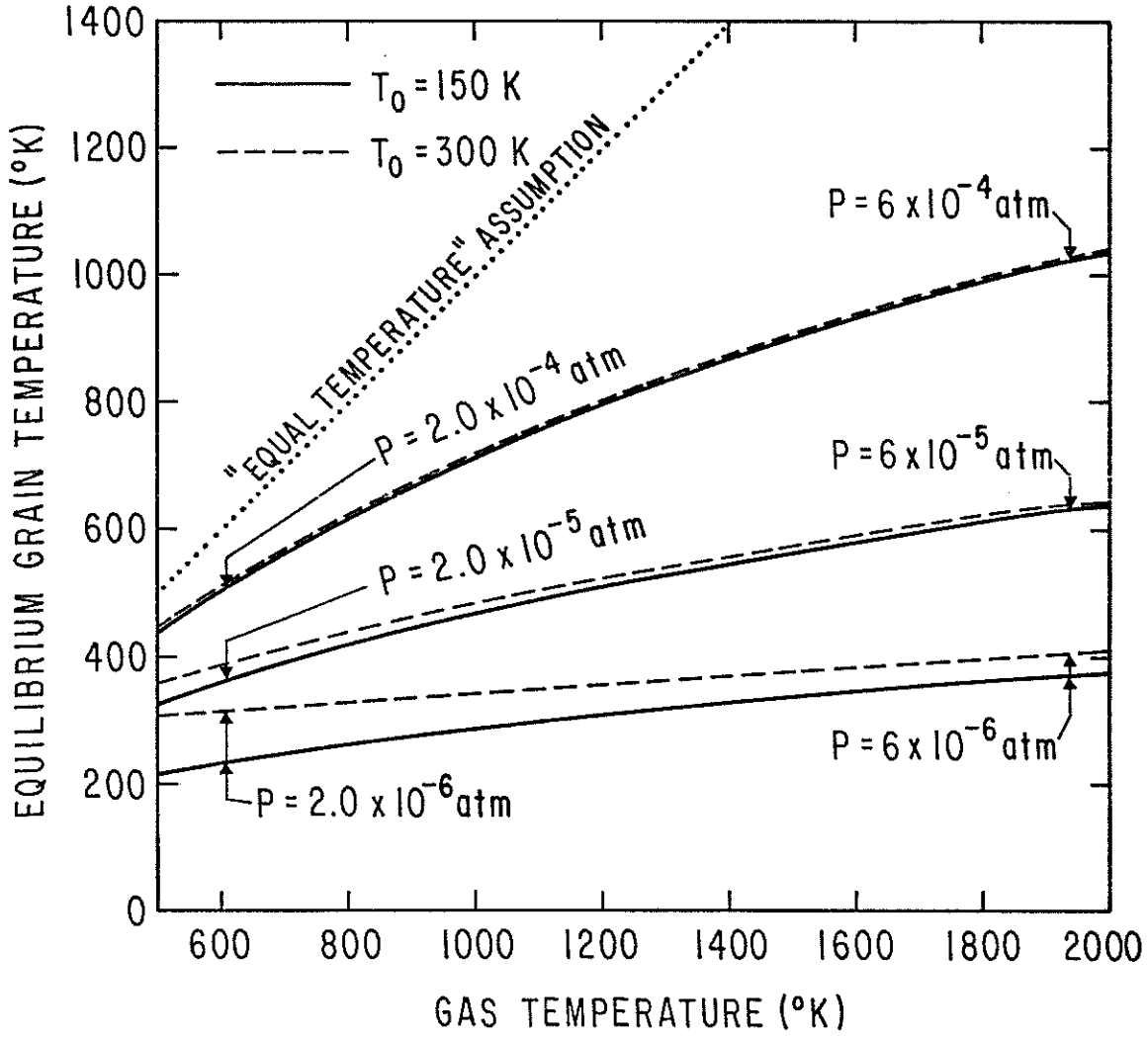
1400
1200
1000
800
600
400
200
0
600
800
1000
1200
1400
1600
1800
2000
EQUILIBRIUM GRAIN TEMPERATURE (°K)
GAS TEMPERATURE (°K)
T_0 = 150 K
T_0 = 300 K
"EQUAL TEMPERATURE" ASSUMPTION
P = 6 x 10^{-4} atm
P = 2.0 x 10^{-4} atm
P = 6 x 10^{-5} atm
P = 2.0 x 10^{-5} atm
P = 6 x 10^{-6} atm
P = 2.0 x 10^{-6} atm

(a)

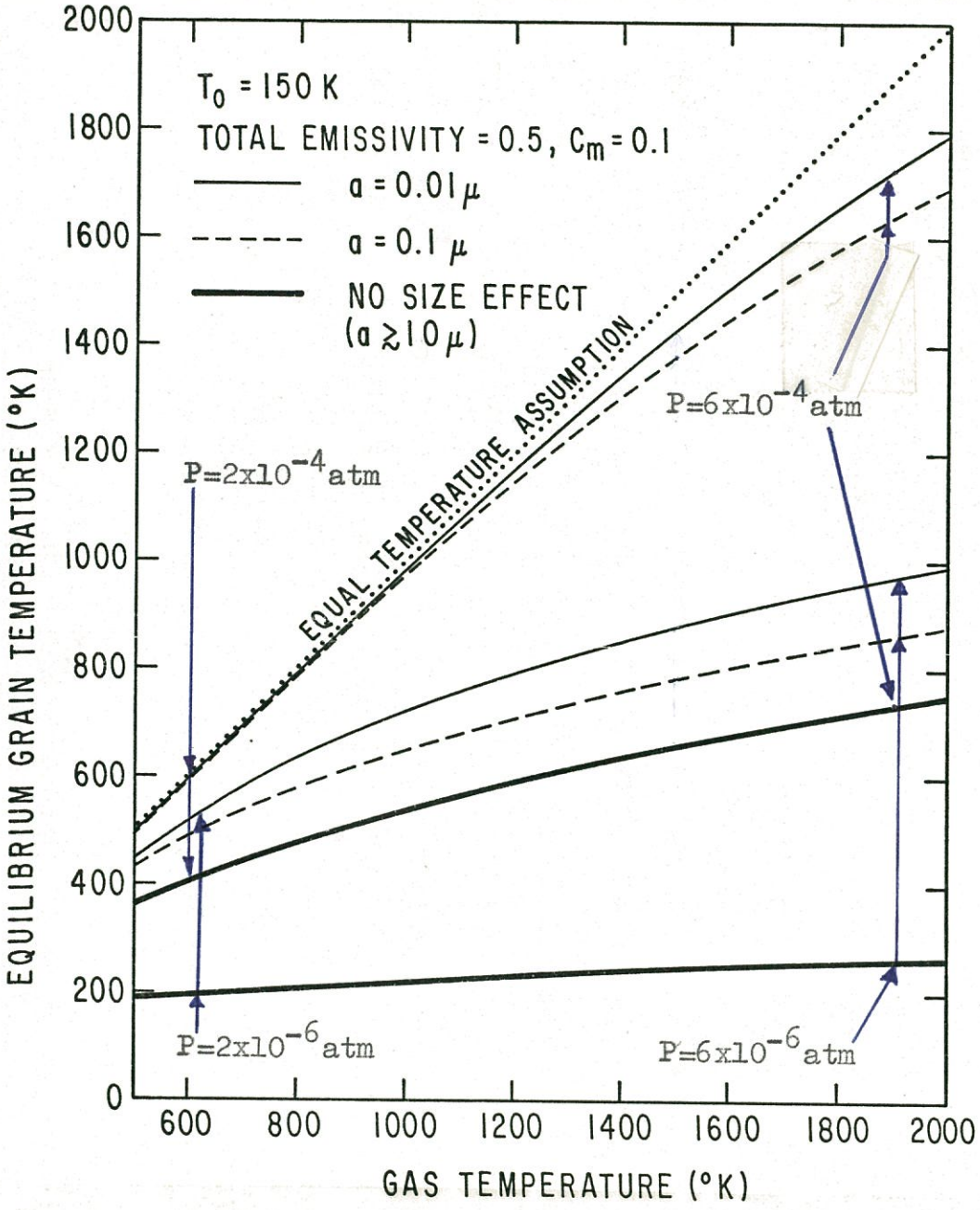
T_0 = 150 K
TOTAL EMISSIVITY = 0.5, C_m = 0.1
a = 0.01 μ
a = 0.1 μ
NO SIZE EFFECT
(a ≳ 10 μ)
EQUAL TEMPERATURE ASSUMPTION
P=6x10^{-4}atm
P=2x10^{-4}atm
P=2x10^{-6}atm
P=6x10^{-6}atm
EQUILIBRIUM GRAIN TEMPERATURE (°K)
GAS TEMPERATURE (°K)
0
200
400
600
800
1000
1200
1400
1600
1800
2000

(b)

asteroidal region (a commonly assumed source region for meteorites) where we have assumed $T_o = 150°K$. The range of gas densities are chosen so as to cover approximately the pressure range of 10^{-6} to 10^{-3} atmospheres. Note that the equilibrium grain temperatures are several hundreds of degrees to over a thousand degrees lower than the gas temperatures in the range shown. For very high grain temperatures, in the range 1800°K, commonly assumed for most refractory phases, the gas temperature exceeds 10,000°K on the lower gas density curves.

Equation (15) and Figure III-2(a) were obtained under the assumption that for a given grain the radiation from the neighboring grains do not constitute a significant heat source. The need for this assumption in discussing the condensation environment will be evident from Section 2.9.

Note that the grain temperatures given in Figure III-2 represent an upper limit - the realistic temperatures would be lower than these values depending on the value of the accommodation coefficient C_m. Note also that for the upper two pairs of gas density curves the grain temperatures in the terrestrial and the asteroidal regions are approximately the same - indicating that G_r is an insignificant heat source in these cases. Thus, even if the solar temperature were somewhat different in the formative era, our conclusion about a significant gas-grain temperature differential would still hold.

Another conceivable heat source for the grains under the

conditions visualized is the association of H atoms on the grain surface to form H_2 molecules. This contributes a term $G_{assoc.}$ to the left hand side of equation (15) such that

$$G_{assoc.} = \frac{1}{2} N_a \left(\frac{kT}{2\pi m_a}\right)^{1/2} \chi_a W_a \qquad (16)$$

where W_a is the association energy, m_a is the mass of hydrogen atom, N_a is the density of atomic hydrogen and χ_a is the fraction of impacting atoms that undergo association on the grain surface. For a liberal estimate of grain temperatures let us put $\chi_a = 1$ and $N_a/N = 10^{-1}$, (see Section 2.7). If we now solve equation (15) including the term $G_{assoc.}$, then for the uppermost pair of curves in Figure III-2 and for a gas temperature of 2000°K, the grain temperature becomes about 1200°K, instead of about 1100°K.

2.4 The accommodation coefficient C

In our discussion in the previous section we used the value 1.0 for the accommodation coefficient C_m for H_2 molecules. Clearly this is an unrealistic case, for this means that all the H_2 molecules colliding with the grains are either brought to rest on the grain surface or return to the gas with a temperature T_g. We can obtain a very simple theoretical estimate for C basing on the laws of impact, if we assume that an impinging atom of mass m collides only once with a single atom of mass m_g on the grain surface (Baule, 1914). Then

$$C = 1 - \frac{m^2 + m_g^2}{(m+m_g)^2} \qquad (17)$$

This simple relation gives $C_m = 0.07$ for H_2 molecules incident on iron grains (since metallic iron constitutes a major component of meteoritic sample, we shall use this as an example of meteoritic material throughout this discussion).

In reality, the atoms on the grain surface are bound to one another in lattices and the collision may not be thought of as taking place with a single surface atom. McCarroll and Ehrlich (1963) have treated this problem by assuming that the gas particle strikes at one end of a semi-infinite linear chain of harmonically coupled particles. From this analysis they obtain the values of C as a function of m/m_g and K/K_o, where K is the force constant corresponding to the harmonic coupling of the particles in the chain and K_o is a modified harmonic potential describing the interaction between the gas particle and the first lattice particle. The accommodation coefficient obtained in this way is independent of the energy of the incident particle. In the case of hydrogen molecules or atoms incident on iron grain ($m/m_g \leqslant 0.04$), the value of C is of the order of 0.1 or less.

Even the above analysis is at best a very simplified one. The accommodation coefficient for molecules also involve the exchange of rotational and vibrational energies besides the translational energy.

It further depends on the chemical and electrical states of the surface and the presence of other gases. There do not seem to be any detailed theoretical or experimental information about the accommodation coefficient when the gas is at a much higher temperature than the solid - and particularly when the gas is diatomic. An experiment on H_2 molecules impinging on iron surface at room temperature gives a value $C = 0.09$ (Kaminsky, 1965; p. 89).

In absence of a more concrete basis for this discussion, it seems reasonable to adopt an order-of-magnitude value $C = 0.1$. This would make the grain temperatures in Figure III-2 lower roughly by a factor $(0.1)^{1/4} \approx 0.6$.

2.5 The assumption of Stefan's law for the grains

In our discussion so far we have assumed that the grains emit and absorb radiation according to Planck's law. Let us examine to what extent this assumption is justified. For very small grains the efficiency for absorption and emission of radiation is impaired for radiation wavelengths larger than the dimension of the grain. Thus, rather than assuming that the efficiency for emission and absorption is unity at all wavelengths as in the case of a blackbody, a more realistic assumption would be that the efficiency Q_λ varies as $1/\lambda$ (see e.g. Spitzer 1968), so that we may write

$$Q_\lambda = 1 \qquad 0 \leq \lambda < a$$

$$= \frac{a}{\lambda} \qquad a \leq \lambda \leq \infty \qquad (18)$$

Thus instead of the Stefan's law of radiation

$$E = \frac{c}{4} \int_0^\infty B_\lambda(T_g)\, d\lambda = \sigma T_g^4 \tag{19}$$

where $B_\lambda(T_g)$ is the Planck function, we now have

$$E' = \frac{c}{4} \int_0^\infty B_\lambda(T_g)\, Q_\lambda\, d\lambda \tag{20}$$

For very small grains (in the submicron range), very little energy exists in the Planck spectrum shortward of $\lambda = a$. Hence we shall not make any significant error if we evaluate the integral in equation (20) by assuming $Q_\lambda = a/\lambda$ for all values of λ from 0 to ∞. When this is done we get a law analogous to Stefan's law

$$E' = \sigma' T_g^5 \tag{21}$$

with

$$\sigma' = \frac{2\pi a k^5}{c^3 h^4} \sum_{r=1}^{\infty} \frac{24}{r^5}$$

$$\approx 2.66\, \sigma a \quad \text{erg cm}^{-2} \text{ sec}^{-1} {}^\circ\text{K}^{-5} \tag{22}$$

where h is the Planck constant and c is the velocity of light.

A departure from Stefan's law will however occur for grains of all sizes due to the non-blackness of the grain material (of course there are no ideal blackbodies). But the emission from a non-black

body can be expressed in terms of the Stefan's law if we write it as

$$E_{nb} = q \sigma T_g^4 \tag{23}$$

or, including the size effect as given by equation (21)

$$E'_{nb} = q \sigma' T_g^5 \tag{24}$$

where the subscript nb stands for non-blackbody and q is the total emissivity of the grain material (q = 1 for blackbody). The quantity q can be determined experimentally and its values for a number of substances have been listed in Table III-I (data from McAdams 1954).

Finally, including all the effects discussed so far, we can rewrite equation (15) as

$$q \sigma' T_o^5 + N\left(\frac{kT}{2\pi m_m}\right)^{1/2} C_m 2k(T - T_g) = q \sigma' T_g^5 \tag{25}$$

In Figure III-2(b) we have plotted the solution of this equation for identical pressure ranges as in the uppermost and lowermost pairs of curves of Figure III-2(a), assuming $C_m = 0.1$ and $q = 0.5$, a rather conservative value of emissivity if the grain material is iron (see Table III-I). Note that for the highest pressure range and for very minute grains (0.01 μm), an approximate equality between the gas and the grain temperature is obtained. In all other cases, the

Table III-1. Total Emissivity of Various Non-Black Substances*

Substance	Temperature (°K)	Emissivity q
Cast iron (metallic surface or very thin oxide layer)	1160 - 1260	0.60 - 0.70
Smooth oxidized electrolytic iron	400 - 800	0.78 - 0.82
Cast iron oxidized at 87°K	470 - 870	0.64 - 0.78
Iron oxide	770 - 1470	0.85 - 0.89
Rough ingot iron (oxidized surface)	1200 - 1390	0.87 - 0.95
Nickel (electroplated, not polished)	290	0.11
Nicel oxide	920 - 1530	0.59 - 0.86
Alumina (99.5-85 Al_2O_3; 0-12 SiO_2; 0-1 Fe_2O_3) Effect of mean grain size:		
10 μ	1280 - 1840	0.30 - 0.18
50 μ	1280 - 1840	0.39 - 0.28
100 μ	1280 - 1840	0.50 - 0.40
Silica (98 SiO_2; Fe free) Effect of grain size:		
10 μ	1280 - 1840	0.42 - 0.33
70-600 μ	1280 - 1840	0.62 - 0.46
Carbon, rough plate	370 - 770	0.77 - 0.72
Glass, smooth	300	0.94

*Total emissivity data as compiled in McAdams (1954). The temperatures have been converted to absolute scale and rounded off to the nearest multiple of 10.

conclusion regarding the existence of a significant gas-grain temperature differential holds.

The effect of grain size on the emission of radiation becomes unimportant when the size of the grain is larger than a few times λ_m, the wavelength of maximum radiation for the Planck curve corresponding to temperature T_g. For our case, the size effect becomes unimportant for grains with a radius of about 10 μm or larger. We shall not discuss the size effect on the emission of radiation by the grains any further in order to keep the discussion manageable, although it will be understood that our conclusions will be subject to some modification if the major part of condensation took place as submicron size grains.

2.6 Approach to equilibrium of an initially hot grain

Suppose that due to some instantaneous process (electrical discharges in the gas, inelastic collision between grains, etc.) the grain temperature is raised to a value close to that of the gas and much higher than T_o. It may then be suggested that the grains would approach their low equilibrium temperature so slowly that the entire condensation process may be thought to take place under conditions of approximate equality of the gas and the grain temperatures. In order to explore this possibility let:

N_c = density of condensing molecules

V_c = effective inflow velocity of condensing molecules

m_c = mass of condensing molecules

M_g = mass of growing grain (instantaneous)

a = radius of growing grain (instantaneous)

a_o = radius of grain at $t = 0$

ρ = density of grain material

s = specific heat of grain material

Then an upper limit to the rate of grain growth is given by

$$\frac{da}{dt} = \frac{N_c m_c V_c}{\rho} \tag{26}$$

so that

$$a(t) = a_o + \left(\frac{N_c m_c V_c}{\rho} \right) t \tag{27}$$

assuming that N_c does not change appreciably during the period of cooling of the grain to its equilibrium temperature. The rate of heat loss of the grain is then given by

$$\frac{d}{dt} (M_g s T_g) = 4\pi a^2 \left[N \left(\frac{kT}{2\pi m_m} \right)^{1/2} C_m 2k(T - T_g) + \sigma(T_o^4 - T_g^4) \right] \tag{28}$$

Hence the rate of cooling of the grain is

$$\frac{dT_g}{dt} = \frac{3}{s\rho a} \left[-s\rho T_g \frac{da}{dt} + N \left(\frac{kT}{2\pi m_m} \right)^{1/2} C_m 2k(T - T_g) + \sigma(T_o^4 - T_g^4) \right] \tag{29}$$

Figure III-3 shows the cooling of an iron grain (with $T_o = 300°K$ and $T_k = 2000°K$) for various grain radii with $C_m = 0.1$. We find that the time to cool to the equilibrium temperature is of the order of seconds. If we use the size-dependent "Stefan's law" of Section 2.5 instead of the blackbody law, the cooling times will be somewhat longer or shorter depending on the grain size, but they will be of the same order as shown in Figure III-3. The conclusion obviously is that if due to some instantaneous process the temperature of a grain is raised, it will very quickly relax back to its equilibrium temperature.

2.7 Cooling of gas

Let us next turn our attention to the physical conditions in the nebular gas which consists predominantly of hydrogen, and to begin with, without any condensed particles. The abundance of molecular hydrogen in this gas is somewhat uncertain since photodissociation of H_2 molecules has to be taken into account. An upper limit to the abundance of H_2 is given by assuming dissociative equilibrium, so that the density N_a of atoms and N_m of molecules are related by

$$\frac{N_a^2}{N_m} = \frac{K_P(T)}{kT} \tag{30}$$

where the value of the dissociation constant $K_P(T)$ as a function of temperature is given for instance by Tsuji (1964). At temperatures of the order of 2000°K and a gas density of 10^{15} cm^{-3} (i.e. a gas pressure

FIGURE III-3

Cooling to equilibrium temperature of an iron grain which has been raised to a high temperature (here 2000°K) by some transient process. The numbers alongside the curves indicate the grain radii at time $t = 0$.

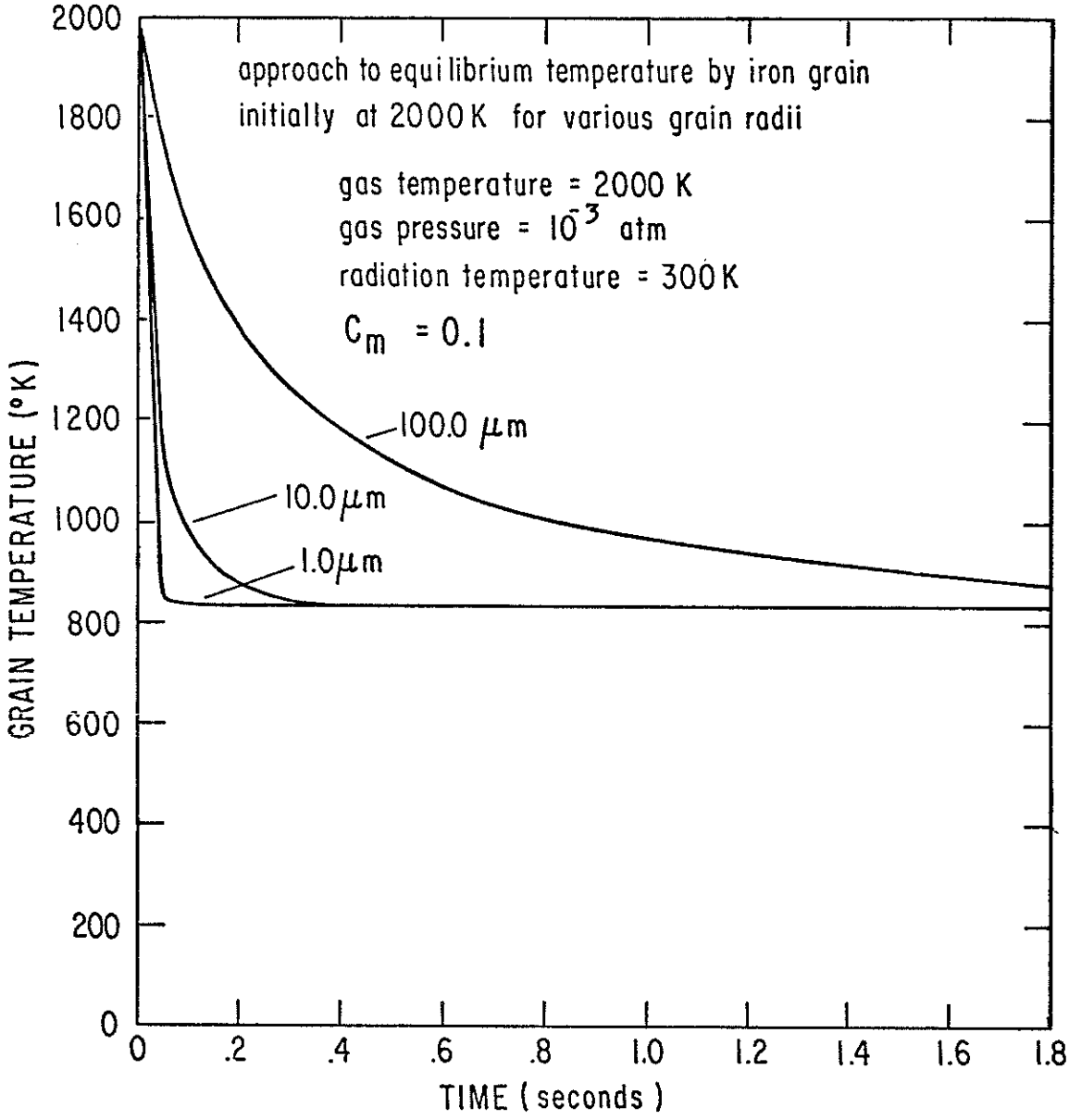
approach to equilibrium temperature by iron grain
initially at 2000 K for various grain radii
gas temperature = 2000 K
gas pressure = 10^{-3} atm
radiation temperature = 300 K
C_m = 0.1
100.0 μm
10.0 μm
1.0 μm
GRAIN TEMPERATURE (°K)
TIME (seconds)
2000
1800
1600
1400
1200
1000
800
600
400
200
0
0
.2
.4
.6
.8
1.0
1.2
1.4
1.6
1.8

of the order of $2 \cdot 10^{-4}$ atm), the ratio N_a/N (N = total number density is about 0.1. At a temperature 1500°K, this ratio falls to 10^{-3}. Hence we may conclude that as soon as the gas temperature is somewhat below 2000°K, it becomes predominantly molecular. In the theories under discussion it is generally assumed that the adiabatic heating of the contracting nebula brought the temperature to the level of about 2000°K at the onset of condensation. The only available source of energy to the gas during the condensation would be the solar luminosity. This source is inefficient in communicating heat energy to a molecular hydrogen gas (see, e.g. Kahn and Dyson 1965).

The predominant source of radiative energy loss would be the excitation and deexcitation of the rotational levels of H_2 molecules. The self-absorption optical depth for this radiation is very large in nebula, and hence cooling due to this process would be confined initially to a thin layer at the edge, which would proceed inward with time. However, by far the most important cooling mechanism, once the solid grains have started to condense, is the cooling due the radiation from the grains in contact with the gas. The grains being at a temperature higher than the radiation field radiate energy faster than

they absorb from the field. The excess energy comes from the kinetic energy of the gas molecules impinging on the grains. This energy loss far exceeds the radiative energy loss or the energy gain from the solar radiation by the gas. Consequently, the gas continues to cool, and so do the grains, but each at a different rate. This cooling process also is confined to the edge of the nebula due to large infrared opacity in the nebula (see Section 2.8), and the cooling front proceeds inward with time. If N_g is the number density of the grains, then the rate of cooling of the gas is given by

$$\frac{d}{dt}\left(\frac{3}{2} N k T\right) = -4\pi a^2 N_g (T_g^4 - T_o^4) \tag{31}$$

where T_g is a function of T as given by equation (15) and a is given by equation (27). Note that due to the assumption $Q_\lambda = 1$, the cooling rates obtained here would represent an upper limit.

In Figure III-4 we have computed the cooling rates for various values of N_g assuming $C_m = 0.1$ and $N = 10^{15}$ cm^{-3}. We find that the cooling times would typically be of the order of days. Hence the gas and the solid in the edge region of the nebula would cool rapidly, each one at its own rate and with T_g always intermediate between T and T_o. This condition persists in the region of cooling as the cooling front proceeds inward.

FIGURE III-4

Cooling of gas due to refrigeration by the grains. The curves are calculated for various grain number densities. The cooling times shown here are a lower limit. If the equilibrium value of the grain temperatures (Figure III-2) is lower, the cooling times would be longer.

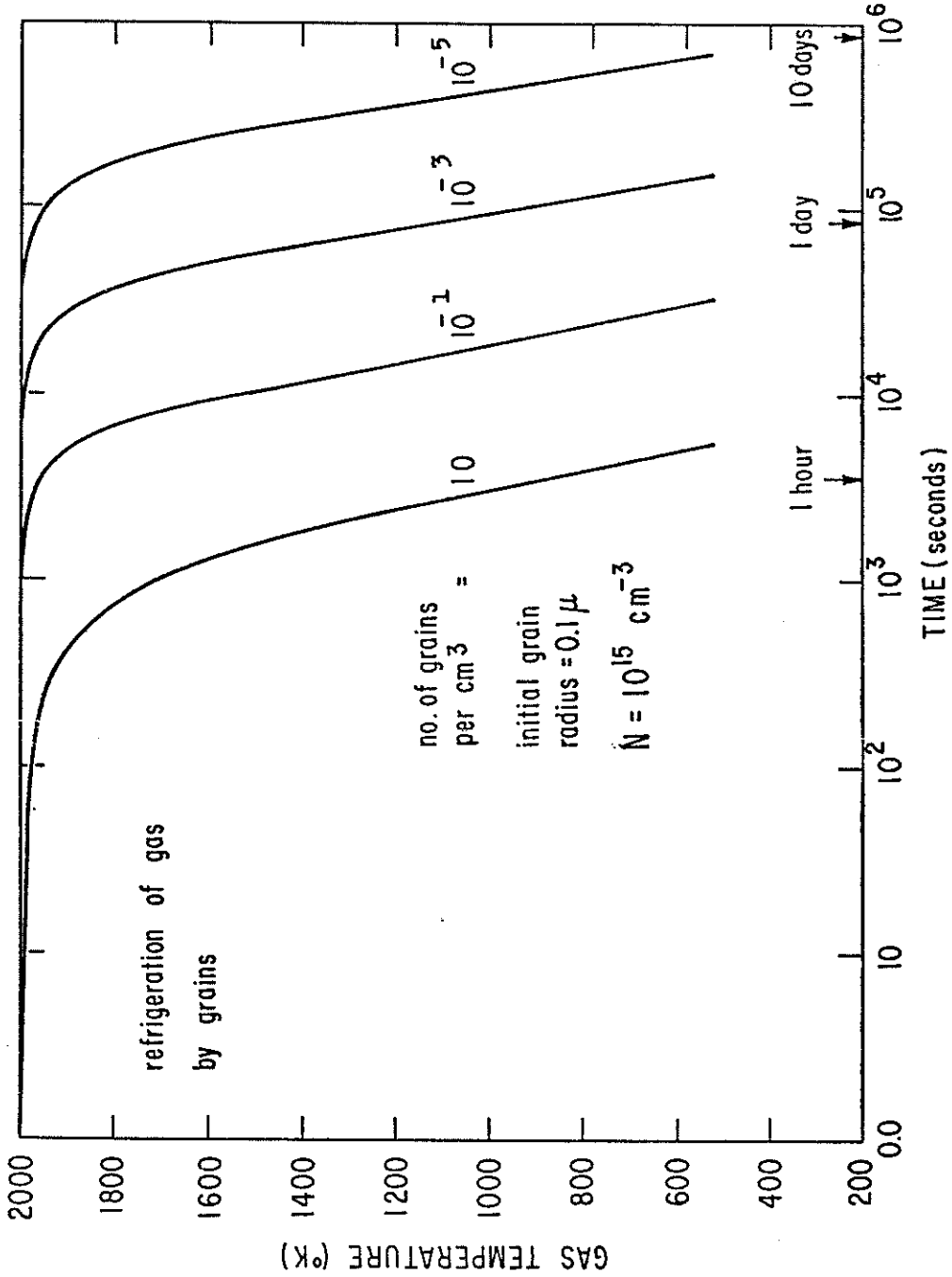
refrigeration of gas
by grains
no. of grains
per cm^3 =
10
10^{-1}
10^{-3}
10^{-5}
initial grain
radius = 0.1 μ
$N = 10^{15}$ cm^{-3}
1 hour
1 day
10 days
GAS TEMPERATURE (°K)
TIME (seconds)
2000
1800
1600
1400
1200
1000
800
600
400
200
0.0
10
10^2
10^3
10^4
10^5
10^6

The assumption of a nebula of neutral gas implies that there are no substantial energy sources for the gas, which results in a catastrophically rapid cooling of the gas once the condensation process ensues, with the condensing grains always at a lower temperature than the gas until the common equilibrium temperature T_o is reached (i.e. until $T = T_g = T_o$). The primordial condensate would consist of a quenched undifferentiated smoke. This conclusion was drawn on similar premises by Urey in 1952.

Since then extensive investigations of meteorites have been carried out suggesting a primordial condensate instead largely consisting of well crystallized, differentiated solids, representing a sequence of crystallization temperatures. Hence it has become necessary, also for this reason, to replace the nebular concepts of the kind under discussion with models that satisfy the requirements of the chemical observations as well as those of energy conservation.

2.8 The greenhouse effect

The grain temperatures that we have obtained in Section 2.3 were calculated under the assumption that the infrared (IR) radiation emitted by the grains can escape freely from the region of the grains, i.e., the IR opacity in the gas-grain cloud is negligible. It is often suggested, however, that the cloud would, for some reason, be opaque to IR radiation, so that the radiation field in the deep interior of the cloud would be modified due to the capture of IR photons. This would

mean that another term, G_τ would have to be added to the left-hand side of equation (15), to represent this additional heat source.

An IR opacity may be produced either by IR-absorbing gas components or by grains. First we shall assume that the opacity is produced by the grains alone. Let us, for the sake of simplicity, visualize the gas-grain cloud as a disc of half-thickness Z, as sketched in Figure III-1. Suppose that the gas has a uniform temperature of 2000°K throughout the cloud, and that the pressure is 5×10^{-4} atm, so that in the absence of any greenhouse effect the grain temperature would be about 1000°K, according to equation (15). Let T_g be the grain temperature at any point in the cloud, and T_{gc} and T_{ge} be its values at the midplane and at the edge (surface) of the cloud, respectively. If τ is the optical depth for grains situated at a depth z from the edge, then we can write $\tau = \pi a^2 N_g z$. From the elementary theory of radiative transfer in plane parallel layers we then have

$$T_g^4(\tau) = T_{ge}^4 \left[1 + \frac{3}{2}\tau\right] . \qquad (32)$$

Comparing equations (15) and (32), we find that for a grain situated at an optical depth τ, there is an additional energy source over and above those included in equation (15), viz.,

$$G_\tau = \frac{3}{2}\sigma T_{ge}^4 \tau \qquad (33)$$

The equation of heat balance now becomes

$$G_r + G_m + G_\tau = L \tag{34}$$

This equation gives us the variation of T_g with τ, which may be expressed as

$$\frac{dT_g}{d\tau} = 3 T_{ge} \left[8\sigma T_g^3 + 6 N \left(\frac{kT}{2\pi m_m} \right)^{1/2} C_m 2k \right]^{-1} \tag{35}$$

where we have neglected the term G_r compared to G_m. Using this equation and the condition that at $\tau = 0$, $T_g = T_{ge}$, we can now obtain the value of T_g for a given value of τ. However, equation (32) and hence equation (35) were obtained under the assumption that there is a thermodynamic equilibrium between the grains and the radiation field, i.e. the temperature of the radiation field equals the grain temperature. Clearly this is not true at the edge of the cloud, but this would be true in the interior if the opacity due to the grains is large. In order to take this effect into account, let us make the following simplifying but reasonable assumption: At points interior to $\tau = 1$, the radiation field is in equilibrium with the grains. At all points between $\tau = 1$ and the edge the grain temperature is T_{ge}, as would be given by equation (15) -- that is, in the present case $T_{ge} = 1000°K$. The temperature of the radiation field can be estimated roughly by making the simple assumption that the mean intensity of radiation declines as $\exp(-\tau')$, where τ' is the optical depth due to grain opacity measured outward from $\tau = 1$. Hence the temperature of the radiation

field declines as $\exp(-\tau'/4)$, levelling off to the value T_o at a large distance from the edge.

In order to achieve a temperature equilibrium between the grains and the gas in the central regions of the cloud, we require $T_{gc} = 2000°K$. From equation (35) and the above assumptions, this requires that the optical depth to the midplane be $\tau_c = \pi a^2 N_g z = 11$. With grains of radius $1\ \mu m$, this means that we must have about 10^9 grains per cm^2-column normal to the disc. If, as is often done, we visualize the condensation region as a ring around the sun 3 AU in radius, and of rectangular cross section 0.1 AU on the side, then the above requirement is equivalent to the existence of about $10^{24}\rho$ gm of 1-μm grains. This is the order of magnitude of the total mass in the asteroids. The implication of this order-of-magnitude estimate is that a major fraction of the total available mass must have already condensed in order to produce the desired greenhouse effect. The early condensates would thus form in a transparent cloud under the conditions of a pronounced gas-grain temperature differential persisting throughout the cloud.

We will, however, for the sake of argument, assume conditions of extreme screening to somehow prevail already in the early part of the condensation period, and also assume that all of the micron-sized grains have somehow succeeded to remain in suspension. Under these conditions a temperature distribution such as described

above would be established. In Figure III-5 we have plotted the temperature of the gas, the grains, and the radiation field, as functions of the optical depth. Note that at the edge of the cloud the temperature of the radiation field is on the order of 800°K, and not the solar radiation temperature, T_o = 150°K, that we used to calculate T_{ge}. However, this makes very little difference, since the value of T_{ge} is about 1060°K if we use T_o = 800°K instead.

Turning our attention to the opacity due to the gas, we note that the most dominating IR-absorbing molecule would be H_2O, whose abundance relative to H_2 molecules in the type of models discussed would be $\leq 10^{-3}$. The opacity due to this contribution would vary irregularly with the grain temperature but would always be considerably less than the large grain opacities discussed above.

2.9 Region of condensation

For the condensation of solids, a cooling of the gas is essential. If this cooling is due to radiative processes, then it must be confined to the edges of the cloud where the optical depth for the escape of photons is small. However, it is more likely that the predominant cooling is due to the grains themselves, as discussed in Section 2.7. Note from equation (31) that this cooling requires that T_g and T_o be different. This is true only at the edges of the cloud. In absence of a substantial energy source for the nebula, as is the case here, the region of cooling will gradually expand inward and so will the region

FIGURE III-5

Temperatures of gas, grains and radiation field as a function of optical depth in a disc-shaped cloud around the Sun as sketched in Figure III-1. Equality between the gas and the grain temperatures is achieved at the midplane of the disc if the optical depth to the midplane is 11. Cooling of the gas, whether radiative or via the grains, then takes place at the edges of the cloud which by definition constitutes the region of condensation.

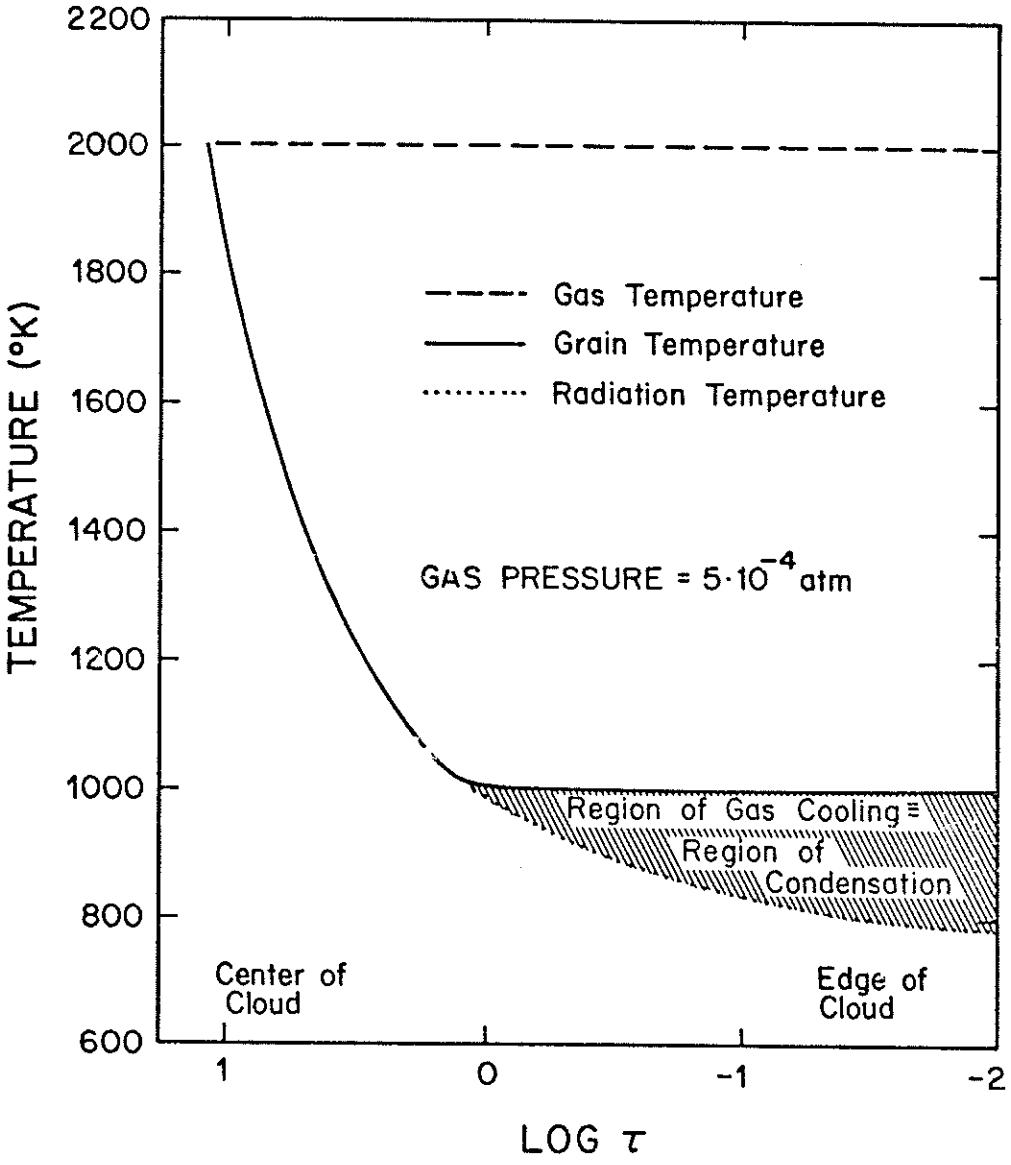
2200
2000
1800
1600
1400
1200
1000
800
600
TEMPERATURE (°K)
Gas Temperature
Grain Temperature
Radiation Temperature
GAS PRESSURE = 5·10⁻⁴ atm
Region of Gas Cooling ≡
Region of
Condensation
Center of
Cloud
Edge of
Cloud
1
0
-1
-2
LOG τ

of condensation with its pronounced gas-grain temperature differential.

Thus, regardless of the cooling mechanism and the opacity assumed, cooling, and hence condensation are confined to the regions of the cloud where a pronounced gas-grain temperature differential always exists.

2.10 Asymptotic realization of the "equal temperature" assumption with increasing pressure

A glance at equation (15) at once tells us that there is one way to increase T_g, that is, to increase the gas density N_m. This results in a larger heat input to the grain, and for very large N_m the grain temperature may become arbitrarily close to the gas temperature, as long as the factor $T - T_g$ does not vanish.

In Figure III-6 we have plotted the temperature differential $T - T_g$ as a function of the gas pressure for two different gas temperatures: $T = 2000°K$ and $1000°K$. The gas pressure is given in units of C_m^{-1} atmospheres. With $C_m = 0.1$, an appproximate equality between T and T_g is obtained for gas pressures $\geq$ 10 atmospheres, for $T = 2000°K$, whereas for $T = 1000°K$, this equality is obtained for pressures $\geq$ 1 atmosphere.

2.11 Summary of Section 2

It is evident from the foregoing discussion that the identification of the temperature of the solid condensate with that of the condensing gas is a postulate which is unacceptable unless the density of the gas is so high that equation (15) results in the gas and grain

FIGURE III-6

Asymptotic approach to the "equal temperature" state. With increasing gas density (and hence gas pressure), the grain temperature approaches the gas temperature, although an exact equality of the two temperatures can never be attained. The pressure scale is in $1/C_m$ atmospheres, where C_m is the accommodation coefficient for the molecules.

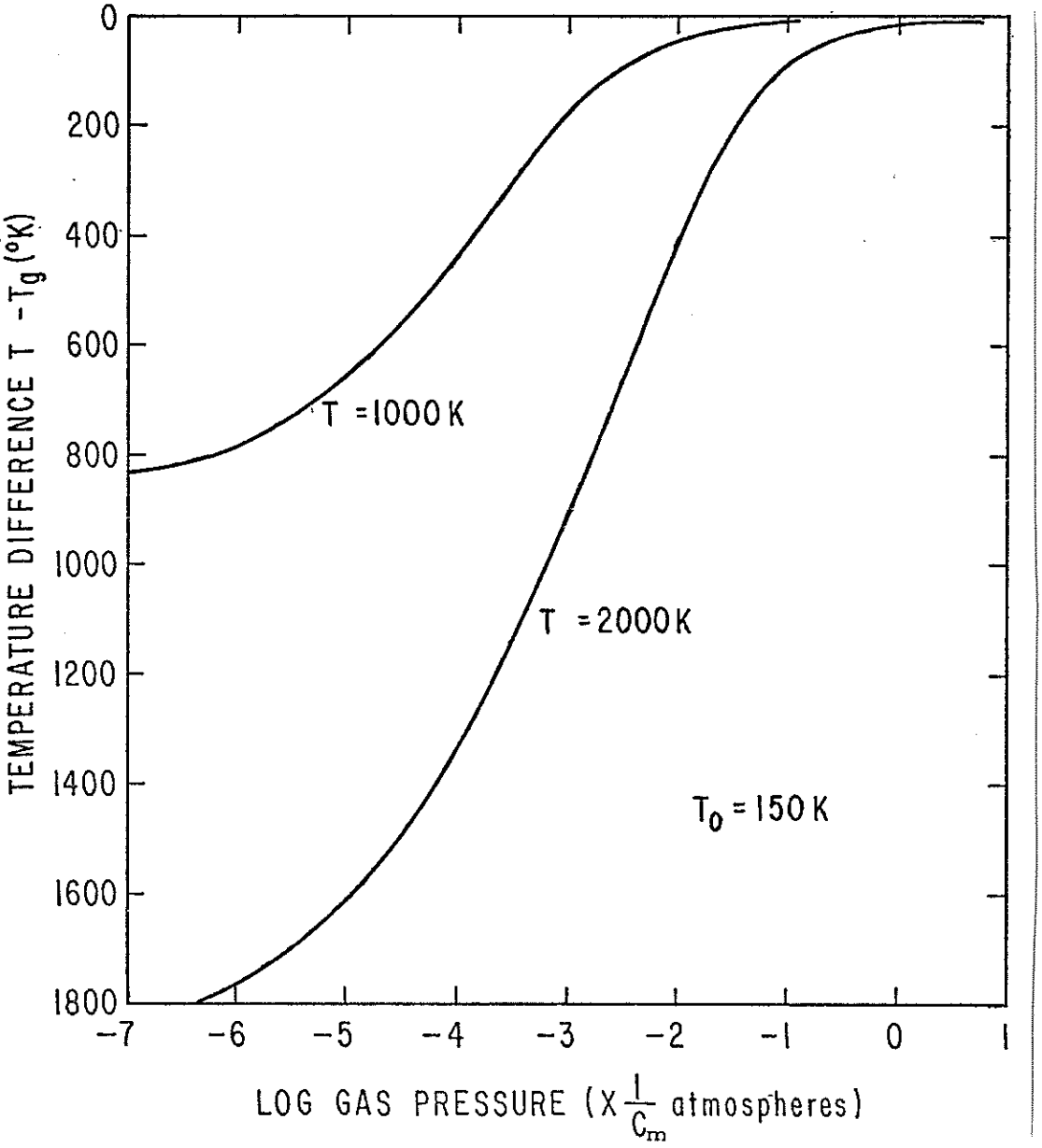
0
200
400
600
800
1000
1200
1400
1600
1800
TEMPERATURE DIFFERENCE T - Tg (°K)
T =1000 K
T =2000 K
T0 = 150 K
−7
−6
−5
−4
−3
−2
−1
0
1
LOG GAS PRESSURE (X 1/Cm atmospheres)

temperature which are very nearly equal. In the temperature range of 1000-2000°K, this requires gas pressures in excess of 1-10 atm. At this point, therefore, we have three clear options open to us, namely:

a) To retain the "equal temperature" assumption and justify by assuming the entire condensation sequence to take place at a very low temperature ($\lesssim$ 400°K). Note from Figure III-2 that an approximate equilibrium between the gas and the grain temperatures is attained in this region for pressures of the order of 10^{-4} atm.

b) To retain the "equal temperature" postulate and justify it by requiring very high pressures in the primordial condensation environment.

c) To abandon the equal temperature assumption. This means that we cannot assume a thermodynamic equilibrium at condensation and hence we have no a priori information about the physical conditions in the gas. Such conditions would have to be deduced in a physically consistent way basing only on information of definitive nature that pertain to the solid condensate.

We have found in this section that the assumption of a nebula of neutral gas necessarily means that there is no substantial energy source for the nebula - which in turn leads to a catastrophic cooling of the gas at condensation. Such a cooling is inconsistent with observed facts.

We have also demonstrated that the process of condensation must take place in regions of the cloud which are transparent to infrared radiation. In such regions, radiation from other grains do not constitute a significant heat source for a grain.

In the next section we shall attempt to make a choice between the options (a), (b), and (c) and try to develop a fresh approach to the problem of primordial condensation environment keeping in mind the above considerations.

3. THE CONDENSATION ENVIRONMENT

3.1 Temperature of solids at condensation

It follows from the discussion of the previous section that the pressures and temperatures of the primordial gas at condensation inferred in a majority of the cosmochemical literature cannot be accpted as realistic because such inferences violate the fundamental principle of conservation of energy by assigning to the condensing grains a much higher temperature than what would be dictated by energy balance. As we shall see in Section 3.3, rather than violating this principle, we can in fact use it to our advantage to deduce the physical conditions in the condensing gas.

Let us note at this point that one direct evidence that we can rely on is the temperature of the solids at condensation. From the crystalline perfection of many of the meteoritic samples, one may conclude

that the temperature of solids at condensation did not exceed their melting points. From the free growth characteristics and lack of significant adhesion of delicate leafy crystals, an origin by crystallization from molten droplets in counterindicated (see Figure IV-1, Part IV). This assigns an upper limit of the solid temperature of the order of 2000°K for most refractory substances. On the other hand, for the condensation of volatile substances, solid temperatures as low as 200°K are necessary. Hence we may reasonably assume that the temperature of the solids at condensation was in the range 200-2000°K. A more accurate specification of temperature on the basis of a condensation curve (Anders 1972a) is not meaningful because of the tacit assumption of thermodynamic equilibrium. We shall not seek, in this thesis, to establish specific condensation temperatures for specific condensates, but rather to establish the limits of physical conditions (pressure and temperature) that would correspond to a given condensation temperature.

3.2 Possible range of gas pressure

We have seen earlier that a physically reasonable condensation environment with approximate equality of gas and grain temperatures is possible if (a) the entire sequence of condensation took place at a very low temperature (below $T \approx T_g \leqslant 400°K$ with a pressure of 10^{-4} atm) or (b) if the gas pressure is very high ($\geqslant$ 10 atm for $T \approx T_g \approx 1000°K$ and $\geqslant$ 10 atm for $T \approx T_g \approx 2000°K$). The

alternative is a state of temperature disequilibration with low gas pressures ($\leqslant 10^{-3}$ atm) and high gas temperature ($T \gg T_g$).

Case (a) above has not been suggested in the "equal temperature" theories that we have discussed, but let us examine this proposition briefly. Consider the condensation of iron in a cooling gas of cosmic composition. If N is the total density of the gas and f_{Fe} is the abundance of iron, then the partial pressure of iron in this gas is

$$P_{Fe} = N f_{Fe} kT \tag{36}$$

The vapor pressure of various elements at a solid temperature T_g for pressures below 1 mm of Hg is given by (Dushman 1962)

$$\log P_v = A - \frac{B}{T_g} \tag{37}$$

where the values of the constants A and B for various elements are given in the above reference. If $T \approx T_g$, then the first temperature T_c at which iron would start condensing if there are condensation nucleii is given by

$$\log (N f_{Fe} kT_c) = A_{Fe} - \frac{B_{Fe}}{T_c} \tag{38}$$

with $N = 10^{15}$ cm^{-3} and $f_{Fe} \approx 10^{-5}$ ("cosmic abundance), we find $T_c \sim 1300°K$. (The corresponding gas pressure being $\sim 10^{-4}$ atm.) If T_g is less than T, then T_c is even higher. Since we may fairly

assume that condensation nucleii were ubiquitous in the primordial condensation environment, it does not seem likely that iron would be held back in the gas phase until the temperature falls down to a few hundred degrees.

The following arguments seem to counterindicate case (b), namely, a high pressure condensation environment:

1) A "smeared out" pressure in the primitive solar nebula may be obtained by spreading out all the matter now in the planets, satellites and the asteroids with their appropriate complement of hydrogen and helium over a solar nebula of reasonable shape and size (see e.g. Alfvén and Arrhenius 1970a, Figure 2.6). The maximum pressure obtainable in this way is of the order of 10^{-3} atm. Assumption of pressures much higher than this require that the nebula contain a very large amount of excess matter at the time of condensation. This excess matter must later somehow be "flushed" out of the solar system. The suggestion of a nebula containing excess matter has been made by Cameron (1972) who postulates T-Tauri like solar wind to flush out this matter. However, Cameron also postulates an initial nebula already containing condensed interstellar grains, and hence his theory does not come under purview of the discussion of condensation process.

2) Investigations of meteorites suggest a span of formation time of the meteorites of about 6.10^{7} years (Podosek 1970). This

seems to indicate that the condensable matter, rather than all being present at any given time, was gradually fed into the region of condensation over a comparable span of time and was continually removed from the gaseous phase by condensation. This would require the pressure at any given time to be much less than the "smeared-out" pressure.

3) Several arguments against a neutral gas nebula with high pressure or even the "smeared out" pressure have been presented by Alfvén and Arrhenius (1970a, 1970b, 1973a). Of primary importance is the question of angular momentum of the nebula. There is no satisfactory explanation as to how a neutral gas nebula can be brought into Kepler rotation around the Sun, and even if there is some way to do so, the process of bringing the nebula into Kepler rotation must necessarily take a long time. Until this happens, there is nothing to prevent a free-fall collapse of the nebula. Let us assume for the sake of argument, however, that a pressure gradient has been established in the nebula in such a way that at each point in the nebula the force of gravity is balanced by the pressure gradient force. From this condition, and assuming that the gas temperature is uniform throughout the nebula, we can derive the following relationship for the pressure P at a distance r from the Sun

$$P = P_o \exp\left[- \frac{GM_\odot m}{kT} \frac{r - R}{rR} \right] \tag{39}$$

where P_o is the pressure at a distance R and $M_\odot$ is the mass of the Sun. Thus, in order to have a pressure of 10 atm at 3 AU, we find that the pressure at 1 AU must be about 10^{15} atm if T = 1000°K and we assume the nebula to be made up of molecular hydrogen gas. Such a pressure is of course absurd. Hence it is impossible to maintain such a high pressure nebula distended in the circumsolar region until it has been brought into Kepler rotation - and we have yet to see how the latter situation could be materialized in this type of nebula.

Another significant fact, but perhaps not an argument, in this connection is that there are no observed nebulae in space that seem to indicate the existence of pressures of the order of several tens of atmospheres.

3.3 Thermal equilibrium of grains in a plasma

We have so far established that the gas is a "low pressure" gas ($\leqslant 10^{-3}$ atm). We shall at the outset assume a very general thermal state for this gas, namely, a partially excited, partially ionized gas. A neutral gas or a fully ionized plasma would be special cases of this general state, depending on whether the degree of ionization is zero or one. In the following discussion, we shall assume the gas to consist only of hydrogen.

3.3.1 Sources of heat energy for the grains

A solid grain immersed in such a gas has the following energy sources besides the solar energy and the kinetic energy of the gas

particles: (1) In a plasma, a grain acquires a negative potential ϕ given by

$$\frac{|e\phi|}{kT} = \psi \approx 1.88 \qquad (40)$$

where e is the electronic charge (see Part II of this dissertation. We shall assume here that we are dealing with the thin sheath case, although in reality the radius of the Debye sheath around a small grain condensing from a low density plasma is likely to be much larger than the grain radius. The difference between the two cases is not significant for our discussion, but the assumption of the thin sheath case simplifies the analysis considerably). Due to this potential ϕ, the ions are accelerated towards the grain surface, so that they arrive at the surface with an increased kinetic energy. The electrons on the other hand, are repelled by the potential and arrive at the grain surface with decreased kinetic energy. (2) An ion and an electron can recombine on the grain surface to form a neutral atom thus releasing the ionization energy W_i onto the grain surface (13.6 eV per event for hydrogen atoms). (3) Atoms can recombine on the grain surface to form molecules, thus releasing their association energy W_a onto the grain surface (4.5 eV per event for H_2 molecules).

The heat loss of the grain is due to radiation. The evaporative heat loss of the grain is insignificant compared to this heat loss in cases where condensation exceeds evaporation.

3.3.2 Thermal energy balance of the grains

Let us consider a gas consisting of molecules, atoms, ions and electrons (referred to by subscripts m, a, i and e, respectively), all of which for the sake of simplicity will be assumed to have the same temperature T and a corresponding Maxwellian velocity distribution. We shall discuss here the thermal energy balance of a grain situated in a region of space which is transparent to infrared radiation, so that radiation from the neighboring grains do not constitute a significant heat source for the grain in question. The reason why this situation is appropriate for the discussion of the condensation process is evident from Section 2.8.

As shown earlier, the grain receives from the radiation field an amount of heat

$$G_r = q\sigma T_o^4 \text{ ergs cm}^{-2} \text{ sec}^{-1} \tag{41}$$

The molecules and the atoms in the gas transfer heat energies to the grain given by

$$G_m = N_m \left(\frac{kT}{2\pi m_m}\right)^{1/2} C_m \, 2k(T - T_g) \tag{42}$$

$$G_a = N_a \left(\frac{kT}{2\pi m_a}\right)^{1/2} C_a \, 2k(T - T_g)$$

$$+ \frac{1}{2} N_a \left(\frac{kT}{2\pi m_a}\right)^{1/2} \chi_a \, W_a \tag{43}$$

where χ_a is the fraction of impinging atoms that undergo association on the grain surface and C_m and C_a are the accommodation coefficients for the molecules and the atoms.

Let N be the density of molecules in the gas if the gas were fully neutral and undissociated. In the general thermal state, there are N_m molecules, N_a atoms, N_i ions and N_e electrons (with $N_e = N_i$). Then,

$$N = N_m + \frac{1}{2} N_a \tag{44}$$

and for our purpose, we shall assume that there is dissociative equilibrium between the atoms and the molecules so that the abundance of the atomic species is given by equation (30). A fraction of the atoms are ionized, and we shall assume that the ionizations are due to electron collisions and the recombinations are radiative. Under these conditions, the degree of ionization is given by (Elwert, 1952).

$$\frac{Ni}{N_a - N_i} = 8.3 \times 10^5 \frac{kT}{W_i} \exp\left[-\frac{kT}{W_i}\right] \tag{45}$$

In Part II, we found that due to the negative potential ϕ on the grain surface, there is a drift of the ions and the electrons with a common drift velocity

$$u_D = \left(\frac{k'T}{2\pi m_i}\right)^{1/2} e^{\psi} = \left(\frac{kT}{2\pi m_e}\right)^{1/2} e^{-\psi} \tag{46}$$

The flux of the ions to the grain surface then has two components: one due to the thermal velocity of the ions and one due to the drift of the plasma towards the grain surface. Hence

$$\Gamma_i = 2\pi N_i \left(\frac{m_i}{2\pi kT}\right)^{3/2} \left[\int_0^{\infty}\int_{-u_D}^{\infty} \exp\left\{-\frac{m_i}{2kT}\cdot[u^2+v^2]\right\}(u+u_D)\, v\, du\, dv\right.$$

$$= N_i \left(\frac{kT}{2\pi m_i}\right)^{1/2} \left[e^{-x^2} + \pi^{1/2} x\{1+\mathrm{erf}(x)\}\right] \tag{47}$$

where

$$x^2 = \frac{m_i}{2kT} u_D^2 = \frac{1}{4\pi} e^{2\psi} \tag{48}$$

Similarly, the energy brought to the grain surface by the ions is

$$E_{i,in} = 2\pi N_i \left(\frac{m_i}{2\pi kT}\right)^{3/2} \left[\int_0^{\infty}\int_{-u_D}^{\infty} \exp\left\{-\frac{m_i}{2kT}[u^2+v^2]\right\}(u+u_D)\right.$$

$$v\,\frac{1}{2}m_i\left[(u+u_D)^2+v^2\right] du\,dv = N_i\left(\frac{kT}{2\pi m_i}\right)^{1/2} kT\left(\frac{1}{4}\right)$$

$$\left.\left\{e^{-x^2} + \pi^{1/2} x\left[1+\mathrm{erf}(x)\right]\right\} + e^{-x^2} + 2.8\, x\, \pi^{1/2} + 3x^2 e^{-x^2}\right] \tag{49}$$

Using equations (46) and (48) and noting that erf $(x) \approx 1$ and $e^{-x^2} \ll 1$, the expressions for Γ_i and $E_{i,in}$ simplify to

$$\Gamma_i = N_i \left(\frac{kT}{2\pi m_i}\right)^{1/2} e^{\psi} \tag{50}$$

$$E_{i,in} \approx N_i \left(\frac{kT}{2\pi m_i}\right)^{1/2} e^{\psi} \, 2kT_i \tag{51}$$

with

$$T_i = T \left[1.2 + \frac{1}{8\pi} e^{2\Psi} \right] \tag{52}$$

Thus T_i is the mean effective temperature with which the ions arrive at the grain surface. Introducing the ion accomodation coefficient C_i, the energy input to the grains from the ions becomes

$$G_i = C_i N_i \left(\frac{kT}{2\pi m_i}\right)^{1/2} e^{\psi} \, 2k \, (T_i - T_g) \tag{53}$$

In the case of the electrons, only the electrons with radial velocity u higher than u_e can reach the grain surface, where

$$\frac{1}{2} m_e u_e^2 = \Psi \, kT \tag{54}$$

Note also that in reaching the grain, each electron loses an amount of energy $\frac{1}{2} m_e u_e^2$. Hence the particle and the energy fluxes for the electrons are given by

$$\Gamma_e = 2\pi N_e \left(\frac{m_e}{2\pi kT}\right)^{3/2} \left[\int_0^\infty \int_{u_e}^\infty \exp\left\{-\frac{m_e}{2kT}\cdot[u^2+v^2]\right\}(u+u_D)\, v\, du\, dv \right. \tag{55}$$

$$E_{e,in} = 2\pi N_e \left(\frac{m_e}{2\pi kT}\right)^{3/2} \left[\int_0^\infty \int_{u_e}^\infty \exp\left\{-\frac{m_e}{2kT}[u^2+v^2]\right\}\left(u+u_D\right)\right.$$

$$\left. v\,\frac{1}{2}m_e\left[\left(u+u_D\right)^2 + v^2 - u_e^2\right] du dv \right| \tag{56}$$

On evaluating the integrals and neglecting the small terms (note that $u_e \gg u_D$), we get

$$\Gamma_e = N_e \left(\frac{kT}{2\pi m_e}\right)^{1/2} e^{-\psi} \tag{57}$$

$$E_{e,in} = N_e \left(\frac{kT}{2\pi m_e}\right)^{1/2} e^{-\psi}\, 2kT \tag{58}$$

Using the accommodation coefficient C_e for the electrons, the energy input to the grain from the electrons is now given by

$$G_e = C_e N_e \left(\frac{kT}{2\pi m_e}\right)^{1/2} e^{-\psi}\, 2k(T - T_g) \tag{59}$$

Finally the energy input to the grain due to the recombination of the ions on the grain surface is given by

$$G_{rec} = N_i \left(\frac{kT}{2\pi m_i}\right)^{1/2} e^{\psi} \chi_i W_i \tag{60}$$

where χ_i is the fraction of impinging ions that undergo recombination on the grain surface.

The overall energy balance equation is now given by

$$G_m + G_a + G_i + G_e + G_{rec} = L \tag{61}$$

with

$$L = q\sigma T_g^4 \tag{62}$$

In Figure III-7 we have plotted the solutions of equation (61) for various values of N with $q = 0.75$ (appropriate for iron; see Table III-1), $T_o = 150°K$ and with all accommodation coefficients and χ_a and χ_i equal to 0.1. We have also plotted the degree of ionization as a function of the gas temperature. Note the following features of these solutions:

1) For gas densities (N) of the order of $10^{10}\ cm^{-3}$ or less, the grain temperature is independent of the gas temperature in the entire range $T = 2000\text{-}20,000°K$.

2) The grain temperature is more sensitive to the gas temperature in an ionized gas than in a neutral gas.

FIGURE III-7

The equilibrium grain temperatures including the effects of dissociation and ionization of the gas.

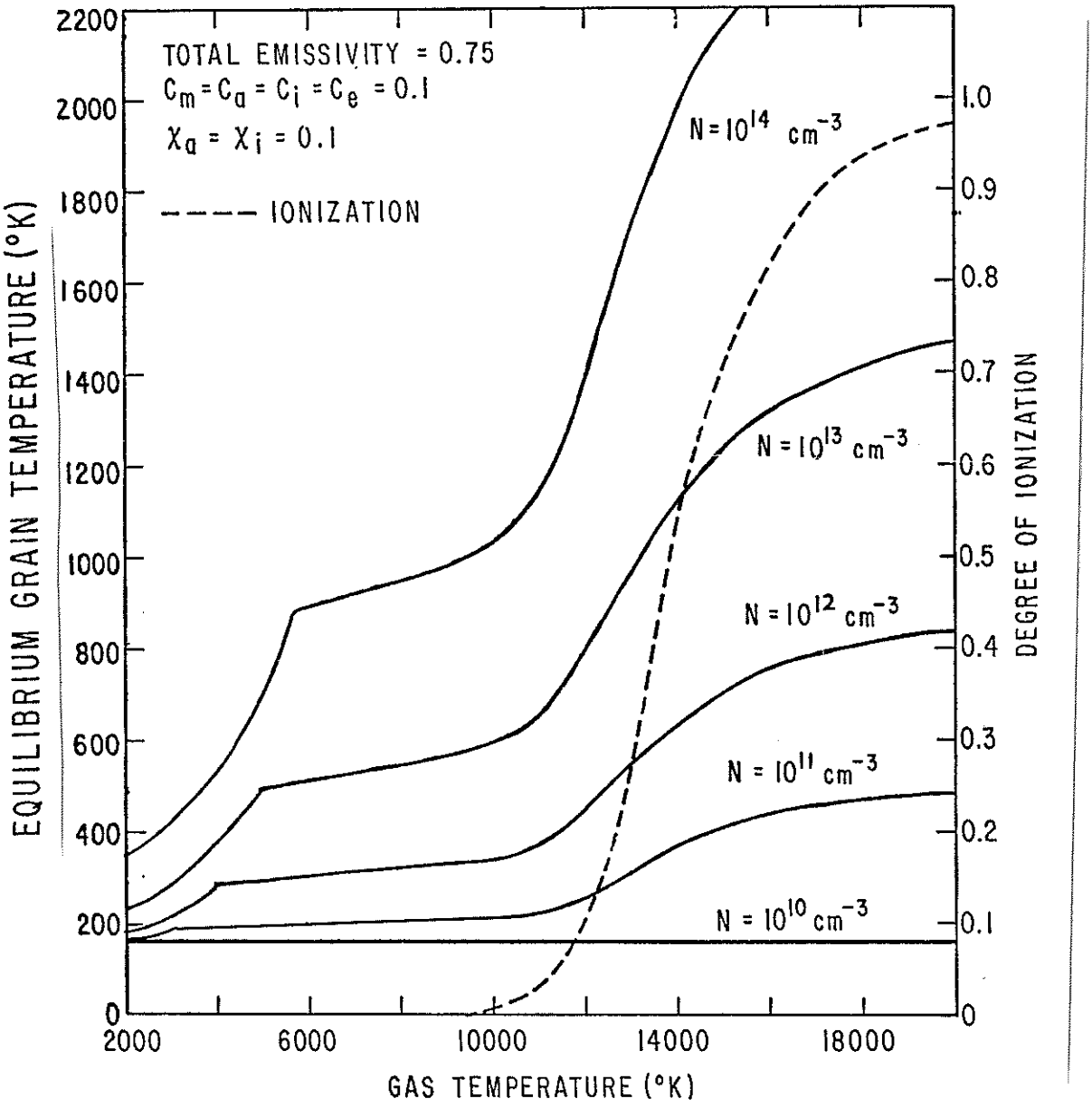
TOTAL EMISSIVITY = 0.75
$C_m = C_a = C_i = C_e = 0.1$
$\chi_a = \chi_i = 0.1$
---- IONIZATION
$N = 10^{14}$ cm^{-3}
$N = 10^{13}$ cm^{-3}
$N = 10^{12}$ cm^{-3}
$N = 10^{11}$ cm^{-3}
$N = 10^{10}$ cm^{-3}
EQUILIBRIUM GRAIN TEMPERATURE (°K)
DEGREE OF IONIZATION
GAS TEMPERATURE (°K)
0
200
400
600
800
1000
1200
1400
1600
1800
2000
2200
2000
6000
10000
14000
18000
0
0.1
0.2
0.3
0.4
0.5
0.6
0.7
0.8
0.9
1.0

3) With $N \sim 10^{14}$ cm^{-3}, the grain temperature exceeds the melting point of even refractory substances for gas temperatures $\geq 13,000°K$.

4) The "knees" of the curves in the gas temperature range 3000-6000°K arise due to the onset of dissociation resulting in substantial heating of the grains by the "atomic hydrogen torch" effect. A similar increase in heating occurs at the onset of ionization due to the large amounts of energy brought in by the ions and the electrons and due to their recombination on the grain surface.

Let $P_\alpha = N_\alpha kT$ represent the pressure of α component of the gas, so that the total gas pressure P is given by

$$P = \sum_\alpha P_\alpha = P_m + P_a + P_i + P_e \tag{63}$$

Let us also define a weighted mean pressure $\hat{P}$ in the following way

$$\hat{P} = \frac{\sum_\alpha w_\alpha P_\alpha}{\sum w_\alpha} \tag{64}$$

where

$$w_m = \frac{1}{\sqrt{2}} C_m$$

$$w_a = C_a + \frac{\chi_a w_a}{2k(T - T_g)}$$

$$w_i = \left[\frac{T_i - T_g}{T - T_g} C_i + \frac{\chi_i w_i}{2k(T - T_g)} \right] e^{\psi}$$

$$w_e = e^{-\psi} C_e \tag{65}$$

With this definition, the energy balance equation (61) may be written as

$$P = \frac{1}{\sum_{\alpha} w_{\alpha}} \left[\left(\frac{\pi m_a T}{2k} \right)^{1/2} q\sigma \frac{T_g^4 - T_o^4}{T - T_g} \right] \tag{66}$$

A will be found later (see Figure III-7), T is much larger than T_g in the situation of our interest. Hence $\hat{P}$ varies roughly as $T^{1/2}$. We shall further show that the maximum and the minimum values of T in our problem should be of the order of 10^4°K and 3×10^3°K respectively. Hence $\hat{P}$ is relatively insensitive to the variation of T. The upper and the lower limits of $\hat{P}$ for a given value of T_g are therefore given by the lower and the upper llimits of the quantity $\sum_{\alpha} w_{\alpha}$.

Let us also note from the theory of averages that the weighted mean is greater than or equal to the geometric mean. Hence

$$\hat{P} \geq P \tag{67}$$

3.4 Upper limit of pressure and lower limit of temperature

From equation (67) it is obvious that if we can find the upper limit of $\hat{P}$, then the maximum value of P will be less than or equal to this value. Let us therefore try to find an upper limit to the quantity $\hat{P}$.

Note from equation (66) that $\hat{P}$ is maximum when the quantity $\sum_{\alpha} w_{\alpha}$ is minimum. The minimum value of this quantity is simply w_m, which obviously occurs for a neutral, undissociated gas. For hydrogen this requires that the gas temperature be less than about 3000°K, above which the dissociation of H_2 becomes important. Since, on the other hand, the gas temperature must be well in excess of 2000°K in order to have grain temperatures in the range 1000-2000°K with pressures $\leq 10^{-3}$ atm (see Figure III-7), it seems that a gas temperature of the order of 3000°K is a reasonable lower limit for the gas at condensation. Thus, the lower limit of gas temperature is associated with the upper limit of the gas pressure.

The upper limit of $\hat{P}$ for a given solid temperature is now found from equation (66) by setting $T = 3000°K$ and $\sum_{\alpha} w_{\alpha} = w_m$. Since in this case $P_a = P_i = P_e = 0$, the corresponding upper limit of the gas pressure is

$$\overline{P} = P_m = \hat{P} \tag{68}$$

In Figure III-8, we have plotted this limit as a function of grain temperature T_g for two different values of the accommodation coefficient C_m: 1 and 0.1. Note that in the case $C_m = 0.1$, which was shown to be a reasonable value in Section 2.4, the upper limit of gas pressure exceeds the value 10^{-3} atm, which we had adopted earlier as a natural upper limit of the gas pressure at condensation. The reason for this discrepancy is that this upper limit - the neutral gas limit - although allowed by the energy conservation law, is unrealistic for the process of condensation. Let us therefore look for the other extreme, the lower limit of the gas pressure as permitted by the law of conservation of energy.

3.5 Lower limit of pressure and upper limit of temperature

The lower limit of $\hat{P}$ occurs when the quantity $\sum_\alpha w_\alpha$ is maximum. This value is obviously given by

$$\left\{ \sum_\alpha w_\alpha \right\}_{max} = w_i + w_e \tag{69}$$

since for hydrogen $w_i > w_a$. The above situation occurs in a fully ionized plasma, for which the minimum gas temperature is somewhat in excess of 10^4°K. A temperature of the order of 10^4°K can be established as the upper limit of the gas temperature from the criterion discussed in the following.

The sputtering threshold for metal surfaces bombarded with ions is about 5 eV (Kaminsky 1965, p. 151). As pointed out earlier,

an ion in reaching a grain surface is accelerated through an energy of the order of 2 kT eV. For a plasma at 10^4°K ($\approx$ 1 eV), an ion receives an additional energy of 2 eV. Thus ions in the plasma which have energies in excess of 3 eV become likely candidates for sputtering. The fraction of such ions in a plasma is given by

$$f_s = 2(\pi k^3 T^3)^{-1/2} \int_{3.0}^{\infty} \exp\left(-\frac{E}{kT}\right) E^{1/2}\, dE \qquad (70)$$

The values of this fraction at gas temperatures 1.10^4°K and 1.5×10^4°K are about 0.1 and 0.2, respectively. However, at temperatures close to 10^4°K, the degree of ionization is very low (see Figure III-7) and hence there do not exist substantial number of ions to cause sputterings. At 1.5×10^4°K, the gas is almost fully ionized and sputtering becomes important. Thus a temperature of the order of 1.10^4°K represents a reasonable upper limit of temperature at condensation.

In order to find a lower limit to the pressure, we shall assume that the plasma is fully ionized, with an order-of-magnitude temperature of 10^4°K. The quantity $\hat{P}$ for a fully ionized hydrogen plasma becomes

$$\hat{P} = \frac{1}{2} P \qquad (71)$$

where we have put $P_i = P_e = \frac{1}{2} P$. Now the minimum value of P can be obtained from equation (66) by substituting in it equation (69) and $T = 10^4$°K. The corresponding value of $\hat{P}$ can be obtained from

equation (71), where we must put $C_i = C_e = \chi_i = 1$ so as to obtain a lower limit to the gas pressure

$$\underline{P} = 2\hat{P} \tag{72}$$

This limit has been plotted in Figure III-8 as a function of the grain temperature and has been labelled the "plasma limit."

3.6 Vapor pressure and partial pressure of the condensing species

Having established the limits of gas pressure in the primordial condensation environment, we must now ask ourselves: Do these gas pressures satisfy the requirement for condensation that the partial pressure of the condensing species in the gas must exceed the vapor pressure of the species at the grain temperature? Since elemental iron is a major constituent of meteorites, we have chosen this element as an example in discussing the above question. In Figure III-8 we have plotted the vapor pressure or iron as a function of the grain temperature using equation (37). We have also plotted the partial pressure of iron in the case of the lower gas pressure limit using "cosmic abundance ratio," i.e. a number ratio of iron to hydrogen of the order of 10^{-5}.

Note that even for the lower gas pressure limit, condensation of iron is possible for grain temperatures up to $\sim$ 1200°K. In fact, if the abundance ratios in the primordial condensation environment were higher than the cosmic abundance ratios as suggested by Anders

FIGURE III-8

The ranges of gas pressure in the meteorite condensation environment as a function of the grain temperature. In the upper limit (the neutral gas limit) the gas is neutral and undissociated. In the lower limit (the plasma limit), the gas is fully ionized. The region between these two limits represents a partially dissociated, partially ionized gas.

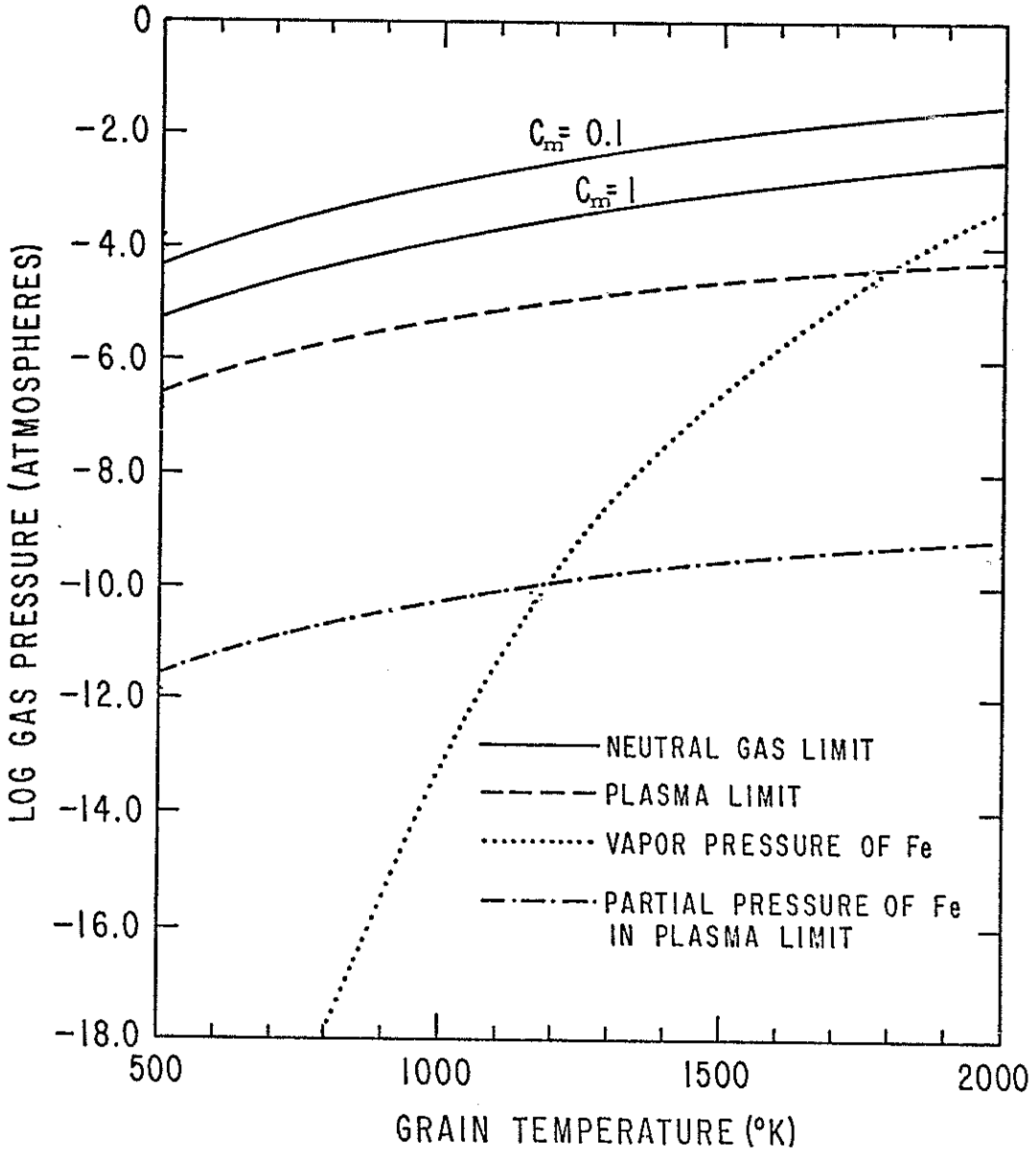
0
-2.0
-4.0
-6.0
-8.0
-10.0
-12.0
-14.0
-16.0
-18.0
LOG GAS PRESSURE (ATMOSPHERES)
500
1000
1500
2000
GRAIN TEMPERATURE (°K)
C_m= 0.1
C_m= 1
NEUTRAL GAS LIMIT
PLASMA LIMIT
VAPOR PRESSURE OF Fe
PARTIAL PRESSURE OF Fe
IN PLASMA LIMIT

(1971b), the upper limit of grain temperature for the condensation of iron would be still higher.

3.7 The case for plasma

In Figure III-8 we have established the two limits of the gas pressure - the upper limit or the neutral gas limit and the lower limit or the plasma limit. The region between these two limits represents a partially dissociated, partially ionized gas and constitutes the domain of condensation. In this section we shall present the following arguments showing that the realistic condensation environment is likely to be closer to the plasma limit than the neutral gas limit:

1) There are a number of observed features in meteorites that suggest that the gas from which their material condensed was at least partially ionized. These features have been discussed by Arrhenius and Alfvén (1971) and by Arrhenius (1971). The sequence of condensation of various elements as observed in meteroties is explainable in a satisfactory way if one assumes that the condensation took place from a partially ionized gas. A certain species which is expected to condense from a neutral gas at a given grain temperature may be held back in the gas phase if it is ionized for the same grain temperature - because of the selective condensation of neutral species compared to the ionized species. Thus the sequence of condensation as expected from a neutral gas may in some cases be different from that expected

from an ionized gas for the same grain temperature. A case in point is that of thallium-mercury pair. Both these elements are highly voltile, mercury even more so than thallium. They differ, however, in their neutralization temperature (the temperature at which the degree of ionization is 0.5) by a factor of 2 - about 11,500°K for mercury and 5900°K for thallium. These elements, due to their volatility, are concentrated in those meteoritic materials which for several reasons appear to constitute relatively low grain temperature condensates. However, in comparison to thallium, this fractionation is found to be much less pronounced in the case of mercury. Arrhenius and Alfvén (op. cit.) have ascribed this effect to the marked differential ionization of the two elements. Mercury as neutral atoms becomes available for occlusion in the low temperature grains already at high plasma temperatures (10,000°K), while thallium is retained in the gas phase and condenses appreciably only in a plasma temperature range well below 5000°K.

Several other similar features in the meteorites all point in favor of a high temperature partially ionized gas. At the same time, laboratory experiments in plasma condensation have demonstrated the possibility of producing by this method condensates with structural properties similar to those observed in meteorites.

2) Note in Figure III-8 that the neutral gas limit with a reasonable value of the constant C_m (= 0.1) yields gas pressures as large as 10^{-2} atm for high grain temperatures. In Section 3.2 we have given several arguments against such high gas pressures. This indicates that the neutral gas limit is an unrealistic condensation environment. The realistic condensation environment must be lower in the diagram, i.e. in the region of partial ionization and partial dissociation.

3) Investigation of remanent magnetization in meteorites (Brecher 1972) indicates that some of the meteoritic samples formed in regions permeated by magnetic field of the order of 0.1 - 1 gauss. If magnetic fields of such strengths in the meteorite formation region (2 - 4 AU) were to be produced by a solar dipole field, it would require a dipole field 10^7 - 10^8 times larger than it is today. A discussion of such assumption involves a long chain of speculation. There is no observational justification at the present time of such high stellar magnetic fields for stars similar to the Sun.

On the other hand, if condensation took place from an ionized gas, magnetic fields of the strengths indicated may arise in a natural way. Flow of electric current is a very common phenomenon in space plasmas (e.g. solar corona, earth s magnetosphere, etc.) and such currents generate their own magnetic fields. Thus the magnetization

of meteorites find a natural explanation if we assume a plasma origin of the solids.

4) An experimentally observed and theoretically explainable ionization phenomena that may ionize the primordial gases during their acceleration towards the Sun has been suggested by Alfvén and Arrhenius (1973b). This is known as the critical velocity phenomenon. When the infall velocity of a gas exceeds a certain value characteristic of the gas, it becomes at least partially ionized if it passes through a region of preexisting ions and electrons. Once such ionization takes place, it can be maintained by the energy liberated in the gas as the central body transfers angular momentum to the gas. The support of the gas against the gravitational pull of the central body is provided by forces arising from the interaction of the currents flowing in the gas with the magnetic dipole field of the central body, until the gases are brought into a special state of rotation, known as the partial corotation.

Hence a plasma condensation environment seems to be experimentally indicated (argument 1), physically consistent (argument 2), observationally called for (argument 3) and astrophysically understandable - at least in a preliminary way (argument 4).

4. THE CONDENSATION PROCESS IN THE STATE OF TEMPERATURE DISEQUILIBRIUM

4.1 Growth and decay of solids

In this section we shall try to examine the rate of condensation and evaporation of solids in the plasma limit, i.e. a gas temperature of the order of 10^4°K with most substances highly ionized. The domain of growth of solids is then given by the range of gas density and grain temperature for which condensation exceeds evaporation. If the latter exceeds the former, the net result is a decay of the solids. This range of gas density and grain temperature will be termed the domain of decay of the solids.

Let f_α be the abundance ratio by number of a species α in the gas phase relative to hydrogen, and χ_α be the sticking probability of this species onto the grain surface and ξ_α, the rate of condensation in gm cm^{-2} sec^{-1}. Then

$$\xi_\alpha = f_\alpha \chi_\alpha N m_\alpha V_\alpha \tag{73}$$

where V_α is given

$$V_\alpha = \left(\frac{kT}{2\pi m_\alpha}\right)^{1/2} \tag{74}$$

Since neither the value of f_α nor χ_α is known with certainty, we can treat $f_\alpha \chi_\alpha$ as a parameter and use a range of possible values of this

parameter. Equation (73) may be written as

$$\xi_\alpha(T_g) = f_\alpha \chi_\alpha m_\alpha V_\alpha N_i(T_g) \tag{75}$$

where $N_i(T_g)$ is the number density of hydrogen ions as a function of the grain temperature as given by equation (61) in the plasma limit. Hence, combining equations (61) and (75) we can now plot ξ_α as a function of T_g. In Figure III-9 we have plotted the condensation rate of iron (for $f_\alpha \chi_\alpha = 10^{-5}$ and 10^{-8}). The upper abscissa in Figure II-9 gives the gas densities corresponding to the grain temperatures in the lower abscissa.

The rates of evaporation η_α in gm cm^{-2} sec^{-1} for various elements are given by Dushman (1962) and may be written as

$$\log \eta_\alpha = C_\alpha - 0.5 \log T_g - \frac{B_\alpha}{T_g} \tag{76}$$

where the values of the constants B_α and C_α are given in the above reference. In Figure III-9 we have also plotted the rates of evaporation of iron as a function of the grain temperature.

The domain of growth of iron extends to $T_g \approx 1150°K$ ($N_i \approx 3.10^{12}$ cm^{-3}) for $f_\alpha \chi_\alpha = 10^{-5}$ and to $T_g \approx 950°K$ ($N_i \approx 2.10^{12}$ cm^{-3}) for $f_\alpha \chi_\alpha = 10^{-8}$. Beyond these limits, the condensation of iron grains is not possible.

FIGURE III-9

Condensation and evaporation rates of solids in the plasma limit. Condensation is possible for ranges of grain temperatures and gas densities (upper abscissa) for which the rate of condensation exceeds the rate of evaporation.

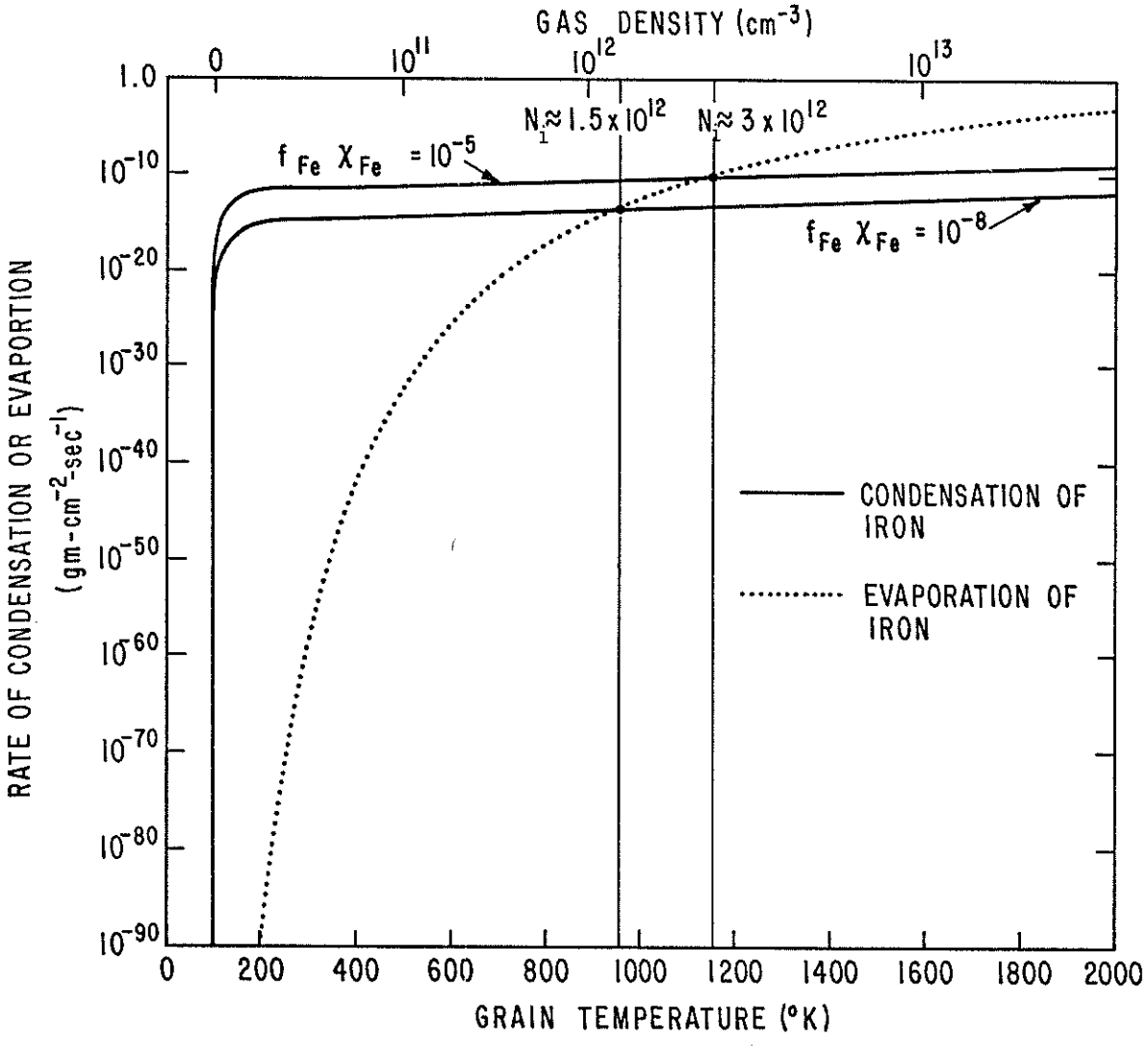
GAS DENSITY (cm^{-3})
0
10^{11}
10^{12}
10^{13}
1.0
10^{-10}
10^{-20}
10^{-30}
10^{-40}
10^{-50}
10^{-60}
10^{-70}
10^{-80}
10^{-90}
$N_1 \approx 1.5 \times 10^{12}$
$N_1 \approx 3 \times 10^{12}$
$f_{Fe}\ X_{Fe} = 10^{-5}$
$f_{Fe}\ X_{Fe} = 10^{-8}$
CONDENSATION OF IRON
EVAPORATION OF IRON
RATE OF CONDENSATION OR EVAPORTION (gm-cm^{-2}-sec^{-1})
0
200
400
600
800
1000
1200
1400
1600
1800
2000
GRAIN TEMPERATURE (°K)

4.2 Growth rates

An estimate of the growth rate for a grain of radius a may be obtained from the relation

$$\frac{da}{dt} = \frac{1}{\rho_\alpha} (\xi_\alpha - \eta_\alpha) \tag{77}$$

where ρ_α is the density of the condensing substance. Thus for iron grains in the case $f_\alpha \chi_\alpha = 10^{-5}$ and $T_g = 1000°K$, we find from Figure III-9 that $\xi_\alpha - \eta_\alpha \approx 10^{-10}$ gm cm^{-2} sec^{-1}. The corresponding growth rate is about 100 Å per day.

We have discussed the domain of growth for the case of the plasma limit since according to our discussion in Section 3.7 the actual condensation environment is likely to be closer to the plasma limit than to the neutral gas limit. If, however, the gas temperature is somewhat lower than $10^4°K$, e.g. in the range 6000 - 8000°K, then hydrogen is largely neutral, but almost fully dissociated. In this case the major heat source for the grain will be the association of H atoms on the grain surface rather than the recombination of H^+ ions. Calculation in this case shows that the domain of growth for iron for $f_\alpha \chi_\alpha = 10^{-5}$ shifts to about $T_g \approx 1200°K$ and the corresponding gas density is about 5.10^{13} cm^{-3}. This gives us a rough idea of how the domain of growth is affected by lowering of the gas temperature.

It is suggested here that the method briefly outlined above may be useful in the study of condensation processes and the condensation

sequence of various species under the condition of temperature disequilibrium. The critical parameter involved in such an analysis is the sticking probability. Laboratory experiments under simulated space environment may provide important information about this parameter.

5. SUMMARY AND IMPLICATIONS

We have shown that a physically consistent meteorite condensation environment, particularly for the condensation of the major component iron, which is also consistent with the observations in meteorites, has the following properties:

1) The temperature of the gas is in the range 3000 - 10,000°K, but is likely to be closer to the upper limit.

2) The upper limit of the total gas density that permits growth is about 10^{13} - 10^{14} cm^{-3}. The corresponding upper limits of the gas pressure is of the order of 10^{-5} - 10^{-4} atm.

3) The upper limit of the growth rate of iron grains is about 100 Å per day. Thus the condensation is essentially a slow, and not a catastrophic process.

Much of the discussion in this paper may also apply to the condensation environment of the planetary material - in particular the material in the terrestrial planets. In that case the above conclusions should be applicable to this environment - thus providing us with important clues to the origin and evolution of the solar system.

REFERENCES FOR III

Alfvén, H. and Arrhenius, G.: 1970a, Astrophys. Space Sci. 8, 338.

Alfvén, H. and Arrhenius, G.: 1970b, Astrophys. Space Sci. 9, 3.

Alfvén, H. and Arrhenius, G.: 1973a, Astrophys. Space Sci. 21, 117.

Alfvén, H. and Arrhenius, G.: 1973b, Structure and evolutionary history of the solar system, IV (preprint)

Anders, E.: 1971a, Ann. Rev. Astron. Astrophys. 9, 1.

Anders, E.: 1971b, Geochim. Cosmochim. Acta 35, 516.

Anders, E.: 1972a, On the Origin of the Solar System, H. Reeves, ed., Centre Nationale de la Recherche Scientifique, Paris, 179.

Anders, E.: 1972b, From Plasma to Planet, Proc. Nobel Symp. 21, A. Elvius, Ed., Wiley, N. Y., 133.

Arrhenius, G.: 1972a, On the Origin of the Solar System, H. Reeves, ed., Centre National de la Recherche Scientifique, Paris, 80.

Arrhenius, G.: 1971, Proceedings of Nobel Symposium 21, from Plasma to Planet, A. Elvius, ed., Almqvist and Wiksell, Stockholm.

Arrhenius, G., 1972b. From Plasma to Planet, Proc. Nobel Symp. 21, A. Elvius, ed., Wiley, N. Y., 117.

Arrhenius, G. and Alfvén, H.: 1971, Earth Planet. Sci. Letters 10, 253.

Baule, B.: 1914, Ann. Physk, 44, 145.

Brecher, A. and Arrhenius, G.: 1971, Nature 230, 107.

Brecher, A.: 1972, Ph.D. Thesis, University of Calfornia, San Diego, La Jolla, Ca.

Cameron, A. G. W.: 1972, Accumulation Processes in the Primitive Solar Nebula, (preprint).

Dushman, S .: 1962, Scientific Foundations of Vacuum Technique, Wiley, New York.

Elwert, G.: 1952, Z. Naturforsch. 72, 432.

Grossman, L.: 1973, Geochim. Cosmochim. Acta 37, 635.

Kahn, F. D. and Dyson, J. E.: 1965, Ann. Rev. Astron. Astrophys. 9, 47.

Kaminsky, M.: 1965, Atomic and Ionic Impact Phenomena on Metal Surfaces, Springer-Verlag, Berlin.

Lehnert, B.: 1970, Cosmical Electrodyn. 1, 219.

McAdams, W. H.: 1954, Heat Transmission, McGraw-Hill, New York.

McCarroll, B. and Ehrich, G.: 1963, J. Chem. Phys. 38, 523.

Podosek, F. A.: 1970, Geochim. Cosmochim.Acta 34, 341.

Spitzer, L.: 1968, Diffuse Matter in Space, Interscience, New York.

Tsuji, T.: 1964, Annals of the Tokyo Astonomical Observatory Second Series, vol. IX, No. 1, p. 1.

Urey, H. C.: 1952, The Planets: Their Origin and Development. Yale Univ. Press, New Haven, 245.

IV. ORIGIN OF THE OCEAN

1. SOURCES OF NEW INFORMATION

Our records of the early history of the ocean and of the composition and evolution of the interior of our planet are fragmentary. Inquiries based on modern geophysical and geochemical data were made in the classical studies by Rubey (1951, 1955) and Urey (1952) and in other important papers related to this subject and referred to in context below.

Lars Gunnar Sillén's interest was drawn to the early phase of the Earth's history as a logical extension of his fundamental work on the chemical dynamics of the ocean. The question of how the controlling chemical processes differed from now at the time when life was possibly absent was one of the last scientific problems that he embarked on (Sillén, 1965, 1966). He also began to devote his interest to the primordial condensation processes in space, using thermodynamic equilibrium considerations as a first, although admittedly unrealistic, approximation. The usefulness of such an approach in guiding necessary disequilibrium considerations (Arrhenius 1972, Arrhenius and Alfvén 1971) has subsequently been demonstrated by Lord (1965), Larimer (1967), Anders (1971) and most recently by Grossman (1972).

In the last five years results of great significance have been obtained and new insights have been gained from theoretical developments inspired largely by the exploration of space. Among materials that cast new light on the early history of the planet are the oldest

known preserved sedimentary rocks from South Africa (~ 3.0 Gy; Engel et al., 1968) and preserved crustal sections as old as 3.9 Gy recently found in Greenland (Black et al., 1971). The intensified studies of meteorites have also given important clues to the sources of the Earth's atmosphere and ocean (Wasson, 1969; Fanale, 1971). Most importantly, the exploration of the Moon has placed the planetary evolution and the history of the Earth in an entirely new perspective. This is being further broadened by missions to still more primitive objects in the solar system: comets, asteroids and planetary satellites.

The new facts accumulating from measurements on the lunar surface and on samples returned from the Moon are providing perhaps the most important guidance in assessment of the various possibilities for the evolution of the Earth. These observations have drawn attention to circumstances of crucial importance in the early history of the planet which now appear straightforward but which were nonetheless largely ignored in the Earth-limited era of Earth Sciences. In general, these results emphasize the fact that the problems of the origin and evolution of the ocean and the atmosphere cannot be resolved realistically without referring to the processes by which the Earth itself formed. The observational data pertinent to these problems do not support the previously common notion that the differentiation takes place and the ocean and the atmosphere develop after the Earth had

already formed. On the contrary, the processes leading to the formation of the Earth must themselves play a decisive role in producing the differentiation and in giving rise to the precursors for ocean and atmosphere while the Earth was still in a state of formation.

2. FORMATION OF THE SOLAR SYSTEM

It is now generally believed that the creation of planets can only take place by accumulation of small solid bodies (planetesimal accretion). Formation of planets from individual contracting gas clouds is excluded because of insufficient gravitation; such a process seems impossible even for a giant planet like Jupiter (Hattori et al., 1969; Kumar, 1972). Hence, it is likely that the Earth has accumulated from a large number of small bodies in space. Considerations of orbital and spin characteristics of the Earth and other planets and their satellites place stringent requirements or limitations on the assumed dynamic state of these building blocks referred to here as grains, aggregates, embryos and planetesimals (Alfvén, 1942-5; Schmidt, 1944; Safronov, 1954; Alfvén, 1954; Levin, 1972; Alfvén and Arrhenius, 1970a, 1973).

When the formation of our solar system began, matter in the form of gas and dust must somehow have become emplaced in the circumsolar region. Several different explanations of this emplacement have been suggested; reviews of these are given by ter Haar (1967) and Hartman (1972). Most theories attempt an explanation of the present

properties of the planetary system but ignore the three well developed satellite systems.

In an evolutionary scheme that attempts to account for the present state of both planetary and satellite systems (Alfvén and Arrhenius, 1970a, b, 1973), the Sun at the outset attracted gas and dust by gravitation. The history of formation of the Sun itself is highly uncertain; it could have been formed by collapse of a gas cloud but equally well by a stellesimal accretion process similar to the planetesimal process. None of these processes have been observationally verified. In contrast, the processes that can realistically be invoked to explain the late evolution of the solar system and, with less certainty, the formative state, can all be identified with processes observable today.

The neutral gas particles in the circumsolar region presumably became ionized upon reaching their critical velocity for ionization by gravitational acceleration toward the Sun. The same process occurred around the magnetized protoplanets (Jupiter, Saturn and Uranus) after their formation. The resulting plasma was stopped by the magnetic field at various distances from these central bodies, determined by the atomic mass and the ionization potential of the controlling chemical species in the neutral gas. The plasma was brought into its necessary rotational state by magnetohydrodynamic transfer of angular momentum from the central bodies.

Under the combined action of the gravitational and the magnetic fields, the plasma acquired a state of motion referred to as partial co-rotation. The plasma rotating around the Sun provided the material that, after condensation to small particles, aggregated to larger bodies which ultimately gave rise to the planets. The theory draws on the similarity between the planetary system and the three regular satellite systems (Jovian, Saturnian and Uranian) and stresses that the regular satellites must have formed around the planets by the same series of processes by which the planets formed around the Sun. The existence of four analogous systems thus removes the constraint of relying solely on the Sun-planet system for relevant information.

3. OCCLUSION OF VOLATILES IN SOLID CONDENSATES

Condensation from the partially corotating plasma around the Sun led to the formation of solid grains, which by inheriting the momentum of the parent plasma, assumed eccentric Kepler orbits. Such grains appear to have been preserved to this day in space as aggregates; some fragments of these are dense and strong enough to survive passage through the atmosphere and are known to us as meteorites.

Individual grains of this kind are abundant components of certain types of meteorites (carbonaceous chondrites). Such grains often form isolated crystals and twins of high regularity (Figure IV-1) or rounded crystalline aggregates with cavities preserving the

FIGURE IV-1

Delicate leafy crystals of the magnesium-iron silicates of olivine and pyroxene, frequently twinned, and loosely adhering to each other. These crystals form a characteristic component of the porous regions of the carbonaceous chondrite Allende. The thickness of the crystal leaves is of the order of 100 Å, tapering off toward the edges.

The crystal habit and the lack of significant adhesion show that the crystals and twinned aggregates grew from a vapor phase. The preservation of their delicate features indicates their relative velocities at aggregation must have been low, perhaps in the range of meters per second or lower (from Arrhenius and Asunmaa, 1973).

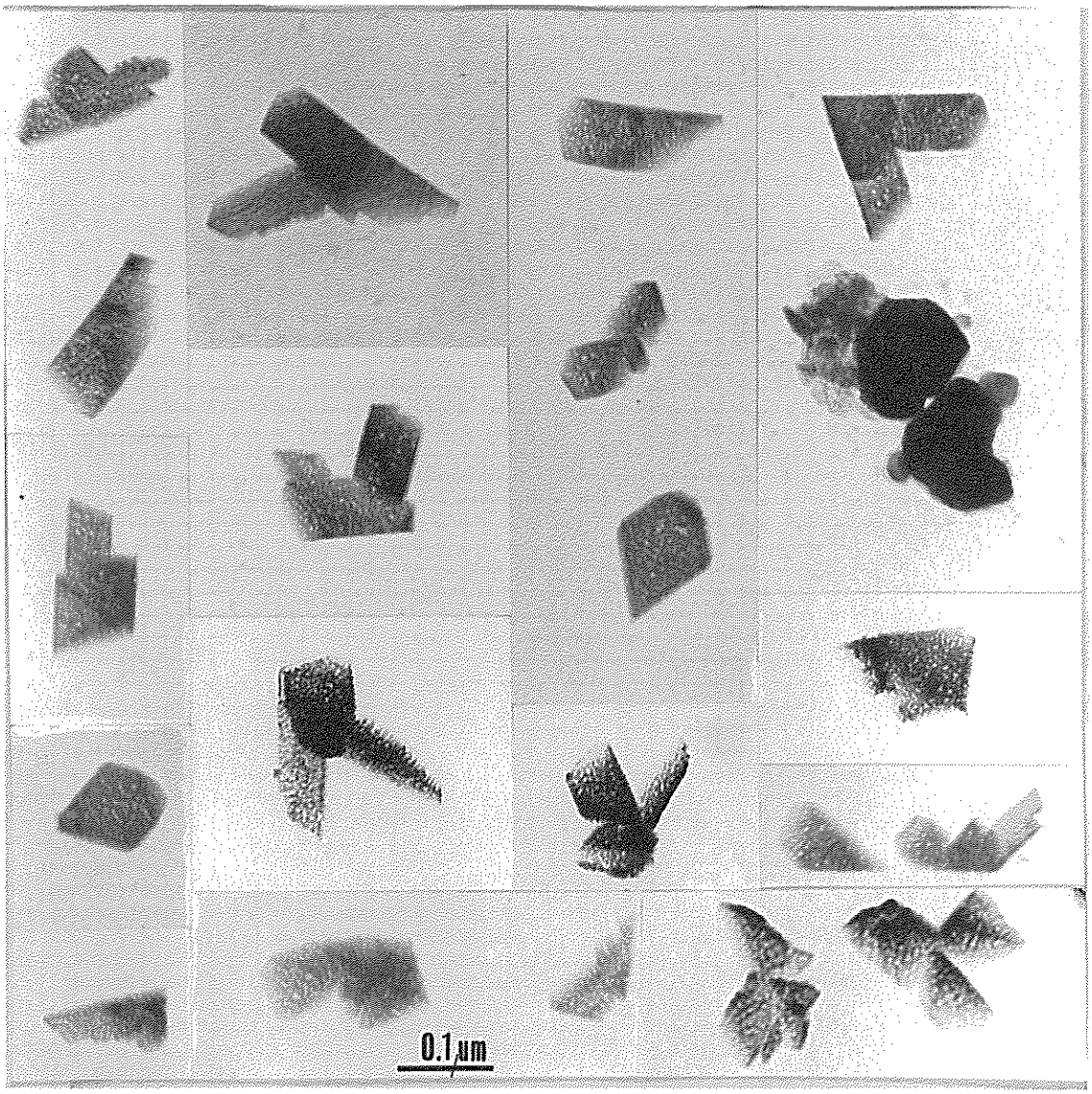
0.1 µm

crystal-vapor interface and showing delicate growth features such as freely grown calcium silicate fibers (Fuchs, 1969).

This meteoritic material, believed to represent a primordial condensate but not necessarily to be identified with the material that formed the Earth, also has chemical features indicative of the conditions of growth. Among these is the incorporation of volatile components such as noble gas atoms and halogen- and hydroxyl ions in some types of crystals. The noble gas components are particularly useful for the study of the mode of incorporation since they do not develop strong chemical bonds with the host structure.

Aside from surface implanted and radiogenic components which have different and characteristic signatures and which will not be discussed here, the noble gas component of particular interest to the problems of the Earth is the component which is strongly bound through the volume of the crystals and requires high activation energies for release. This indicates that the noble gas atoms were incorporated as impurities in crystal imperfections at growth from the vapor phase.

The fact that the occluded noble gas component is strongly bound internally in the crystals shows that the incorporation took place as a part of the crystallization process and not by subsequent surface adsorption or other low energy processes. Furthermore, it is well known from experiments that for such noble gas occlusion to be significant, the temperature of the crystals has to be below the range

400-600°K. The vapor phase temperature, however, must have been an order of magnitude higher for several reasons. One such reason is the requirement for sufficient concentration of vapor components to permit growth; at the low vapor pressures of silicates and oxides this is not possible if the vapor were in temperature equilibrium with the grains at the temperature indicated (Arrhenius and Alfvén, 1971). Another reason is the need for the gas particles to provide sufficient kinetic energy to heat the grains at the relevant plasma densities ($< 10^{12}$ cm^{-3}). These maximum densities are required to permit the momentum transfer process to operate. In this density range, gas temperatures of the order 10^4 K are required (Lehnert, 1970; Arrhenius, 1972; De and Arrhenius, 1973) to maintain grain temperatures in the range 300-900°K indicated by the chemical record (Larimer, 1967; Larimer and Anders, 1967, 1970; Grossman, 1972).

Hence we are concerned here with a thermal steady state which must be common in gas-solid systems in space and where crystallizing grains at comparatively low temperature are immersed in, and exchange matter and energy with, a hot, optically thin, partially ionized gas.

4. PRIMORDIAL GRAINS AS CARRIERS OF ATMOSPHERIC AND OCEANIC COMPONENTS

The composition of the occluded noble gas component in primordial condensates gives useful clues to the origin of the atmosphere of the Earth and the formation of its ocean. Measurements on

meteorites show that this component characteristically has a relative abundance distribution of primordial noble gas species which is closely similar to that of the Earth's atmosphere (Singer and Suess, 1963). In contrast, the solar abundances more or less accurately represented by solar wind, and by the components implanted in the surface skin of lunar rocks and meteorite grains were realized to be markedly different with a much higher abundance of light noble gases.

These facts suggest that the special noble gas composition as found in meteorites and in the terrestrial atmosphere, was established in the gas phase from which the primordial condensates grew, both in the region of space where the parent materials of meteorites formed, and in the region where the parent material of the Earth condensed. Several mechanisms may have contributed to the observed noble gas fractionation in the circumsolar region (see reviews in Arrhenius, 1972; Black, 1972a and b).

The Earth could then have acquired its atmosphere and ocean as it grew from primordial grains and aggregates similar to, but not necessarily identifiable with those found in meteorites, by the release of the volatiles mainly during the accretion process into a primordial atmosphere from which the present one has gradually developed (Aston, 1924).

Although the important discovery of the "planetary" component of noble gases in meteorites was made over a decade ago, the full

implications of a genetic relationship were not realized until recently (Wasson, 1969; Fanale, 1971). Fanale aptly ascribes this delay to a climate of opinion which for a long time fostered a belief that the primordial atmosphere of the Earth must have been entirely removed by some ad hoc process. The present atmosphere would under these circumstances have evolved entirely by degassing of the interior of the planet, which then would need from the outset to have retained a sufficient mass of volatile components.

As demonstrated by Fanale, this is not likely to have been the case; the primordial noble gases with the possible exception of xenon must at accretion onto Earth have been transferred in quantity to the atmosphere where they still reside. They do not appear to play a significant role in the present gas flux from the Earth's interior, where the noble gas component is dominated by radiogenic species, nor do they occur in measurable quantities in igneous rocks. Other chemically reactive volatiles show a more complex partition between the atmosphere and the solid Earth as discussed below.

The component of primordial solids of major importance as a source of oceanic water is hydroxyl ion. This ion forms a regular structural element in magnesium and iron hydroxysilicates with sheet structure, which form the major mass of carbonaceous chondrites of Type I (Wiik, 1956). (Crystal hydrates of magnesium and sodium sulfates found in carbonaceous chondrites are probably not generated in

space where they are unstable; they are likely to be forming by reaction with water vapor in terrestrial museums.)

It was previously believed (on the basis of geological experience) that the hydroxysilicates in meteorites must be understood as a secondary reaction product between anhydrous silicates and water in vapor form, or even as liquid water in rivers and swamps on a planet from which the sediments would subsequently have been removed as meteorites. It is know known from experiment (Meyer, 1969, 1971) that magnesium hydroxysilicates, analogous to those in meteorites, crystallize directly from partially ionized gas containing magnesium, silicon, hydrogen and oxygen species and at grain temperatures below about 500°K. Furthermore, substitution with hydroxyl occurs also in the terrestrial varieties of silicates common in space such as olivine and pyroxene (Martin and Donnay, 1972). Such partial hydroxylation is likely to occur at the growth of these silicates also in free space, particularly in vapor crystallization at high relative pressure of atomic and ionic species of oxygen and hydrogen.

In view of the small mass of the hydrosphere compared to the mantle (1/3000) concentrations as small as 300 to 1000 parts per million of available hydroxyl in the accreting silicates are sufficient to generate the total mass of the hydrosphere, considering also the initial loss process discussed in Section 3 below. Thus the space condensates that we know from meteorites and from the Moon (Gibson

and Moore, 1973a; Apollo 16 PET, 1973) would provide ample sources for both the ocean and the atmosphere.

This should not be taken to mean that the Earth formed from any of these specific materials, which represent different condensation regions in space. But the observations imply that primordial condensates in different parts of the solar system, although varying markedly in chemical composition (Alfvén and Arrhenius, 1973, Part IV) have incorporated substantial amounts of volatiles, which were subsequently released in the accretional heat front at the formation of planets (Alfvén and Arrhenius, 1970b).

An important related question concerns the chemical composition of the Earth's total store of primordial volatiles, determined by the average composition of the planetesimals from which the Earth was built and modified by the loss processes discussed in the following. In the case of the primordial noble gases the observations mentioned above indicate relative proportions similar to those found in meteorites and concentrations within the range of those in meteorites.

The content and proportion of reactive volatiles in the Earth's source material (primarily species of H, C, N, O, S, halogens and Xe) is obscured by the fact that the fraction of each one of these, hidden in the Earth's interior, is totally unknown. Analyses of crustal rocks and extrusions from the upper mantle are not informative on this point since they are likely to be contaminated by the ocean's atmospheric

reservoir. Extraterrestrial materials do not provide much quantitative guidance on this point either since their absolute and relative contents of reactive volatiles are extremely variable (Gibson and Moore, 1973b; Gibson and Johnson, 1971, 1972; and Gibson, 1973).

5. THE IMMEDIATE PRECURSOR STAGES

As shown above, we can trace the Earth's ocean and atmosphere with some certainty into the plasma phase which preceded the formation of solid grains around the Sun. We shall now turn our attention to those stages of the protoplanetary development which have a most immediate effect on the formation of the ocean.

The first problem we must solve is that of the orbital evolution of a large number of grains born in eccentric Kepler orbits around the Sun and undergoing mutual collisions that result in loss of orbital energy. The result of analysis of this many-body problem (Alfvén, 1970; Baxter and Thompson, 1971, 1973; Trulsen, 1971) is contrary to intuitive application of experience from scattering of particles in a stationary frame of reference. If the particles are orbiting in a gravitational field, and if the collision time is long compared to the orbital period, the particle orbits instead of spreading increasingly widely in space, contract into a torus (Figure IV-2) whose thickness decreases with time until a state is reached where the collision velocity is low.

The exchange of energy at the particle collisions tends to equalize eccentricity, orbital inclination and orbital radius for all

FIGURE IV-2

Formation of jet streams. The condensation process will result in a large number of small grains in eccentric Kepler orbits (top).

Inelastic collisions between the grains will not spread the orbits because of the negative diffusion coefficient (Baxter and Thompson, 1971, 1973). Instead the collisions will lead to equalization of the orbital elements (bottom) so that a jet stream is formed (from Alfvén and Arrhenius, 1972).

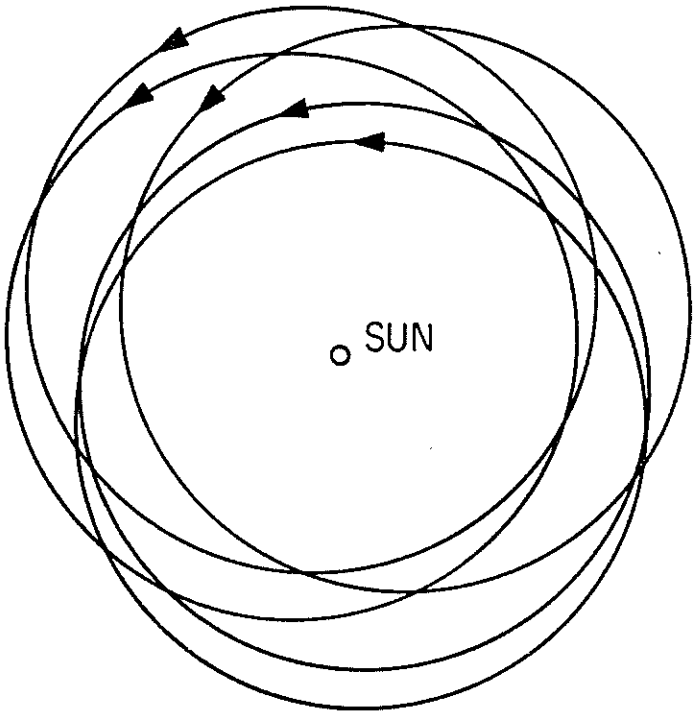
SUN

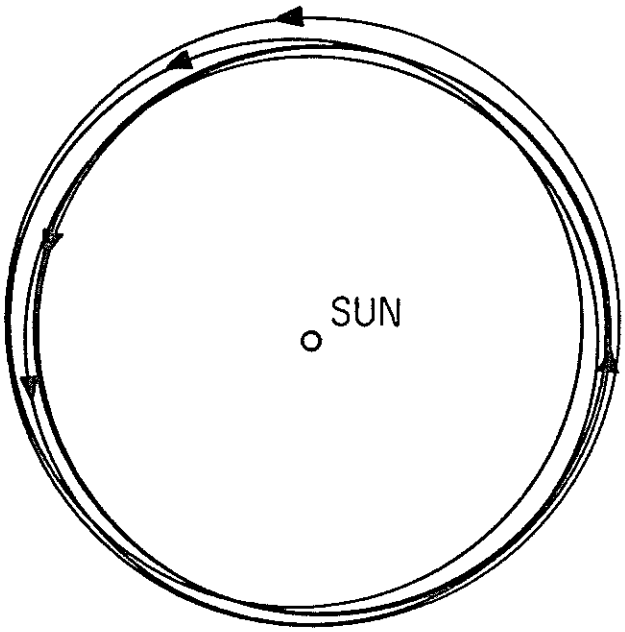
SUN

particles in the assemblage. Particle assemblages with these characteristics are properly called jet streams. Such jet streams are today probably represented by groups of asteroids moving in closely similar orbits (Arnold, 1969; Danielsson, 1969, 1971). It is also possible that the particles that make up comets and meteor streams have these characteristics (Mendis, 1973).

6. ACCRETION OF PLANETARY EMBRYOS

Investigations on the lunar surface have demonstrated a number of processes leading to adhesion of colliding particles and resulting in a net growth of aggregate size (Asunmaa et al., 1970; Arrhenius and Asunmaa, 1973). This occurs when the relative velocity between the particles is low enough, or if the target is an already accreted fluffy aggregate, large enough to dissipate the projectile energy within it. Before this stage of low relative velocities in the jet stream is reached, particle collisions result in fragmentation or vaporization. Their effect is mainly a decrease of the particle size while the resultant fragments or condensates remain parts of the stream and eventually collide again. The importance of high energy impact processes is reflected by the large fraction of melted and quenched silicate droplets (chondrules) which form a major part of the most common meteorites. However, it is also likely that the presence of gas in jet streams leads to viscous dissipation of particle energies, thereby reducing the relative velocities at collision. The need for assuming this comes from

the observation in carbonaceous chondrites of abundant crystals likely to be of primordial origin and having fragile texture, which have been brought together into the ultimate aggregate now observed, without destruction of temperature or impact sensitive features (Figure IV-1). This requires that the crystals were aggregated without suffering high energy collisions and such an effect can be produced only by gas friction.

The approximate dimensions of the Earth's original jet stream can be visualized in the form of a torus with the large radius r_o approximately equal to the Earth's orbital radius and with the small diameter $2x$ such that the characteristic volume U of the jet stream is

$$U = 2\pi^2 r_o x^2 = \frac{1}{2} r_o T_K^2 v_i^2 \qquad (1)$$

where T_K is the Kepler orbital period of the Earth and v_i is the "internal velocity" in the stream representing the relative velocity between the particles in the jet stream. The results quoted in this section are derived in detail in Alfvén and Arrhenius, 1970b, Section 9).

When the condition has been reached such that the relative velocities in the jet stream are low enough to permit net accretion, a number of individual aggregates (embryos) in the stream begin to accrete, and continue to grow further by collision with individual grains and with each other.

The rate of mass increase of an embryo (assumed spherical) is

$$\frac{dM_e}{dt} = v_i \rho \pi R^2 (1 + v_e^2/v_i^2) \qquad (2)$$

where ρ is the space density of condensable substances in the jet stream, πR^2 is the geometrical cross section of the embryo for capture of the condensable substances and v_e is the escape velocity for the embryo, given by

$$v_e = \left(\frac{2 \varkappa M_e}{R}\right)^{1/2} = \left(\frac{8}{3} \pi \varkappa \theta\right)^{1/2} R \qquad (3)$$

θ being the density (assumed here to be uniform) of the embryo, and $\varkappa$ the gravitational constant. The factor in parenthesis in equation (2) represents the increase in the effective capture cross-section of the embryo due to gravitational attraction. The gravitational accretion becomes important when the embryo has reached a size of the order of 100 km, and the rate of accretion increases rapidly afterward.

The rapid increase in the growth rate with the size of the embryo results in a runaway accretion process (Safronov, 1954). The rate of accretion becomes catastrophically rapid at a time τ_c after the beginning of accretion when the largest embryo in the jet stream sweeps up all the other material in the jet stream to form the protoplanet. If there were an unlimited supply of particles to the jet stream, the radius of this protoplanet would theoretically become

infinite in a finite time τ_a, given by

$$\tau_a = \left(\frac{3\pi}{2\kappa}\right)^{1/2} \theta^{1/2} = 8.4 \times 10^3 \frac{\theta^{1/2}}{\rho} \tag{4}$$

If M is the final mass of the planet, the distributed density ρ of condensables may be approximated by $\rho = M/U$, so that equation (4) may also be written as

$$\tau_a = 8.4 \times 10^3 \theta^{1/2} \frac{U}{M} \tag{5}$$

The time τ_c at which the catastrophic growth takes place may be approximated by

$$\tau_c = (2 \tau_i \tau_a)^{1/2} \tag{6}$$

where the injection time τ_i is the time during which condensing grains are continuously fed to the jet stream, replenishing those removed by accretion. This represents the time span during which the grains were condensing from the plasma and hence the total time during which gas was injected into the circumsolar region. In the part of this region where meteorites formed, measurements of formation intervals (Podosek, 1970) indicate that the injection time cannot possibly have been less than $0.15 - 0.5 \times 10^8$ years. As, on the other hand, it could not possibly be of the order 10^9 years, an intermediate value of 3×10^8 years has been used for τ_i. Other estimates have led to the order of 10^8 years (Safronov, 1954, 1958, 1960, 1969; Urey, 1962). As

shown in Section 8 the exact value is not very important in the case of the Earth.

The order of magnitude consideration of the time parameter is, however, of crucial importance. As pointed out by Levin (1972) much of the confusion in the discussion of the origin of the Earth arises from ignoring the strictures that the accretion mechanism imposes on the time factor, and from the resulting ad hoc assumptions of accretion times many orders of magnitude shorter than the time indicated by any quantitative accumulation theory.

Applying the above relationships to the bodies in our solar system and adopting the above value for τ_i we find essentially three types of cases. Mercury, Venus, Earth and Jupiter all have values for τ_c of the order 10^7 years (3.5×10^7 years for Earch), which is much shorter than the total time of injection of material, τ_i. At the other extreme are Uranus and Neptune for which the values of τ_c calculated in this manner would be larger than the age of the solar system. An intermediate group is formed by the Moon, Mars and Saturn, for which τ_c most likely are of the same order of magnitude as τ_i.

We conclude that for Uranus and Neptune, significant growth of embryos cannot have occurred while the parent jet streams were maintained at constant volume U by continuous injection of material during τ_i. Only after τ_i could a contraction of the jet stream occur, first slowly and then rapidly increasing the space density of matter

and thereby accelerating the process leading up to a catastrophic accumulation. The accumulation process would consequently continue for a time substantially longer than 10^8 years for these two planets.

In the case of the Moon, Mars and Saturn the catastrophic termination of accretion roughly coincided with the end of injection of matter by condensation; the present uncertainty in the value of τ_i makes it impossible to state which time was the longer.

In the third case which includes the Earth and hence is of particular interest to us, the catastrophic accumulation of the protoplanet and the exhaustion of the parent jet stream occurred very early in the process of formation of the solar system, according to equation (6), 3.5×10^7 years after the onset of condensation in the terrestrial region of space. The mass present at that time sufficed to give rise to a protoplanet with about half the present radius (Figure IV-3). During the remaining part of the time period of injection of material, assumed to last approximately 3×10^8 years, growth was maintained at a low and steady rate, determined by the rate of injection of newly condensed material into the jet stream and hence by the rate of inflow of gas into this part of the circumsolar region. At the end of the injection time τ_i the jet stream was rapidly exhausted and the accretion of the planet terminated, as shown in Figure IV-3.

FIGURE IV-3

Heat structure and the accumulation of water. The dashed curve and the left hand ordinate scale show the thermal power (in abritrary units) delivered per unit surface area of the growing Earth by impacting planetesimals. The lower abscissa scale shows the radius of the growing Earth in fractions of the present size.

The upper (non-linear) abscissa scale shows the time elapsed from inception of accretion.

The three solid curves show the accumulation of water on Earth according to equation (17). The left curve represents the amount retained in the coolly accreted inner core. The middle curve shows the accumulated water in the atmosphere and the right hand curve shows the accumulated liquid water.

The final mass of accumulated water has been adjusted to equal the present ocean mass.

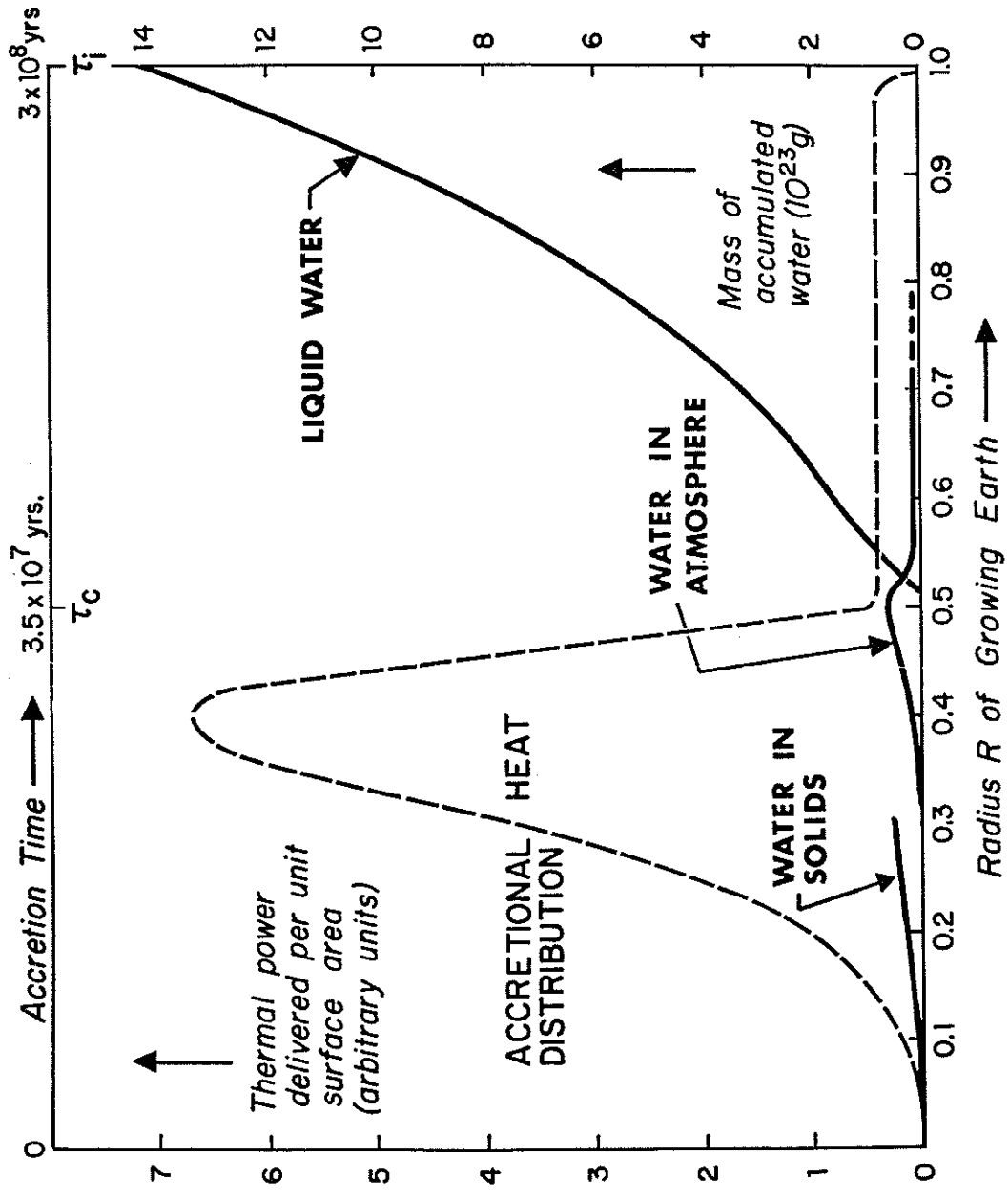
Accretion Time
0
3.5 x 10^7 yrs.
τ_c
3 x 10^8 yrs
τ_i
Thermal power delivered per unit surface area (arbitrary units)
ACCRETIONAL HEAT DISTRIBUTION
LIQUID WATER
WATER IN ATMOSPHERE
WATER IN SOLIDS
Mass of accumulated water (10^{23}g)
Radius R of Growing Earth
0.1
0.2
0.3
0.4
0.5
0.6
0.7
0.8
0.9
1.0
1
2
3
4
5
6
7
2
4
6
8
10
12
14

7. HEAT RELEASE AND VOLATILIZATION OF WATER AT ACCRETION

We have shown above the mass and time relationships of accretion of planets in general with special consideration of the Earth. The heating of the accreted material, carrying in it the volatile sources of the ocean and the atmosphere is of crucial importance for fractionation of the volatiles and their ultimate disposition. The major amount of heat in the accretion process derives from the conversion of kinetic energy of the infalling bodies into thermal energy at impact.

When a grain hits an embryo, the velocity at impact is

$$v_p = (v_e^2 + v_i^2)^{1/2} \tag{7}$$

where v_e is the escape velocity for the embryo given by equation (3), and v_i is the original velocity of the grain relative to the embryo. In the later state of accretion, v_i becomes small compared to v_e. Hence, the amount of kinetic energy released at each impact is at least $\frac{1}{2} m v_e^2$, where m is the mass of the impacting grain. A fraction γ of this energy will be converted to thermal energy of fusion within the grain, melting a mass-fraction α of the grain, given by

$$\alpha = \frac{\gamma v_e^2}{2L} \tag{8}$$

L being the latent heat of fusion for the grain material. If we take iron-magnesium silicates to be representative of the solid material in

the grains, the latent heat of fusion (Fe_2SiO_4: 295 J/g, $MgSiO_3$: 616 J/g, Mg_2SiO_4: 455 J/g) may be taken to be of the order of 500 J/g for our estimate. As an example, when the embryo has grown to a size of half the present size of the Earth, we find on putting $R = 0.5\ R_\oplus$, $\theta = 5.5$ g cm^{-3} and $L = 500$ J/g.

$$\alpha = 25\ \gamma$$

Thus, even if γ is as low as one per cent, one-fourth of the grain will be melted. It is likely that also some of the target material will be heated at the same time. The above is, however, a very conservative estimate since γ is likely to be larger. Hence we can conclude that a considerable fraction of the grain will be heated to sufficiently high temperatures for the major part of its volatile components to be released in the form of gas.

The extent to which water vapor and other volatile compounds will be retained as an atmosphere around the protoplanet is determined by the balance between thermal escape of the molecules and the increasing gravitational retention by the protoplanet as its mass grows. Thus there will be a gradual accumulation of water vapor with time, and under suitable conditions this may condense to form liquid water.

These conditions are largely determined by the temperature at the surface of the growing protoplanet, which in its turn depends on the heat release at the impact of individual bodies on it as discussed above, and on the rate at which such impacts occur. Before we

proceed in Section 9 below to outline the process of the accumulation of water, we shall therefore briefly review the characteristics of the accretional heat distribution.

8. TEMPERATURE DISTRIBUTION IN THE GROWING PROTOPLANET

The kinetic energy of an impacting planetesimal is almost entirely converted to heat energy when it is brought to rest on the surface of the embryo. The thermal power w delivered per unit area of the surface of a growing embryo by the impacting planetesimals is given by

$$4\pi R^2 w = \frac{v_p^2}{2} \frac{dM_e}{dt} \tag{9}$$

Substituting equation (2) into this equation, we obtain

$$w = \frac{\rho}{8} \frac{(v_i^2 + v_e^2)^2}{v_i} \tag{10}$$

If a fraction $\gamma' w$ of this heat is dissipated in melting and vaporization of projectile and target material, then the rest, $(1-\gamma')w$, will be used up in heating the surface of the embryo. Equations (3) and (10) now give us the profile of $(1-\gamma')w$ as a function of radius R of the growing embryo, assuming γ' to be constant. It is reasonable to assume that this heat is balanced by radiation from the surface of the embryo. Hence the profile of $(1-\gamma')w$ will also represent the profile

of the temperature of the surface layer of the growing embryo as a function of its radius. This profile has been plotted in Figure IV-3, where we note that the temperature first reaches a maximum and then falls to a very low value at the end of the time τ_c. The fraction of the mass accumulated by the time τ_c is reached is

$$\phi = \tau_c/\tau_i = (2\tau_a/\tau_i)^{1/2} \tag{11}$$

The radius of the protoplanet at this time, R_c, equals $\beta R_\oplus$ where $R_\oplus$ is the final radius, with

$$\beta = \phi^{1/3} = (2\tau_a/\tau_i)^{1/6} \tag{12}$$

Using the values 2×10^6 years found for τ_a for the Earth and taking $\tau_i = 3 \times 10^8$ years, we find

$$\beta = (4/300)^{1/6} \approx 0.5 \tag{13}$$

The result is not very sensitive to the choice of value for τ_i; values of 10^8 and 10^9 years change the value for β to 0.58 and 0.40 respectively.

We conclude, therefore, that the inner core of the Earth accreted cold (Figure IV-3), the accretion temperature rose to maximum at the formation of the outer core and then fell abruptly and remained low (averaged over the entire surface of the Earth) during the accretion of the mantle. It is tempting to see in this primeval

heat distribution of the Earth an explanation of the facts that in its present state, our planet is known to have a solid inner core and mantle and a liquid outer core. This requires that since the formation, the heat distribution has not changed very much due to the thermal conduction. However, radioactive decay would add another component to the heat profile in a manner depending on the largely unknown distribution of uranium, thorium and potassium. Hence, it is possible that also the central part of the Moon, although accumulated cold, is now partially melted as suggested by seismic evidence (Latham et al., 1973).

9. A SIMPLE MODEL FOR ACCUMULATION OF WATER

The rate of increase of mass with radius of an embryo of uniform density is

$$\frac{dM_e}{dR} = 4\pi R^2 \theta \tag{14}$$

Let us suppose that each mass unit of impacting matter releases ϵ mass units of water. Then the rate of increase of water content in the environment of the embryo is

$$\frac{dM_{H_2O}}{dR} = \epsilon \frac{dM_e}{dR} = \epsilon 4\pi R^2 \theta \tag{15}$$

The water vapor will approach an equilibrium temperature T and a corresponding Maxwellian velocity distribution. The molecules which have thermal velocity v in excess of the escape velocity v_e

for the embryo can escape immediately from the neighborhood of the embryo. As shown by Jeans, if the root mean square velocity of a gas is only of the order of 20 per cent of the escape velocity, the gas can escape entirely in the course of a billion years or so. Let us make a conservative estimate of the retention of water molecules and assume that all molecules having velocities higher than $0.2\ v_e$ will escape from the gravitational field of an embryo. Hence, we have to multiply the right hand side of equation (15) by the fraction representing the number of molecules that are retained:

$$\frac{dM_{H_2O}}{dR} = \epsilon\, 4\pi R^2 \theta\, \frac{4}{\sqrt{\pi}} \int_0^{X(R)} e^{-x^2} x^2\, dx \qquad (16)$$

with

$$x = v \left(\frac{m_{H_2O}}{2kT}\right)^{1/2}$$

$$X(R) = 0.2\, v_e \left(\frac{m_{H_2O}}{2kT}\right)^{1/2} = 0.2 \left(\frac{8}{3}\pi\varkappa\theta\right)^{1/2} R \left(\frac{m_{H_2O}}{2kT}\right)^{1/2}$$

where m_{H_2O} and k are the mass of a water molecule and the Boltzmann constant respectively. Therefore, the total mass of water that has accumulated when the embryo has a radius R is

$$M_{H_2O}(R) = \epsilon\, 16\pi^{1/2}\, \theta \int_0^R R^2 \left\{ \int_0^{X(R)} e^{-x^2} x^2\, dx \right\} dR \qquad (17)$$

Is the accumulation of water described by equation (17) up to the time when the planet has attained its final size sufficient to account for the ocean mass? In order to answer this question, we need to specify the value of the parameter ϵ. Instead, we will turn the question around and ask what value of ϵ will give a total accumulation equal to the present ocean mass; we can then examine the implications of this value of ϵ.

The relevant temperature T of the water vapor that will determine its rate of gravitational escape is a characteristic temperature at the top of the atmosphere that forms by the release of the occluded gases. This temperature is not related to the accretionally heated surface temperature of the embryo but is determined by the radiation fields of the Sun and of the plasma in the primordial magnetosphere surrounding the Earth (De and Arrhenius, 1973). Assuming that the thermal conditions at the top of the atmosphere were comparable to those in the Earth's exosphere today, we choose a characteristic temperature of 1000°K. Our analysis does not change appreciably if T is lower than 1000°K. If T were as high as 3000°K, this would lower the total accumulation of water by about a factor of 2.

For the density θ, we adopt for convenience the average density 5.5 g cm^{-3} of Earth. It is possible that the Earth formed from relatively homogeneous material of lower density. The high density core would in this case be produced by a phase transformation setting in when the Earth had reached about 0.8 of its present radius

(Lodochnikov, 1939; Ramsey, 1948, 1949, 1967; see also discussion in Levin, 1972 and Alfvén and Arrhenius, 1973b). The original density of this material is then likely to be of the order of 3 to 4 g cm^{-3} - but as far as the present analysis is concerned, the assumption of average density is not critical.

Figure IV-3 shows the accumulation of water with increasing radius of the protoplanet calculated on the basis of equation (17). The total accumulation when the radius reaches the present value has been matched to equal the present ocean mass. The value of ϵ needed for this is $\epsilon \approx 3.2 \times 10^{-4}$.

Meteorite materials of the type discussed in Section 4 have values of ϵ in the range 10^{-2} - 10^{-3}, hence primordial grains in principle would satisfy the required value for ϵ. Figure IV-3 also shows the primeval heat structure of the Earth resulting from accretion as discussed in Section 8. The ordinate (left) for this curve is given in arbitrary units and is proportional to the temperature. We note that after the low temperature accretion of the inner core, the temperature of the surface layer of the embryonic Earth continues to rise and culminates at $R \approx 0.4\ R_{\oplus}$. Hence water vapor cannot condense during this period and must remain in the atmosphere. However, the gravitational retention of water vapor at this stage is very small. As the accretion proceeds, now at a low rate determined by the injection of source gas into the terrestrial region, the surface temperature of the protoplanet falls to a low average value which is probably close to the

present surface temperature of the Earth. This would allow the water vapor to condense and begin the formation of a proto-ocean.

10. ACCRETIONAL HEAT FRONT AND STATE OF WATER

As was shown in Section 6 above and in Figure IV-3 for the case of the Earth, heat delivery to the surface layer of the protoplanet first reached a maximum and then declined to a low mean value when the size of the present outer core was reached. After this culmination, the accretion of the outer regions of the Earth proceeded at a low rate, controlled by the continued injection rate of matter (assumed here to be constant) into the terrestrial region of space and terminating at the time τ_i when this injection ceased. During the era preceding τ_i the average rate of heating of the surface of the protoplanet hence must have been low. At the same time, however, the local heating at each individual impact site continued to be high and actually increased as a function of R as the escape velocity of the Earth increased due to its increasing mass. The transformation of kinetic energy of the infalling bodies to thermal energy has been discussed in Section 7 above. Since the major fraction of mass, and hence potential thermal energy, is concentrated in the largest embryos impacting on the growing Earth (Gurevich and Lebedinskij, 1950), it is these large projectiles that control the thermal evolution.

Assuming that the size distribution of accreting planetesimals was such as to place the major fraction of mass in bodies larger than

10^{10} kilograms, the major fraction of heat was delivered in large impacts repeated relatively rarely at any given location (once every ten to a few hundred years in any impact area) during the era of mantle and crust formation. Each major impact is likely to have created a deep subsurface region of molten rock which, in contrast to secondary ejecta and a thin surface crust, would cool slowly. In such melt reservoirs differentiation of magma could take place with the heavy components sinking to the bottom and the light materials accumulating at the top. Although the average surface temperature of the Earth during this era would have remained low, each individual impact region would, in the course of time, be remelted and differentiated many times over. Radial progression of this accretional heat front, discontinuous in space and time, resulted in the selective removal toward the surface of light differentiates forming the Earth's crust, and of volatiles forming the atmosphere and the ocean.

The water vapor released at individual impacts would after time τ_c condense and contribute to the growing proto-ocean due to the low average surface temperature during this era.

11. DETAILS OF MODEL

The development discussed in Sections 8 and 9 above has purposely been made simplistic in order to illustrate in principle the energetics of growth of the planet and the course of retention of oceanic and atmospheric components with time. There are several

complicating factors, some of which can be discussed qualitatively with some assurance at the present time; for others observational basis is still lacking. Some of the resulting modifications and uncertainties are discussed in the following sections.

11.1 Atmospheric loss mechanism

In the calculation in Section 9, it was assumed that water vapor is lost from the exosphere by molecular evaporation. If one assumes solar energy flux of at least the present magnitude, water vapor in the upper atmosphere will be dissociated and form a number of species including atomic and molecular hydrogen, hydroxyl and oxygen ions; of these the hydrogen species have a high escape rate and are preferentially lost to space. The escape rate is probably controlled by the transfer rate of water vapor from the troposphere across the stratospheric cold trap (Harteck and Jensen, 1948; Urey, 1952, 1959).

It is thus generally believed that a part of the terrestrial oxygen is the residue of water from which the hydrogen component has escaped. An estimate of the relative importance of this selective loss can be obtained from the budget shown in Table IV-1.

Table IV-I. Oxygen Reservoir of the Earth

Oxygen Reservoirs	Mass of Stored Oxygen (10^{23} g)
Hydrosphere (including sediment pore water)	16.7
Limestone	4
Excess in oxidized iron compounds	0.2
Atmosphere	0.05
Sulfates	0.04

The table shows that if we make the extreme assumption that the oxygen now present in carbonates derives entirely from dissociated water by reaction of such oxygen with primordial carbon compounds, then limestone would be a major store of such oxygen. However, the carbonates may partly or entirely have formed by other reactions instead; carbon dioxide may have been a primordial gas component of planetesimals (Gibson and Moore, 1973a), it may have been produced by reaction of planetesimal carbon with oxygen in iron silicate in the accretional heat front (Ringwood, 1959) or carbonates could have formed by reaction of methane and water with silicates (Urey, 1952). Hence the largest conceivable loss of water by escape of hydrogen would amount to about 25 per cent of the present mass of water; the actual amount is probably much smaller.

The amount of atmospheric oxygen used up by oxidation of transition element compounds, primarily those of iron, has been estimated on the basis of the extreme assumption of an original oxygen-iron average oxidation state corresponding to FeO, furthermore all iron in present day sediments occurring as Fe_2O_3 and forming on the average 3.5 per cent of shale and deep sea sediments. The total thus obtained is only a small fraction of the oxygen in the present ocean. However, this calculation ignores the unknown amount of water-derived oxygen bound to divalent or trivalent iron in the mantle and in crustal igneous rocks (see Holland, 1964). Particularly the amount in the mantle constitutes a substantial uncertainty.

The rate of removal of gas from bodies in space is also affected by interaction with corpuscular radiation from the Sun. It is sometimes assumed that a "solar gale" arose after the planets had formed, removing all planetary atmospheres in the inner part of the solar system.

The need for such an ad hoc mehanism was rooted in the belief that the primordial components were missing from the Earth's atmosphere. As discussed in Section 4, it is now realized that on the contrary our present atmosphere can only be understood as a product of the primordial accumulation, modified by loss of hydrogen and helium, by photochemical and biological processes, and by reaction with the solid earth, from which radiogenic gases have also been added. The

records from the Moon and from meteorites also have failed to give evidence of any major enhancement of solar corpuscular radiation after the formative era. For a discussion of the corpuscular radiation effects during this era, see Alfvén and Arrhenius, 1973, Section 11.8.

11.2 Effect of atmosphere and ocean on accretional heating

The developing hydrosphere and atmosphere could in principle introduce effects on the distribution of heat received in the accretional process. This is partly due to the fact that some of the projectile energy will be dissipated by frictional heating of the atmosphere and the ocean, and partly to the fact that these will decrease the efficiency of cooling by reradiation into space from collision-heated spots on the surface. The latter effect would become important if a large fraction of accumulated water were evaporated into a hot atmosphere. This is, however, not likely to have taken place since such a runaway greenhouse effect (Rasool and de Bergh, 1970) would probably be irreversible, whereas the geological record shows existence of sediments and organic life on Earth already at the -3 Gy level (Engel et al., 1968). The lack of development of a hot atmosphere can be understood since the calculated size distribution of accumulating planetesimals place the major amount of mass in large projectiles (Section 10). This concentrates the accretional heat to limited regions, and with sufficient intervening time available for efficient reradiation of surficial heat into space.

At a large projectile mass/surface ratio, the energy dissipation in the atmosphere and the ocean would also become small compared to the energy release after penetration to the solid surface (Lin, 1966). Terrestrial experience gives no guidance concerning the nature of impact processes of the magnitude involved here. As was pointed out by Urey (1952), until these effects could be studied directly in the preserved impact record of the Moon it would be difficult to predict the relative distribution of projectile matter between ejecta dissipating energy over wide regions, and the retained projectile fraction implanted in the target and melting itself as well as the target material. In the projectile mass range covered by controlled experiments the mass of ejecta exceeds that of the projectile in hypersonic impacts (Gault et al., 1968; Neukum et al., 1970). At projectile masses far beyond this range, however, the fraction of projectile material retained in the target would be expected to increase particularly at impact speeds several times the sound velocity in the projectile material. This is indicated by the effects of the largest impacts on the lunar surface. Hence local implantation of kinetic energy converted to heat is likely to have been an important process at the accretion of the Earth.

12. VOLATILES IN THE LITHOSPHERE

Crustal igneous rocks on Earth have a low but persistent content of water and occasionally very high contents of carbon dioxide (von Eckermann, 1948, 1958; Tuttle and Gittens, 1966). Because of the unknown extent of these components with depth in the Earth, the total store of volatiles in the solid Earth is highly uncertain. The question how and when these volatiles became buried is important to the problem of the formation of the ocean. One suggestion has been that an excess over the present amount was introduced into the interior of the Earth during its early history. This situation would be or become metastable, causing a net transport of water from the lithosphere to add to the volume of the ocean during a substantial fraction of geological time and possibly still today. No observational basis seems to exist for this assumption which was originally made to secure a storage place for the present ocean and atmosphere while the original atmosphere was supposed to be destroyed. As discussed above, such a catastrophy is counterindicated by the noble gas distribution in the atmosphere and hence the need for temporary ocean storage has disappeared.

To explain the present content of reactive volatiles (primarily water and carbon dioxide) in igneous rocks, Fanale (1971) on the basis of a proposal that the Earth became completely melted (Hanks and Anderson, 1969) suggested that the volatiles were partitioned in

equilibrium between the melted Earth and a hot atmosphere in contact with it. This would seem excluded on the basis of quantitative considerations of the accumulation process (Safronov, 1954, 1958, 1959, 1960, 1969; Alfvén and Arrhenius, 1970a and b; Section 6 above). These indicate early exhaustion of the Earth's jet stream, and slow subsequent growth during the major part of the approximately 10^8 year accretion period. If this is correct, the average temperature of the Earth's surface must have been low during accumulation of the mantle and the crust. The thorough outgassing of the noble gases recognized by Fanale is, as demonstrated by the late bombardment effects on the Moon, the natural consequence of the local heating at each individual impact and does not in itself require simultaneous heating of the whole Earth. It is furthermore doubtful that a thoroughly melted Earth would have had time to cool enough to yield a still preserved crust 0.7 Gy after formation, particularly with a hot atmosphere containing a major part of the present ocean and of the carbon dioxide reservoir. Finally, the spotty occurrence of deep seated igneous rocks rich in carbon dioxide suggests that it was introduced locally by a mechanism such as described below, rather than by equilibration of a molten Earth with a hot, massive atmosphere.

There is indeed a straightforward and observationally supported way in which the igneous rocks of the crust and upper mantle would seem to be continuously impregnated with reactive volatiles from the

atmosphere and the ocean. The evidence for convection driven lateral movement of large plates of the Earth's crust suggests strongly that water and carbonate containing sediments and hydrated submarine eruptives are sinking and assimilating into the upper mantle in subduction zones, compensating for the rise of magma and generation of new crust in the sea floor spreading zones. This vertical mixing is sufficiently fast (approximately 5 cm/year) to have drowned all ocean sediments appreciably older than a few per cent of the estimated age of the Earth. Hence all reactive volatiles now found in igneous rocks can be understood as contamination mainly from the ocean, introduced into the solid Earth much later than the time of formation of the primordial crust. A potential measure of the efficiency of this cycling is the remaining effusion from the Earth's interior of stable end products from such radioactive species which decayed practically completely a short time after the formation of the Earth (Xe^{129} from I^{129}, half life approximately 15 My; see Boulos and Manuel, 1971). Another suggested indicator would be He^{3} possibly inherited as a cosmic ray spallation product from primordial material (Clarke et al., 1969). It would, however, seem difficult to understand how helium could survive accretional degassing while neon, argon and krypton were transferred to the primordial atmosphere with such efficiency that no traces have been found of their primordial component in terrestrial igneous rocks.

It should be clear from this discussion that an efficient mechanism for circulation of volatiles between the ocean-atmosphere system and the upper mantle has been operating through the geological eras recorded on the ocean floor and presumably during the entire history of the Earth after its formation. This does not exclude the possibility that a fraction of the primordial volatiles were left behind in the growing lithosphere as a result of incomplete outgassing at accumulation of the Earth.

At atmospheric pressure the equilibrium solubilities in silicate melts of most gases are modest. However, considerable excess amounts of gas can be incorporated, at the moment of shock, in melted gas rich materials and can be retained in disequilibrium in such melts when they solidify due to the inefficiency of diffusion-limited removal processes. On the other hand, convection in such melts, and stripping by boiling of components such as hydrocarbons and monoxides of carbon, silicon and potassium contribute toward relieving such disequilibria. These retention and removal phenomena are exemplified in the lunar rocks. Conditions in the lunar crust also indicate that in the culminating stage of accretional heating (which on Earth probably occurred at the outer core and on the Moon not far below the present surface), the removal of any water vapor possibly associated with the molten and vaporized projectile material was highly efficient, resulting in oxygen partial pressures less than 10^{-14} b. The sporadic occurrences of volatiles in

lunar materials are considered to derive from post-formative impact of volatile-rich projectiles on the cold lunar surface and in some instances perhaps to be due to vapor transport through crustal fractures from the coldly accreted inner core (which could be considerably warmer today due to radioactive heating).

During the accretion of the Earth's mantle and crust, the large impacts could well have implanted hydroxyl containing material sufficiently deep so that the solubility in the melt remained comparatively high, and removal was not complete before solidification in spite of repeated remelting by new impacts and gravitational upward removal of light components resulting in formation of the crust. Because of the complexity of these processes and our lack of knowledge of large scale impact effects, it is difficult now to estimate the ultimate efficiency of the materials separation by the accretional heat front.

A continued systematic search for primordial gas components in the effluents from the Earth's crust and mantle could narrow the limits of uncertainty. Improved knowledge of the temperature distribution in the mantle would also contribute to the vertical transport efficiency problem, since at least at moderate pressures the large cations of the elements contributing to radioactive heating, are concentrated in the light component migrating toward the surface in the accretional heat front.

13. THE OCEAN AND THE EARTH-MOON SYSTEM

It is likely that the evolution of the ocean has been markedly affected by the fact that an abnormally massive body causing significant tidal effects exists in the vicinity of the Earth. A similar case is that of Neptune with the captured satellite Triton which has a tidally modified orbit (McCord, 1966).

After the recent exploration of the Moon, two types of theories for its origin remain to be discussed. One postulates the formation of the Moon in an independent solar orbit (Gerstenkorn, 1969) or coupled by resonance to the Earth (Alfvén and Arrhenius, 1969, 1972) and in either case subsequently captured by tidal interaction. The other (Ringwood, 1970) proposes that the Moon formed around the Earth by hydromagnetic transfer of angular momentum to a primordial plasma emplaced around the planet in the same way as the (structurally very different) regular satellite systems seem to have formed.

The former hypothesis would appear more likely in view of the fact that the Moon is much more massive (mass ratio 1:80 relative to Earth) than the regular satellites of Jupiter, Uranus and Saturn where the ratios of satellite mass to central body are less than $1:10^4$.

A comparison of Earth with the regular planet-satellite systems of Jupiter, Saturn and Uranus (Alfvén and Arrhenius, 1972, Figure 1) suggests that the Earth indeed may have had a regular satellite system, composed of about half a dozen bodies, each with a mass of only a

FIGURE IV-4

Noncatastrophic capture. Spin-orbit resonance prevents the Moon from reaching the Roche limit. The retrograde lunar capture orbit contracts due to tidal dissipation, until resonance between the lunar orbit period and the spin period of the Earth locks the Moon in a slowly expanding orbit. Since the Moon never comes very close, no breakup or autoejection occurs and the tides do not reach catastrophic heights. When the orbital inclination has decreased below a critical angle (suggested in the diagram at about 25°), the resonance locking is broken and the Moon recedes to its present orbit at 60 $R_{\oplus}$. (from Alfvén and Arrhenius, 1969).

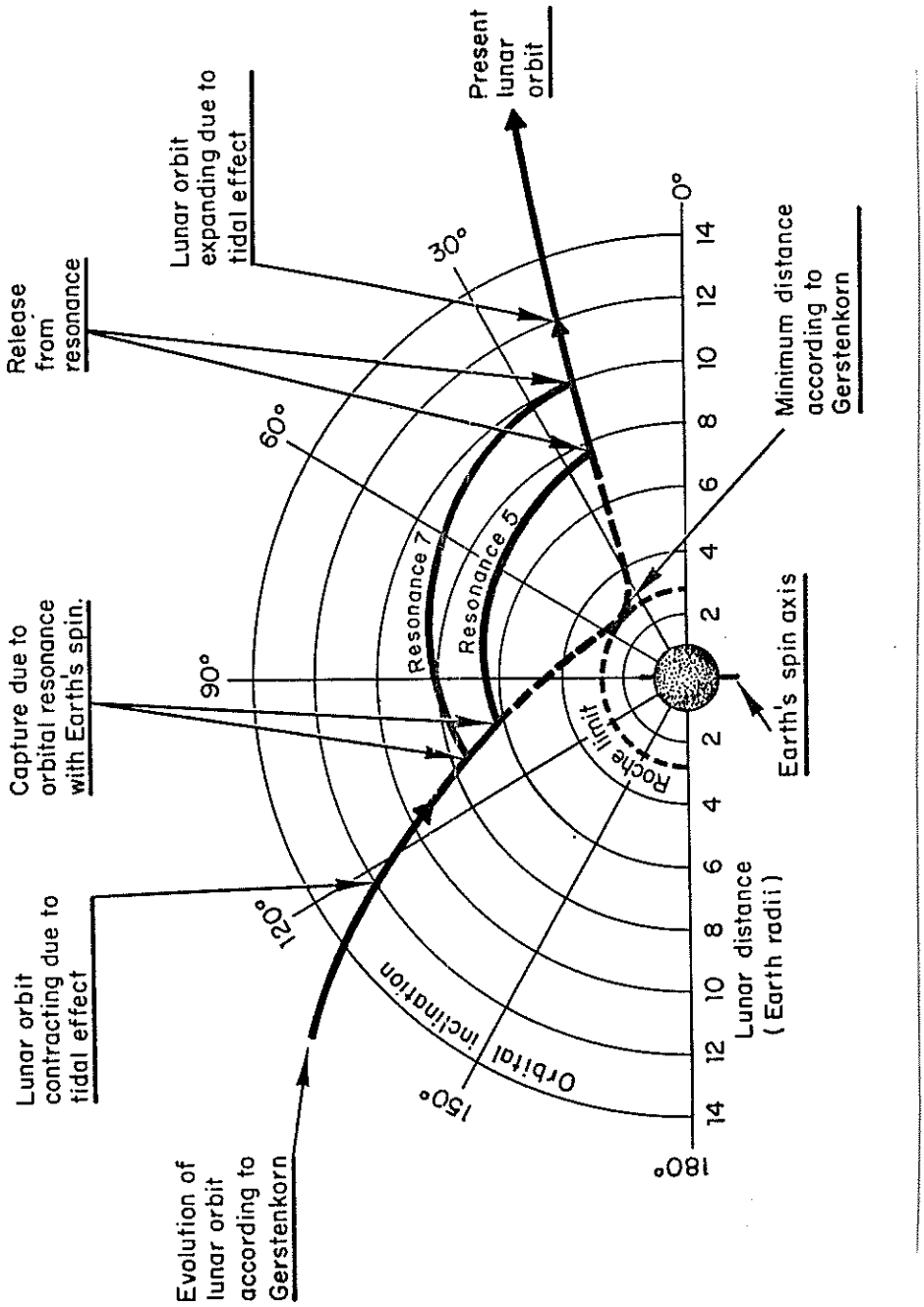
Release from resonance
Lunar orbit expanding due to tidal effect
Present lunar orbit
Capture due to orbital resonance with Earth's spin.
Minimum distance according to Gerstenkorn
Lunar orbit contracting due to tidal effect
Earth's spin axis
Evolution of lunar orbit according to Gerstenkorn
Orbital inclination
Resonance 7
Resonance 5
Roche limit
Lunar distance (Earth radii)
0°
30°
60°
90°
120°
150°
180°
2
4
6
8
10
12
14

fraction of a percent of the lunar mass. These proper satellites could have been swept up by the Moon during the post-capture evolution of its orbit; the major maria may be the impact sites, and the active time interval -4.0 to -3.0 Gy would mark this series of events.

Regardless of the ultimate origin of the Moon, tidal forces in the early evolution of the Earth-Moon system should be of considerable importance, and the question arises of the relative role of the ocean in the tidal dissipation. Since dissipation in the solid Earth is considered insignificant (Munk, 1968) the ocean would provide the most important medium for tidal energy exchange.

It was believed earlier that capture of the Moon must have catastrophic tidal effects on Earth leading to complete evaporation of the ocean to form a hot atmosphere. However, the long duration of the high magnetic field immersion indicated by the magnetization of lunar rocks in the time interval -4 to -3 Gy (Strangway et al., 1972; Alfvén and Lindberg, 1973), suggest that the capture and the subsequent approach and recession of the Moon to its present orbit were associated with resonance effects (Figure IV-4). These could possibly also limit the closest approach of the Moon to distances much larger than the Roche limit.

14. FUTURE DEVELOPMENTS

We have attempted to demonstrate here how the knowledge gained by exploration of the solar system has made possible a new

approach to some of the fundamental geological and oceanographic problems, which previously lacked observational basis and frequently were ignored. It is also clear, however, that much of the quantitative clarifications of the relevant processes is still ahead of us. It is likely that considerable refinement of our concepts can be achieved with the new experimental material already existing or within reach in the near future. The awareness of the problems and of the means for their solution are bound to intensify the search for further experimental evidence both on Earth and in space around us. It was at this new frontier of oceanography that Lars Gunnar Sillén's inquisitive and exacting work came to an end.

REFERENCES FOR IV

Alfvén, H.: 1942-45. On the cosmogony of the solar system. Stockholm Observatorium Ann. 14, No. 2; 14, No. 5; 14, No. 9.

Alfvén, H.: 1954, On the Origin of the Solar System. Oxford University Press, London.

Alfvén, H.: 1970, Astrophys. Space Sci. 6, 161.

Alfvén, H. and Arrhenius, G.: 1969, Science 165, 11.

Alfvén, H. and Arrhenius, G.: 1970a, Astrophys. Space Sci. 8, 338.

Alfvén, H. and Arrhenius, G.: 1970b, Astrophys. Space Sci. 9, 33.

Alfvén, H. and Arrhenius, G.: 1972, The Moon 5, 210.

Alfvén, H. and Arrhenius, G.: 1973, Astrophys. Space Sci. 12, in press.

Alfvén, H. and Arrhenius, G.: 1973, Astrophys. Space Sci. in preparation.

Alfvén, H. and Lindberg, L.: 1973, Magnetic Field Production in the Earth-Moon system (in preparation).

Anders, E.: 1971, From Plasma to Planet, Proc. Nobel Symp. 21, A. Elvius, Ed., Wiley, N. Y., 133.

Apollo 16 Preliminary Examination Team, 1973. Science 179, 23.

Arnold, J. R.: 1969, Astron. J. 74, 1235.

Arrhenius, G.: 1972, From Plasma to Planet, Proc. Nobel Symp. 21, A. Elvius, ed., Wiley, N. Y., 117.

Arrhenius, G. and Alfvén, H.: 1971, Earth Planet. Sci. Letters 10, 253.

Arrhenius, G. and Asunmaa, S. K.: 1973, The Moon, in press.

Aston, F. W.: 1924, Nature 114, 786.

Asunmaa, S. K., Liang, S. S. and Arrhenius, G.: 1970, Proc. Apollo 11 Lunar Science Conf., Vol. 1, Pergamon Press, N.J., 1975.

Baxter, D. and Thompson, W. B.: 1971, Physical Studies of Minor Planets, NASA SP-267, T. Gehrels, ed., 319.

Baxter, D. and Thompson, W. B.: 1973, Astrophys. J., in press.

Black, D. C.: 1972a, Geochim. Cosmochim. Acta 36, 347.

Black, D. C.: 1972b, Geochim. Cosmochim. Acta 36, 377.

Black, L. P., Gale, N. H., Moorbath, S., Pankhurst, R. J. and McGregor, V. R.: 1971, Earth Planet. Sci. Letters 21, 245.

Boulos, M. S. and Manual, O. K.: 1971, Science 174, 1334.

Cameron, A. G. W.: 1964, The Origin and Evolution of Atmospheres and Oceans, P. J. Brancazio and A. G. W. Cameron, eds., Wiley, N. Y., 235.

Clarke, W. B., Beg, M. A. and Craig, H.: 1969, Earth Planet. Sci. Letters 6, 213.

Danielsson, L.: 1969, Astrophys. Space Sci. 5, 53.

Danielsson, L.: 1971, Physical Studies of Minor Planets, NASA SP-267, T. Gehrels, ed., 353.

De, B. and Arrhenius, G.: 1973, Inhomogeneous plasmas and primordial condensation: inferences from present-day observations (in preparation).

v. Eckermann, H.: 1948, Sveriges Geol. Undersokn Arsbok, Ser. Ca. 36, 176.

v. Eckermann, H.: 1958, Kungl. Svenska Vetenskaps Akademiens Handl., 4th Series, 7, no. 2.

Engel, A. E. J., B. Nagy, L. A. Nagy, C. G. Engel, G. O. W. Kremp and C. M. Drew: 1968, Science 161, 1005.

Fanale, F. P.: 1971, Chem. Geol. 8, 79.

Fuchs, L. H.: 1969, Amer. Mineralogist 54, 1645.

Gault, D. E., Quaide, W. L. and Oberbeck, V. R.: 1968, Shock Metamorphism of Natural Materials, B. M. French and N. M. Short, eds., Mono Book Corp., Md., 87.

Gerstenkorn, H.: 1969, Icarus 11, 189.

Gibson, E. K., Jr.: 1973, Thermochim. Acta, in press.

Gibson, E. K. and Johnson, S. M.: 1971, Geochim. Cosmochim. Acta 2 (Suppl. 2), 1351.

Gibson, E. K. and Johnson, S. M.: 1972, Thermochim. Acta 4, 49.

Gibson, E. K. and Moore, G. W.: 1973a, Science 179, 69.

Gibson, E. K. and Moore, G. W.: 1973b, Geochim. Cosmochim. Acta, in press.

Grossman, L.: 1972, Geochim. Cosmochim. Acta 36, 597.

Gurevich, L. E. and Lebedinskij, A. I.: 1950, Izv. Akad. Nauk S.S.S.R., Ser. Fiz. 14, 765.

Hanks, T. C. and Anderson, D. L.: 1969, Phys. Earth Planet. Inter. 2(1), 19.

Harteck, P. and Jensen, J. H. D.: 1948, Z. Naturforschung 3a, 591.

Hartmann, W. K.: 1972, Moons and Planets: An Introduction to Planetary Science, Bogden and Quigley, Tarrytown-on-Hudson, N. Y. and Belmont, Ca., 404.

Hattori, T., Nakano, T. and Hayashi, C.: 1969, Prog. Theoret. Phys. 42, 781.

Holland, H. O.: 1964, The Origin and Evolution of Atmospheres and Oceans, P. J. Brancazio and A. G. W. Cameron, eds., Wiley, N. Y., 86.

Kumar, S. S.: 1972, Astrophys. Space Sci. 16, 52.

Larimer, J. W.: 1967, Geochim. Cosmochim. Acta 31, 1215.

Larimer, J. W. and Anders, E.: 1967, Geochim. Cosmochim. Acta 31, 1239.

Larimer, J. W. and Anders, E.: 1970, Geochim. Cosmochim. Acta Acta 34, 367.

Latham, G., Dorman, J., Duennebier, F., Ewing, M., Lammlein, D. and Nakamura, Y.: 1973, Lunar Science IV, J. W. Chamberlain and C. Watkins, eds., The Lunar Science Institute, Houston.

Lehnert, B.: 1970, Cosmical Electrodyn. 1, 219.

Levin, B. J.: 1972, The Upper Mantle, A. R. Ritsema, ed., Tectnophysics 13, 7.

Lin, S. C.: 1966, J. Geophys. Res. 71, 2427.

Lodochnikov, V. N.: 1939, Zap. Mineral. O-va. 64, 207.

Lord, H. C.: 1965, Icarus 4, 279.

Martin and Donnay: 1972, Amer. Mineralogist 57, 554.

McCord, T. B.: 1966, Astron. J. 71, 585.

Mendis, D. A.: 1973, Astrophys. Space Sci., in press.

Meyer, C., Jr.: 1969, Ph. D. Thesis, University of California, San Diego, La Jolla, Ca.

Meyer, C., Jr.: 1971, Geochim. Cosmochim. Acta 35, 551.

Munk, W. H.: 1968, Q. J. R. Astron. Soc. 9, 352.

Neukum, G., Mehl, A., Fechtig, H. and Zahringer, : 1971, Earth Planet. Sci. Letters 8, 31.

Podosek, F. A.: 1970, Geochim. Cosmochim. Acta 34, 341.

Ramsey, W. H.: 1948, Monthly Not. R. Astron. Soc. 108, 406.

Ramsey, W. H.: 1949, Monthly Not. R. Astron. Soc., Geophys. Suppl. 5, 409.

Ramsey, W. H.: 1967, Planet. Space Sci. 15, 1609.

Rasool, S. I. and de Bergh, C.: 1970, Nature 226, 1037.

Ringwood, A. E.: 1959, Geochim. Cosmochim. Acta 15, 257.

Ringwood, A. E.: 1970, J. Geophys. Res. 75, 6453.

Rubey, W. W.: 1951, Bull. Geol. Soc. Amer. 62, 1111.

Rubey, W. W.: 1955, Geol. Soc. Amer., Special Paper 62, 631.

Safronov, V. S.: 1954, Astron. Zh. 31, 499.

Safronov, V. S.: 1958, Vopr. Kosmog., Akad. Nauk S.S.S.R. 6, 63.

Safronov, V. S.: 1959, Izv. Akad. Nauk S.S.S.R., Ser. Geofiz. 1, 139.

Safronov, V. S.: 1960, Vopr. Kosmog., Akad. Nauk S.S.S.R. 7, 59.

Safronov, V. S.: 1969, Evolution of the Preplanetary Cloud and the Formation of the Earth and Planets, Nauka, Moscow, (in Russian).

Schmidt, O. Yu.: 1944, Dokl. Akad. Nauk S.S.S.R. 45, 245.

Signer, P. and H. E. Suess: 1963, Earth Science and Meteorites J. Geiss and E. D. Goldberg, eds., North-Holland Publ. Co., Amsterdam, 241.

Sillén, L. G.: 1965, Arkiv. Kemi. 24, 431.

Sillén, L. G.: 1966, Arkiv. Kemi. 25, 159.

Strangway, D. W., Gose, W. A., Pearce, G. W. and Carnes, J. G.: 1972, J. Appl. Phys., in press.

ter Haar, D.: 1967, Ann. Rev. Astron. Astrophys. 5, 267.

Trulsen, J.: 1971, From Plasma to Planet, Proc. Nobel Symp. 21, A. Elvius, ed., Wiley, New York, 179.

Tuttle, O. F. and Gittens, J., editors, 1966. Carbonatites, Interscience, N. Y.

Urey, H. C.: 1952, The Planets: Their Origin and Development, Yale Univ. Press, New Haven.

Urey, H. C.: 1959, Handbuch der Physik, 52, 363.

Urey, H. C.: 1962, The Moon, Proc. 14th I. A. U. Symp., Z. Kopal and Z. K. Mikhailov, eds., Academic Press, London, 133.

Wasson, J. T.: 1969, Nature 223, 163.

Wiik, H. B.: 1956, Geochim. Cosmochim. Acta 9, 279.